High-order harmonics from laser-irradiated plasma surfaces

U. Teubner

Fachhochschule Oldenburg/Ostfriesland/Wilhelmshaven, University of Applied Sciences, Fachbereich Technik, Photonik, Constantiaplatz 4, 26723 Emden, Germany and Institut für Physik, Carl von Ossietzky Universität Oldenburg, D-26111 Oldenburg, Germany

P. Gibbon

Institute for Advanced Simulation, Jülich Supercomputing Centre, Forschungszentrum Jülich, 52425 Jülich, Germany

(Published 3 April 2009)

The investigation of high-order harmonic generation (HHG) of femtosecond laser pulses by means of laser-produced plasmas is surveyed. This kind of harmonic generation is an alternative to the HHG in gases and shows significantly higher conversion efficiency. Furthermore, with plasma targets there is no limitation on applicable laser intensity and thus the generated harmonics can be much more intense. In principle, harmonic light may also be generated at relativistic laser intensity, in which case their harmonic intensities may even exceed that of the focused laser pulse by many orders of magnitude. This phenomenon presents new opportunities for applications such as nonlinear optics in the extreme ultraviolet region, photoelectron spectroscopy, and opacity measurements of high-density matter with high temporal and spatial resolution. On the other hand, HHG is strongly influenced by the laser-plasma interaction itself. In particular, recent results show a strong correlation with high-energy electrons generated during the interaction process. The harmonics are a promising tool for obtaining information not only on plasma parameters such as the local electron density, but also on the presence of large electric and magnetic fields, plasma waves, and the (electron) transport inside the target. This paper reviews the theoretical and experimental progress on HHG via laser-plasma interactions and discusses the prospects for applying HHG as a short-wavelength, coherent optical tool.

DOI: 10.1103/RevModPhys.81.445 PACS number(s): 42.65.Ky, 42.65.Re, 52.38.−r, 52.50.Jm

CONTENTS

I. INTRODUCTION

Since the invention of the laser in 1960 by Maiman (1960), it has been possible to generate ever more intense light fields: the past decade in particular has seen the emergence of laser systems delivering unprecedented power. Multiterawatt systems have become standard, and at the time of this writing, several peta-

watt laser systems exist or are under construction worldwide (Mourou, 1997; Norreys *et al.*, 2004; Mourou *et al.*, 2006). This progress has been made possible by a dramatic reduction of the pulse duration from nanosecond pulses in the 1960s to femtosecond pulses approximately ten years ago. Subsequently, the newly developed chirped pulse amplification technique (CPA) (Strickland and Mourou, 1985; Perry and Mourou, 1994) has been improved to allow laser pulses to be amplified to high peak power and applied to laser-matter interaction.

Driven by these laser developments, early research using linear optics at low intensities graduated to nonlinear optics in the mid-1960s when light power exceeded the kilowatt range and the intensity in the interaction regime reached around 10^9 W/cm^2.

Approximately ten years later, the inertial confinement fusion programs led to the construction of lasers capable of reaching 10^{14} W/cm^2 on a nanosecond time scale. This can be regarded as the advent of plasma optics or "coronal physics" (Mulser, 1979; Kruer, 1988), based on the interaction of light with a moderately dense free-electron gas. Later, dense plasmas of ultrashort lifetimes were produced on the surface of solid targets (see, e.g., Luther-Davies *et al.*, 1992), offering interesting laboratory sources of incoherent electromagnetic radiation at short wavelength and of short pulse duration (Murnane *et al.*, 1994; Teubner *et al.*, 1995, 1996; Andiel *et al.*, 2001). Only recently—a further two decades on—was the domain of relativistic nonlinear optics achieved, based on the interaction of light with relativistic free electrons. This progress also shows up in the generation of short-wavelength radiation (high harmonics of the laser fundamental, soft, and hard x rays) and in ever shorter durations of those short-wavelength pulses (from nanoseconds down to femtoseconds and most recently to attoseconds). Altogether, the considerable progress in laser physics has led to a new science of intense light interaction with matter (Gibbon, 2005).

The motivation for the investigation of high-order harmonics is twofold. First, with respect to future applications in the extreme-ultraviolet region (XUV) such as nonlinear optics at short wavelengths, the aim is to enhance their optical properties, that is, to reduce their wavelength, to enhance the XUV intensity, and also to shorten the duration of the XUV pulses (in particular, of coherent radiation). On the other hand, one can use such harmonics in a diagnostic sense to gain insight into femtosecond laser interaction physics, including the physical process of harmonic generation itself. Short-wavelength, coherent radiation can be used to probe dense plasma properties (such as density, electrical conductivity, and opacity) via interferometry or absorption spectroscopy, or to examine high-energy electron jets and gigagauss magnetic fields from the interaction process. For these reasons, high-order harmonic generation has become a dynamic field in its own right, attracting more and more research groups.

This paper reviews high-order harmonic generation (HHG) from the interaction of intense picosecond and femtosecond laser pulses with dense plasmas, surveying the early investigations up to recent results. It is structured as follows. First we discuss the generation of harmonics at dense plasma surfaces with references to early work. We make a brief comparison of the different situations in which the harmonics are produced with relatively long and short pulses, respectively, and we also point out differences from harmonic generation in gases, clusters, and underdense plasmas. In Sec. III, we describe the theoretical framework for HHG with plasma surfaces, and in Sec. IV we discuss more recent investigations of harmonic generation with femtosecond pulses at higher laser intensities and contrast, together with the dependence of their properties on the experimental conditions, such as the emission direction and angle. We show how such harmonics can form very powerful coherent pulses of femtosecond or even attosecond pulse duration. Recent results from experiments and simulations of harmonics from the front and rear sides of thin foil targets are also reviewed; these shed new light on the generation mechanisms. Finally, Sec. V considers future perspectives and potential applications of high-order harmonics.

Throughout the paper, we use the following terms and notation. Femtosecond (fs) pulses denote pulses from several fs up to approximately 100 fs. Longer pulses of the order of several hundred fs (e.g., 500 fs) up to the picosecond range are termed picosecond (ps or sub-ps) pulses. HN, where N stands for the Nth order ($N=1,2,3,4,\ldots$), denotes harmonics observed in the direction of the (specular) reflected laser light and from the laser-irradiated side of the target. Sometimes a subscript is used that indicates the wavelength of the laser fundamental in nm (e.g., $H15_{800}$ stands for the 15th harmonic of the fundamental at 800 nm wavelength). Similarly, hN denotes the Nth-order harmonic observed from the rear side of a thin target. Indices such as 0 or L correspond to the incident fundamental laser pulse and $N=1$ corresponds to the first-order harmonic, that is, light of the same wavelength as the incident fundamental. A subscript H denotes that the corresponding quantity is from a harmonic in general.

II. HARMONIC GENERATION IN PLASMAS: BACKGROUND AND EARLY EXPERIMENTS

A. Physical mechanisms of harmonic generation

It has long been recognized that laser-produced plasmas offer various means of frequency conversion, particularly up-conversion into low-order harmonics of the fundamental. These mechanisms include resonance absorption (Erokhin *et al.*, 1969), parametric instabilities (Bobin, 1985), transverse density gradients associated with light filaments (Stamper *et al.*, 1985), ionization fronts (Brunel, 1990), photon acceleration (Wilks *et al.*, 1989), lattice radiation (Hüller and Meyer-ter-Vehn, 1993), and relativistic nonlinearities (Mori *et al.*, 1993).

Resonance absorption is of particular significance for overdense plasmas because it provides an efficient means of converting an electromagnetic wave with an-

gular frequency ω_0 and wave number $\mathbf{k}_0$ into a localized electrostatic mode $(\omega_p, \mathbf{k}_p)$, where ω_p is the plasma frequency and $\mathbf{k}_p$ is the corresponding wave vector. At the critical density surface n_c, the frequencies of the electromagnetic and plasma modes match, $\omega_0 = \omega_p$, so these two waves can mix to produce a second harmonic $\omega_2 = \omega_0 + \omega_p = 2\omega_0$. Parametric instabilities such as Raman scattering and two-plasmon decay (Drake *et al.*, 1974) also result in frequency conversion of the form $\omega_0 \rightarrow \omega' + \omega_p$, where the scattered wave ω' is shifted by the local plasma frequency ω_p. In a density gradient, these instabilities grow fastest at $n_c/4$, so that $\omega' = \omega_0/2$. Mixing of this wave with the fundamental leads to emission at $3\omega_0/2$. Integer and noninteger harmonics generated in laser-ablated fusion plasmas have attracted much interest in the past because they can yield useful diagnostic information on the properties of the plasma (density gradient, expansion velocity, etc.) especially in the vicinity of the critical density surface (Tarasevitch *et al.*, 2000; Veisz *et al.*, 2004). A classic example of this is second-harmonic emission, which is routinely used to track the passage of high-intensity laser pulses through underdense plasma targets (such as gas jets) (Stamper *et al.*, 1985). Here the second-harmonic light is generated via the interplay between the oscillatory motion of electrons in the laser field and a transverse density gradient. For example, an electromagnetic field $\mathbf{E} = \hat{\mathbf{y}} E_L \sin(\omega_0 t - k_0 x)$ will induce plasma oscillations parallel to this gradient, leading to a current $J_y(2\omega_0)$ and a corresponding electric field $\mathbf{E}(2\omega_0) = \hat{\mathbf{y}} E_L^2$ radiated perpendicular to the laser propagation axis.

Fluid nonlinearities caused by relativistic electron motion (Akhiezer and Polovin, 1956) have been regarded as a potential means of frequency up-shift for some time (see Gibbon, 1997, and references therein), beginning with the early work on Thomson scattering (Sarachik and Schappert, 1970) and perturbation theory in underdense plasmas (Montgomery and Tidman, 1964). To see this, it is instructive to examine the electron fluid motion in an oscillating laser field $E_L \sin \omega_0 t$, which is assumed to be polarized along the y axis as above. To lowest order, the transverse momentum p_y is given by

$$p_y = \frac{eE_L}{\omega_0} \cos \omega_0 t = m_e c a_0 \cos \omega_0 t, \tag{1}$$

where $a_0 = eE_L/m_e\omega_0 c$ is the dimensionless laser "pump strength" or quiver amplitude, m_e is the electron mass, ω_0 is the laser angular frequency, and c is the velocity of light. A simple Taylor expansion of the fluid velocity

$$v_y = \frac{p_y}{m_e \gamma} = \frac{p_y}{m_e \sqrt{1 + p_y^2/m_e{}^2 c^2}} \tag{2}$$

for $a_0 \ll 1$ reveals that the corresponding nonlinear current $J_y = n_e v_y$ will contain terms like $a_0^3 \cos 3\omega_0 t$, $a_0^5 \cos 5\omega_0 t$, etc., sources that will produce radiation at odd harmonics of the fundamental.

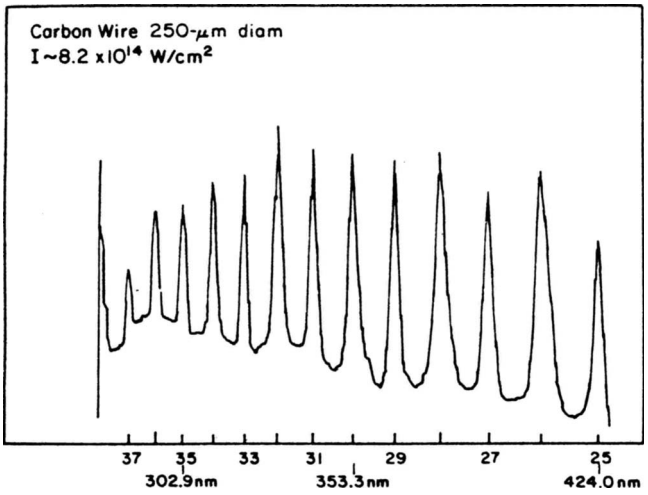

FIG. 1. Harmonic spectrum produced with a nanosecond CO_2 laser on a carbon wire. From Carman *et al.*, 1981b.

B. First experiments using nanosecond lasers (CO_2-laser pulses)

The first measurements on HHG were performed by Burnett *et al.* (1977) and Carman *et al.* (1981a, 1981b) more than 20 years ago. In those experiments, harmonics of a nanosecond CO_2-laser pulse were observed up to the 11th and 46th order, respectively (see, e.g., Fig. 1). As already mentioned, in an extended density profile the laser interacts with electrons at the critical electron density n_c, where an electron plasma wave is generated at $\omega_0 = \omega_p$ via resonance absorption (Kruer, 1988). If the light is sufficiently intense, the density profile will become steeper because of the ponderomotive force: electrons subsequently dragged back and forth across the density step can generate highly nonlinear, asymmetric currents (Bezzerides *et al.*, 1982; Grebogi *et al.*, 1983). Mixing of the plasma wave with the electromagnetic (EM) laser pump again generates radiation at $2\omega_0$. This wave is mainly reflected, but part of it can propagate up the density profile to $4n_c$, where it excites a plasma wave at $2\omega_0$. This in turn generates a third harmonic, $\omega_3 = 3\omega_0$, which is resonant at $9n_c$, and so on (Gibbon, 1997). Thus the maximum harmonic order is determined by the highest electron density available in the plasma,

$$M = \sqrt{\frac{n_e}{n_c}}. \tag{3}$$

According to this "cutoff" rule, the lowest achievable harmonic wavelength would appear to be independent of the driver: a CO_2 laser should generate more harmonics than a glass laser, but their intensities are likely to be lower, depending on the spectral falloff.

C. First experiments using femtosecond and picosecond lasers

With the advent of the CPA technique and the availability of sufficiently intense picosecond and femtosecond pulses, mainly ultrashort pulses have been applied

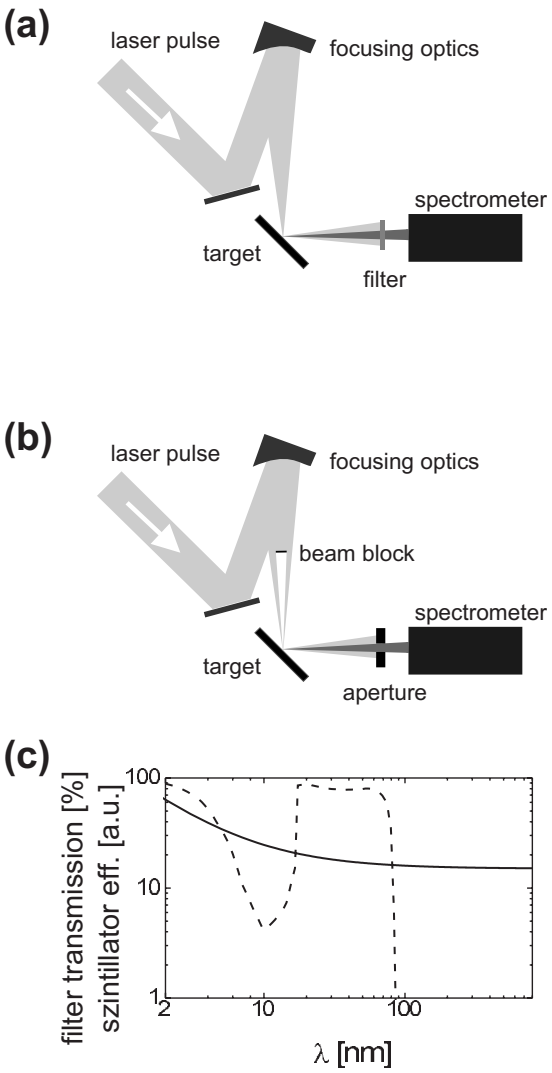

FIG. 2. Typical setup for the measurement of high-order harmonics. (a) Measurement with a thin filter to discriminate against stray light of the laser fundamental (typically a 100 nm Al filter). (b) Measurement without filter, but with a beam block to avoid damage of the spectrometer due to direct illumination with the strong laser fundamental. (c) Relative efficiency of a $Gd_2O_2S:Tb$ szintillator (solid line, data taken from Benitez *et al.*, 1991) and transmission of a 100-nm-thick aluminum filter (dashed line, data taken from Henke *et al.*, 1993).

for HHG in dense laser-produced plasma (LPP). As we will see in Sec. III, this allows the interaction of the laser pulse with a steep-density-gradient plasma, an entirely different regime from that accessible with nanosecond laser pulses. This is apparent even in the early experiments looking at the generation of low-order harmonics ($H2, H3$) (see, e.g., von der Linde *et al.*, 1992).

A typical setup for measurement of the harmonics is shown in Figs. 2(a) and 2(b). Usually, the high-power femtosecond laser pulse is focused with a lens or parabolic mirror onto a flat solid target. The generated harmonics are observed with a spectrometer mainly in the direction of the specular reflected laser light, although in some experiments they are also diagnosed from other directions. Different kinds of spectrometers have been applied; some are based on commercial systems (Kohlweyer *et al.*, 1995; Norreys *et al.*, 1996), some are specially made of a toroidal holographic reflection grating (von der Linde *et al.*, 1995; Földes *et al.*, 1996), and some consist of a large-aperture toroidal mirror together with a planar large-aperture free-standing transmission grating (Jasny *et al.*, 1994; Teubner, Pretzler, Schlegel, *et al.*, 2003).

The spectra in the image plane can then be detected either directly, for example, with a diode array (von der Linde *et al.*, 1995), a combination of a monochromator and a photomultiplier (Ishizawa *et al.*, 2001), a soft-x-ray streak camera (Kohlweyer *et al.*, 1995), a backside-illuminated charge-coupled device (CCD) (Gruner *et al.*, 2002), of an open microchannel plate (MCP) (Jasny *et al.*, 1994; Földes *et al.*, 1996; Norreys *et al.*, 1996), or after conversion into visible light by means of a phosphor (Tarasevitch *et al.*, 2000; Teubner, Pretzler, Schlegel, *et al.*, 2003). A phosphor that covers the broad wavelength range of soft x rays up to the visible region and thus is suitable for the detection of the harmonics is $Gd_2O_2S:Tb$ (Benitez *et al.*, 1991) [Fig. 2(c)]. The visible light of the phosphor is then imaged onto a slow-scan CCD, using either imaging optics (see, e.g., von der Linde *et al.*, 1995) or a fiber-optical taper (Altenbernd *et al.*, 1997; Gruner *et al.*, 2002), sometimes with subsequent light amplification via a MCP.

To discriminate the laser fundamental and stray light in the spectrometer, a light, thin, tight filter is placed in front of the spectrometer, typically an aluminum filter with a thickness between 50 and 200 nm [Fig. 2(a)]. This blocks radiation between 7 and 17 nm and wavelengths greater than 82 nm, respectively [Fig. 2(c)]. Hence, in experiments where harmonics with longer (or shorter) wavelengths are observed, the filter has to be removed and an additional beam stop placed at the center of the incident beam between the laser focusing optics and the target. Furthermore, an aperture before the spectrometer entrance has to be used to suppress the fundamental, which otherwise would be directly reflected into the spectrometer. This was first done by Peatross *et al.* (1994) and von der Linde *et al.* (1995) [Fig. 2(b)].

The first experimental observations of femtosecond high-order harmonics were made independently by Kohlweyer *et al.* (1995) and von der Linde *et al.* (1995) using Ti:sapphire laser systems with wavelengths of $\lambda_0 = 794$ and 800 nm, respectively. The laser pulses with an energy of $E_0 \approx 100$ mJ and a pulse duration of $\tau_0 \approx 100$ fs were focused to an intensity of the order of $I_0 = 10^{17}$ W/cm^2 onto solid targets of aluminum and glass, respectively. These pulses were of *high contrast ratio*, meaning that the background of amplified spontaneous emission (ASE) or prepulse(s) was weak enough to avoid significant preplasma formation. The contrast ratio is defined as the ratio of the intensity of the femtosecond laser pulse to that of the background and/or prepulse(s), respectively. Thus in those experiments the laser pulse interacted with a steep density gradient plasma. Harmonics up to seventh (Kohlweyer *et al.*, 1995) and 15th order (von der Linde *et al.*, 1995), respec-

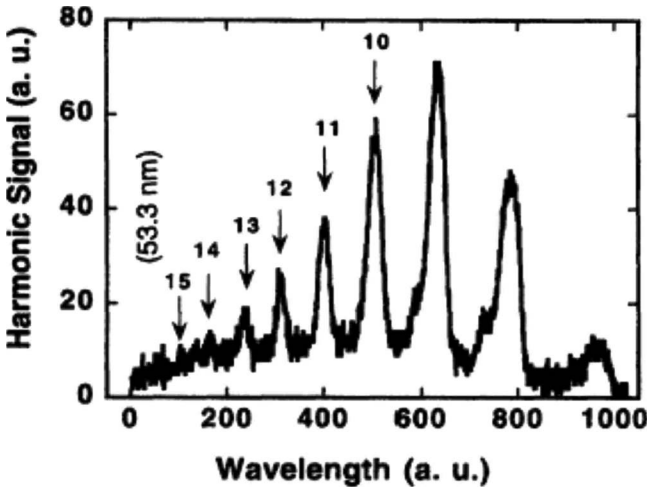

FIG. 3. Harmonics from an aluminum target produced with a 100 fs laser pulse focused to $I_0=10^{17}$ W/cm^2 and measured in reflection geometry. The harmonic orders are indicated. From von der Linde *et al.*, 1995.

tively, were observed (Fig. 3). The estimated conversion efficiency of the incident laser energy into the highest harmonic was approximately 10^{-9}.

Low-order harmonics (but in the same wavelength range) were also observed with high-contrast KrF* lasers (248 nm laser fundamental) and 0.6 ps pulse duration. Földes and co-workers reported the generation of the second- and third-order harmonics with thresholds between 4×10^{14} and 1×10^{15} W/cm^2 (for $H2$) and 3×10^{15} W/cm^2 (for $H3$), respectively (Földes *et al.*, 1996).

D. Comparison with harmonic generation in gases, clusters, and underdense plasmas

Before we review more recent experiments and simulations, it is useful at this point to make a brief comparison to HHG in gases. HHG in gases has now been studied for two decades (L'Huillier and Balcou, 1993; Platonenko and Strelkov, 1998; Balcou *et al.*, 2002; Gavrila, 2002). In most of those experiments, an intense femtosecond laser pulse is focused into a jet of rare gas, such as helium or argon. Harmonic generation in this context is a nonlinear optical process, which can be described with a simple three-step model of tunnel ionizing gas atoms in the strong electric field of the laser pulse, a subsequent acceleration of the free electrons along a trajectory given by the laser field and the atomic (or ionic) potential, and finally the radiative recombination (recollision model). In contrast to the HHG with dense plasmas—the subject of the present work—HHG in gases creates odd-order harmonics only, for symmetry reasons. Thus it is clear that the mechanisms of HHG in gases and from dense plasma surfaces are physically distinct.

Since the first milestone experiments by McPherson *et al.* (1987) and L'Huillier and Balcou (1993), harmonic generation in gases is now possible down to the water window region (Spielmann *et al.*, 1997). Other experiments have demonstrated harmonic pulse durations well below 1 fs (650 as) (Hentschel *et al.*, 2001). However, extraordinary as these achievements may be, fundamental physical restrictions on the utility of gas harmonics arise due to limitations on the laser intensity. In order to avoid strong ionization of the gaseous medium that would suppress harmonic generation, the laser intensity has to be kept below 10^{15}–10^{16} W/cm^2. Of course this results in a generally rather low harmonic intensity. In addition, there is another well-known problem, namely, that of proper phase matching, which can be partially remedied using gas-filled capillaries instead of gas jets (Balcou *et al.*, 2002). Because of the radically different physics involved with ionized material, these limitations and problems are not present in the case of HHG by means of LPP.

Just as for HHG in gases, clusters (see, e.g., Donnelly *et al.*, 1996; Hu and Xu, 1997) or low-density plasmas created on solid surfaces (see, e.g., Akiyama, *et al.*, 1992; Theobald *et al.*, 1995, or Ganeev, Suzuki, Baba, and Kuroda, 2005; Ganeev, Suzuki, Baba, Kuroda, *et al.*, 2005, and references therein) can also be used as the conversion medium. In this case, a picosecond laser pulse generates a preplasma of low density consisting mainly of neutral and singly ionized atoms. Then, after a specific delay, a femtosecond laser pulse is propagated through this preplasma and is partly converted to harmonics. Using this scheme, Ganeev and co-workers reported on harmonics up to 63rd order (i.e., 13 nm) (Ganeev, Suzuki, Baba, and Kuroda, 2005; Ganeev, Suzuki, Baba, Kuroda, *et al.*, 2005). Similarly, harmonic generation has also been observed using preformed plasmas on microdroplets (Flettner *et al.*, 2003).

Phase-matched HHG is also possible in an ionized gas, or underdense plasma, driven by the nonlinear currents arising via relativistic electron motion; see Sec. II.A. Experimentally, this regime has remained largely unexplored because of the difficulty in excluding the harmonics generated by bound electrons. Even at focused intensities of 10^{18} W/cm^2, multiphoton effects can occur near the ionization threshold in the foot, tail, and wings of the pulse, which is typically 10^{14}–10^{16} W/cm^2 depending on the medium. Chen *et al.* (2000) observed phase-matched third-order harmonics scattering into a narrow ring in the forward direction. Phase matching can be arranged in a three-dimensional geometry using a tight focal spot containing higher-order Laguerre-Gaussian modes (Siegman, 1986). The requirement $\Delta\varphi=k_3z'-3k_0z=0$ is then satisfied by allowing the propagation directions of pump z and harmonic z' to differ through $z=z'\cos\theta$. In their experiment, Chen *et al.* found an absolute conversion efficiency for the third-order harmonic, emitted at a cone angle of 5.6°, of 2×10^{-5} at 1.7×10^{17} W/cm^2, two orders of magnitude higher than that predicted by one-dimensional (1D) theory for forward-directed light (Mori *et al.*, 1993).

III. THEORY OF HHG ON DENSE PLASMA SURFACES

A. Nonlinear fluid model

The starting point for most theoretical analyses of HHG is the usual set of Lorentz-Maxwell equations for a preionized, quasineutral, collisionless plasma slab fitting the above description. The ions are assumed to form a fixed background density $Zn_i \equiv n_0$, where Z is the average ionization degree, n_i is the ion density, and n_0 is the initial electron density; the electrons are fluidlike and driven by the laser fields incident on the surface. For normally incident light, these fields can be represented by a vector potential $\mathbf{A}=(0,A_y\{x,t\},0)$, whereby $E_y=-\partial A_y/\partial t$, $B_z=\partial A_y/\partial x$. In this geometry, the transverse electron momentum is

$$p_y = eA_y/c, \tag{4}$$

expressing the fact that the canonical momentum is conserved (Gibbon, 2005). To get a wave equation for A_y, we substitute E_y and B_z into Ampère's law and apply the Coulomb gauge, $\nabla\cdot\mathbf{A}=0$, to obtain

$$\frac{1}{c^2}\frac{\partial^2 A_y}{\partial t^2} - \nabla^2 A_y = \frac{4\pi}{c}J_y. \tag{5}$$

With the help of Eq. (4), the current J_y can be written as

$$J_y = -en_e v_y = \frac{e^2 n_e}{mc}\frac{A_y}{\gamma}, \tag{6}$$

where

$$\gamma = \left(1 + \frac{p_x^2 + p_y^2}{m_e^2 c^2}\right)^{1/2}. \tag{7}$$

The problem of finding the harmonic content of the reflected light spectrum $|A_y(x,t)|^2$ essentially reduces to determining J_y, the source of reemitted radiation from the plasma surface. From Eq. (6), we can immediately see that this transverse current is generally nonlinear, containing both longitudinal density oscillations through n_e and relativistic motion through $\gamma(p_x,p_y)$.

Within this simplified geometry, the longitudinal momentum p_x is given by

$$\frac{dp_x}{dt} = e\frac{\partial\varphi}{\partial x} - \frac{e^2}{2m_e c^2\gamma}\frac{\partial A_y^2}{\partial x}. \tag{8}$$

Collective electron motion results in a change in the local density according to the continuity equation

$$\frac{\partial n_e}{\partial t} + \frac{\partial}{\partial x}\left(\frac{n_e p_x}{m_e\gamma}\right) = 0, \tag{9}$$

and the resulting electrostatic field is determined via Poisson's equation,

$$\frac{\partial^2\varphi}{\partial x^2} = 4\pi e(n_e - n_0). \tag{10}$$

Equations (5)–(10) form a closed set that is in principle sufficient to determine the reflected wave form $A_y(x,t)$ for arbitrary laser amplitude at normal incidence angle, i.e., where the wave vector $\mathbf{k}$ is perpendicular to the plasma surface. An analogous set of equations to describe general fluid nonlinearities for plane waves in homogeneous, *underdense* plasmas was derived 50 years ago by Akhiezer and Polovin (1956). To generalize this set of equations to *oblique* incidence, $\mathbf{k}=(k\cos\theta, k\sin\theta, 0)$—the most relevant geometry for HHG—a simple trick can be employed to make the wave vector appear normally incident. The covariance of Eq. (5) permits addition of a transverse drift momentum $\mathbf{p}_0=-\hat{\mathbf{y}}m_e c\tan\theta=-p_0\hat{\mathbf{y}}$ to both electrons and ions, resulting in a net current (now permitted to be in both the y and z directions, allowing for arbitrary laser polarization),

$$\mathbf{J}_\perp = -\frac{en_e}{m_e\gamma}(\mathbf{p}_\perp + \mathbf{p}_0) + \frac{en_0}{m_e\gamma_0}\mathbf{p}_0. \tag{11}$$

This procedure is equivalent to Lorentz transformation of all fluid variables to a frame moving along the plasma surface with velocity $v_y=ck_y=c\sin\theta$ (Bourdier, 1983). In this frame, the longitudinal momentum acquires an additional driving term,

$$\frac{dp_x}{dt} = e\frac{\partial\varphi}{\partial x} - \frac{e^2}{2m_e c^2\gamma}\frac{\partial A_y^2}{\partial x} + \frac{e}{m_e c\gamma}p_0\frac{\partial A_y}{\partial x}, \tag{12}$$

where the relativistic factor is now given by

$$\gamma^{-1} = \frac{(1 + p_x^2/m_e^2c^2)^{1/2}}{[1 + (|\mathbf{p}|^2/m_e^2c^2)\cos^2\theta - (p_y/m_e c)\sin 2\theta]^{1/2}}. \tag{13}$$

The above model is equivalent to those formulated by Bulanov *et al.* (1994) and Lichters *et al.* (1996). An important feature of HHG that can be rigorously deduced from Eq. (11) is the existence of so-called selection rules for the polarization of reflected harmonics from a perfectly smooth surface (Lichters *et al.*, 1996; Gibbon, 2005). For s-polarized light, $\mathbf{A}=(0,0,A_z)$, the current sources are

$$J_z^s = -\frac{e^2 n_e}{m_e c\gamma}A_z,$$

$$J_y^s = \frac{en_e}{m_e\gamma}p_0 - \frac{en_0}{m_e\gamma_0}p_0. \tag{14}$$

Likewise, for p-polarized light,

$$J_z^p = 0,$$

$$J_y^p = -\frac{e^2 n_e}{m_e c\gamma}A_y + \frac{en_e}{m_e\gamma}p_0 - \frac{en_0}{m_e\gamma_0}p_0. \tag{15}$$

Note that the above equation also contains the ion current due to the streaming plasma $J_y^i=-en_0v_0$. Initially, before the laser arrives ($\gamma\to\gamma_0; n_e\to n_0$), this cancels the corresponding electron component en_0v_0 exactly, so that $J_y^p\to 0$. Inspection of the momentum equation (12) together with the relativistic factor γ shows that

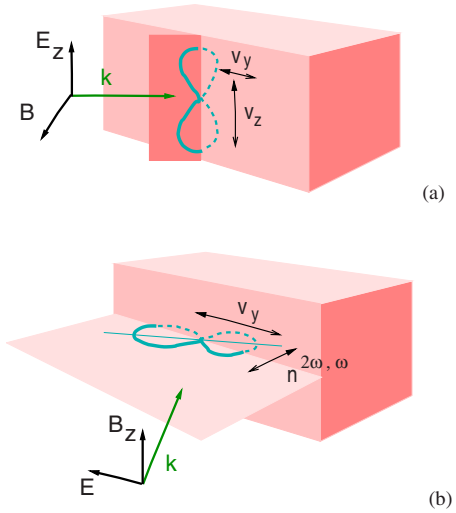

FIG. 4. (Color online) Moving mirror model for obliquely incident laser: relativistic figure-of-8 electron oscillations initially driven by (a) *s*-polarized light, leading to surface currents in both the *y* and *z* directions, and (b) *p*-polarized light, leading to surface currents in the *y* direction only.

$$p_x \sim \frac{p_y^2 + p_z^2}{\gamma} + \frac{p_y}{\gamma},$$

which contains purely even harmonics $\sim p_z^2$ for *s*-polarized light, but both even and odd harmonics $\sim p_y^2$, $\sim p_y$ for *p*-polarized light, as does γ itself. The continuity (9) and Poisson equations (10) imply that n_e and φ will have the same harmonic content as p_x. Therefore, J_z^s will create purely odd harmonics in the reflected light, J_y^s purely even, but J_y^p will create both odd and even. At normal incidence ($p_0=0$), even harmonics vanish for both polarizations.

These rules can also be deduced by simple symmetry arguments, recalling that the electron motion in a relativistic wave initially follows a "figure-of-8" path, containing a transverse component at the laser frequency ω_0 plus a longitudinal one at $2\omega_0$ For obliquely incident light on an overdense plasma surface, this motion takes place in different planes relative to the plasma density (see Fig. 4), thus resulting in net surface currents polarized according to Table I, and hence reflected EM radiation following the same polarization pattern. Note that the actual surface motion is more complex than that suggested by Fig. 4 (as we show later) for two reasons: first, electrostatic restoring forces set up inside the plasma result in a strong asymmetry of motion across the boundary; second, wave breaking leads to absorption of electrons by the target as well as extended, possibly unbounded excursions into the vacuum.

TABLE I. Selection rules for harmonics generated by various polarizations of incident light.

Laser polarization	Odd harmonics ω_{2n+1}	Even harmonics ω_{2n}
Oblique *s*-	*s*-polarized	*p*-polarized
Oblique *p*-	*p*-polarized	*p*-polarized
Normal linear	Linearly polarized	
Normal circular (*C*)		

B. Oscillating mirror model

In contrast to the extended density profiles generated by nanosecond laser pulses, femtosecond laser-produced plasmas have little time to expand, so typical density scale lengths for a high-contrast laser are submicron. During the interaction, the plasma surface can thus be represented to a good approximation by a simple step profile, and assumed to be overdense ($n_e \gg n_c$), so that it acts as a mirror reflecting the incident light specularly. On the other hand, to model the plasma surface dynamics even in this limit, one has to solve the complete equation system Eqs. (8)–(13). Previous analyses have shown that this approach usually breaks down due the onset of wave breaking (Grebogi *et al.*, 1983; Kato *et al.*, 1993; Yu *et al.*, 1998). To get round this obstacle, Bulanov *et al.* (1994) proposed the so-called oscillating (or moving) mirror model (OMM), in which the electron density is treated as a rigid step function oscillating harmonically though a fixed ion background.

In terms of the electron density, we can formally write

$$n_e = n_0 \Theta[x - \xi(t)], \tag{16}$$

where $\Theta(x)=\{0, x<0; 1, x>0\}$ is the Heaviside step function and $\xi(t)$ is the instantaneous mirror position. In general, the mirror motion is highly complex, and depends on the laser polarization, angle of incidence, intensity, and plasma density. For simplicity, we assume that the position has a simple harmonic form $\xi(t) = \xi_s \sin \omega_0 t$. The reflected electric field is therefore emitted from a moving surface, and, omitting constant phase factors, can be approximated by

$$E_r = E_L \sin(\omega_0 t_{\text{ret}}), \tag{17}$$

where $t_{\text{ret}} = t - \xi(t)/c$ is the retarded time at the observation point. Substituting for $\xi(t)$, we find

$$E_r = E_L \sin\left(\omega_0 t - \frac{\omega_0}{c}\xi_s \sin \omega_0 t\right), \tag{18}$$

giving a characteristic anharmonic wave form. Tutorial accounts of the OMM can be found in Teubner, Pretzler, Schlegel, *et al.* (2003) and Tsakiris *et al.* (2006). The OM model was developed further by Lichters *et al.* (1996) and von der Linde and Rzàzewski (1996). These early versions relied on an *ad hoc* treatment of the critical surface motion $\xi(t)$ in order to compute the harmonic spectrum.

More recently, the OMM has been reexamined using asymptotic analysis of the mirror dynamics in the highly relativistic limit (Gordienko *et al.*, 2004). Despite its simplicity, and the fact that it is in fact strictly valid only for normal incidence, this model makes important predictions concerning the reflected light spectra and its har-

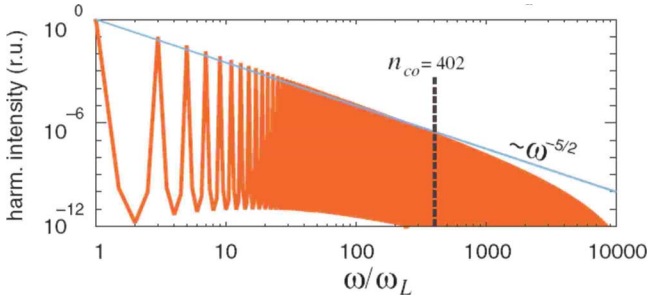

FIG. 5. (Color online) Harmonic spectrum calculated from the oscillating mirror model in the extreme relativistic limit (here $a_0=10$). From Tsakiris *et al.*, 2006.

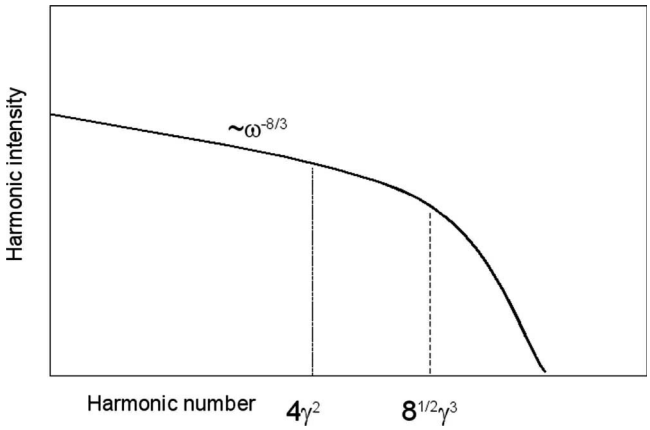

FIG. 6. Properties of harmonic spectrum according to the "spiky" mirror model. For relativistic intensities, the $\gamma_{\max}$ cutoff will be higher than the $4\gamma_{\max}$ value predicted by the standard OMM. The rolloff beyond the second power-law "cutoff" is exponential.

monic content. First, for highly relativistic laser pump strengths ($a_0 \gg 10$), the spectrum rolls off according to a power law,

$$I_\omega \sim \omega^{-5/2}, \tag{19}$$

up to a cutoff frequency $\omega_{\max}$ (see Fig. 5). The latter is just the Doppler-shifted frequency corresponding to the maximum mirror velocity,

$$\beta \approx c^{-1}\left|\frac{\partial \xi}{\partial t}\right|_{\max}.$$

Note that the mirror velocity is limited to $\beta \leqslant 1$. In other words,

$$\omega_{\max} = 4\gamma_{\max}^2\omega_L = \omega_L\frac{1+\beta_{\max}}{1-\beta_{\max}}. \tag{20}$$

For more modest pump strengths ($a_0=1$) and/or finite pulse lengths, a steeper spectral falloff and lower cutoff frequencies are expected, as confirmed by particle-in-cell simulations, which are discussed in the next section.

An improvement on this theory based on a more physically motivated, but still asymptotic, analysis of the surface motion was presented by Baeva *et al.* (2006a). This model also takes into account the surface *acceleration* in a heuristic manner, leading to some subtle but important differences in the harmonic efficiencies. By restricting the analysis of the motion of an accelerated charge to a short period close to the turning points, it is possible to express the spectral intensity of emitted radiation in terms of Airy functions (Jackson, 1975). In the present context of coherent HHG, Baeva *et al.* find that the spectrum has a rolloff given by

$$I_\omega \sim \omega^{-8/3}, \tag{21}$$

slightly steeper than the 2.5 exponent in Eq. (19). Second, the cutoff frequency scales as $\gamma_{\max}^3$ as opposed to $\gamma_{\max}^2$, implying that higher-order harmonic orders can be reached for a given intensity in the extreme relativistic regime. These features are summarized in Fig. 6. Physically the γ^3 cutoff originates from the finite time over which the mirror electrons are accelerated. In fact, there is a close analogy here with synchrotron radiation, which also contains harmonics up to a maximum $\omega_c \approx 3c\gamma^3/R$, where R is the radius of curvature of the device (Jackson, 1975).

A further variation on this approach is the sliding mirror model proposed by Pirozhkov *et al.* (2006). This is valid for highly overdense, thin plasma slabs in which the electron motion along the density gradient can be neglected owing to the high charge-separation field. The only motion relevant for harmonic generation is then along the target surface. The figure of merit characterizing this regime is the so-called normalized plasma density,

$$\varepsilon_p = \frac{\pi d n_e}{\lambda_0 n_c}, \tag{22}$$

where d is the slab thickness. The sliding mirror regime is defined by $\varepsilon_p > a_0$. In this case, the spectrum is predicted to fall off as ω^{-2} up to a critical frequency $\omega_{\rm cr} \approx a_0\omega_0$, after which it decays exponentially.

C. Particle-in-cell simulations

Particle-in-cell (PIC) simulation is one of the most important numerical tools in plasma physics, providing a direct, self-consistent solution of the Lorentz-Maxwell equations for a system of charges interacting with an incident laser pulse. Not surprisingly, PIC codes have also been instrumental in predicting the optical properties of surface harmonics, guiding and even preceding some of the theory described above.

Early simulations of harmonic generation were hampered by a lack of spatial and temporal resolution available with two-dimensional PIC codes needed to adequately treat oblique incidence, a fact that also restricted the modeling performed by Carman *et al.* to fewer than ten harmonics in the early 1980s (Carman *et al.*, 1981b), so that they were unable to accurately model the conditions in their experiment in which nearly 50 harmonics were observed. The first simulations of HHG in the context of relativistic short-pulse laser interactions

were made by Wilks *et al.* (1993), who demonstrated the generation of low-order odd harmonics for normally incident light at intensities of around 10^{19} W/cm^2. At about the same time, the introduction of the relativistic boost technique [described in Sec. III.A by Eqs. (11)–(15)] to PIC simulation by Gibbon and Bell (1992) [see also Gibbon *et al.* (1999)] paved the way for order-of-magnitude improvements in temporal and spatial resolution over traditional 2D codes, and allowed high harmonics to be resolved for the first time. Bulanov *et al.* (1994) applied this technique to verify that low-order harmonics generated by oblique, *p*-, and *s*-polarized light did indeed obey the selection rules predicted by the oscillating mirror analysis.

To model HHG with a PIC code, it is necessary to resolve all physically relevant wavelengths on the spatial mesh and choose a sufficiently small time step to represent the highest frequency of interest. The simulation box must be large enough to prevent electrons from "escaping," which would otherwise upset overall charge neutrality. Typically this latter requirement translates to a simulation region of a few laser wavelengths, or several microns. Resolution of H_{100} would thus require at least 1000 grid points per laser wavelength. The target is usually modeled as a pre-ionized plasma, either as a thin foil surrounded by vacuum regions or as a semi-infinite slab with an absorbing "solid" boundary. Realistic densities ($n_e/n_c \sim 100$) demand a large number of particles per cell in order to resolve the all-important nonlinear surface dynamics. These considerations lead to an overall computational effort of 10–20 CPU hours on a single-processor PC. Equivalent two- and three-dimensional runs with the same resolution remain a challenge even with substantial supercomputing resources, but useful information can be and is still gained with lower resolution.

The large spectral advantage offered by the boost technique was first exploited by Gibbon (1996), who demonstrated that large numbers of harmonics could be generated at high intensities with no cutoff at the upper plasma density as implied by Eq. (3); see Fig. 7. These simulations also showed that in this intensity range, the harmonic efficiencies for *p*-polarized light are one to two orders of magnitude higher than for *s*-polarized or normally incident light. In the latter case, Eq. (14), only the relativistic $\mathbf{v}\times\mathbf{B}$ mechanism is present via γ and $n_e \sim n(2\omega_0)$, whereas strongly driven density bunching, via the net current $J_y^p = n_\omega v_\omega$ (see Fig. 4), makes an important contribution to the nonlinear current for *p*-polarized light.

Since then, particle-in-cell simulations have become an essential component of any theoretical or experimental investigation on HHG (Lichters *et al.*, 1996; Norreys *et al.*, 1996; Zepf *et al.*, 1998; Geissler *et al.*, 2007; and Tarasevitch, Lobov, Wünsche *et al.*, 2007). They are particularly expedient in identifying transitions in the harmonic generation mechanisms responsible for the observed spectra (see Secs. IV.B–IV.F). For example, a study by Tarasevitch, Lobov, Wünsche, *et al.* (2007) unveiled the limitations of the relativistic OMM in describing HHG in finite density-gradients; see Sec. III.D

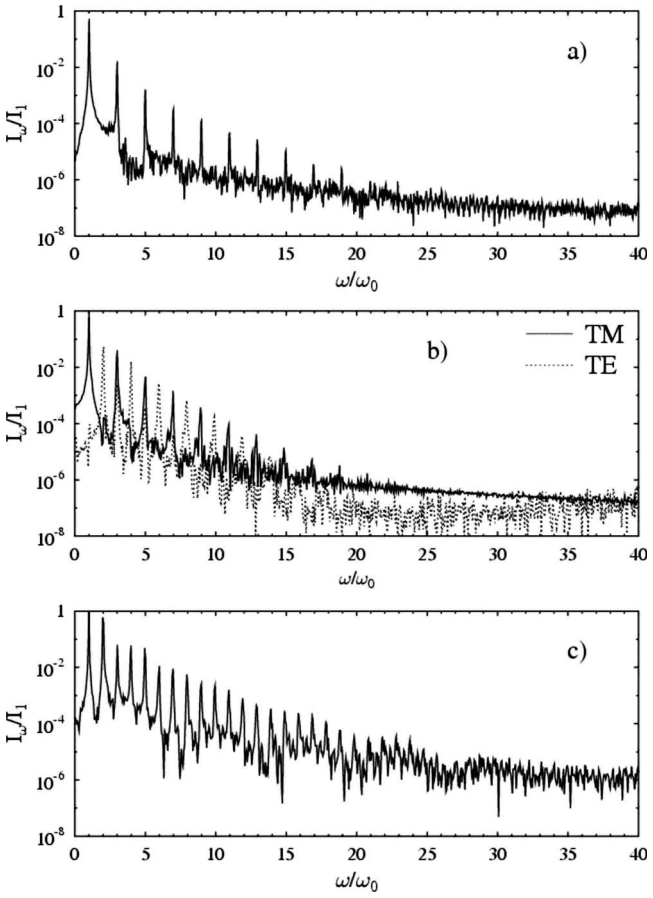

FIG. 7. Harmonic spectra produced by a particle-in-cell simulation at (a) normal incidence, (b) 45°, *s* polarized, and (c) 45°, *p* polarized. The upper shelf density was $n_0/n_c=20$, the laser amplitude is $a_0=1.0$.

The harmonic efficiencies obtained by particle simulations for *p*-polarized light at 45° incidence are shown in Fig. 8. These can be summarized by an empirical relation valid for high orders ($N \gg 1$),

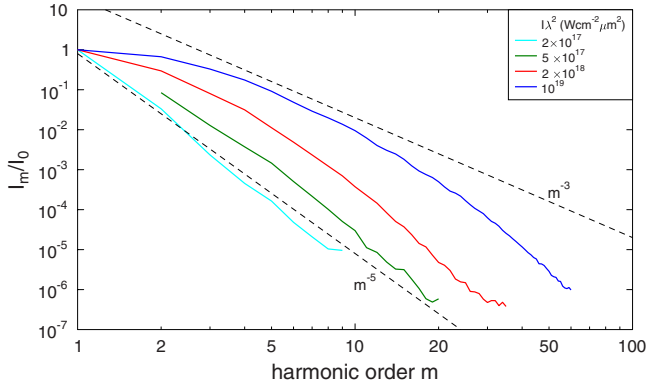

FIG. 8. (Color online) Scaling of harmonic spectra with laser intensity according to PIC simulations for *p*-polarized light at 45° incidence angle.

$$\eta_H \approx 9 \times 10^{-5} \left(\frac{I_0 \lambda_0^2}{10^{18}\ \mathrm{W\,cm^{-2}}\ \mu\mathrm{m}^2} \right)^2 \left(\frac{N}{10} \right)^{-\alpha}, \tag{23}$$

where α also scales inversely with intensity (Gibbon, 1996), ranging from $\alpha=6$ at $I_0=10^{17}$ W/cm^2 to $\alpha=3.5$ at $I_0=10^{19}$ W/cm^2 (at $\lambda_0=1$ μm), indicating a generally steeper rolloff of the spectrum than the asymptotic value predicted by the oscillating mirror model [Eq. (21)] in the extreme relativistic case at normal incidence. This scaling means that the highest harmonic order (down to the detection threshold) is simply determined by $I\lambda^2$, although there is some dependence on upper shelf density and incidence angle. Thus, in contrast to Eq. (3) here a short-wavelength pump beam will generate shorter-wavelength harmonics for the same irradiance. Equation (23) also implies that, for a fixed harmonic wavelength and $I\lambda^2$ (i.e., fixed N), shorter wavelength lasers are more efficient in harmonic generation (see also Sec. IV.C).

D. HHG in finite-scale-length density profiles

The OMM theory presented in Sec. III.A is strictly valid for ideal step profiles. In experiments, the target surface will almost inevitably have expanded into the vacuum to some extent, either due to laser prepulses or via suprathermal ion expansion during the interaction itself (Gibbon, 1994; Kingham *et al.*, 2001). In this more realistic situation, other nonlinear plasma effects come into play, such as resonance absorption and fast electron generation (via wave breaking). Resonant plasma wave excitation is a well-studied phenomenon usually considered in the context of laser absorption. It occurs for p-polarized incidence on a profile with a well-defined critical surface, where the transverse EM wave is converted to a longitudinal plasma (Langmuir) wave. The conversion efficiency of this process can be well approximated by a self-similar function (Denisov, 1957; Ginzburg, 1964),

$$\Phi(\xi) \approx 2.3\xi \exp\left(-\tfrac{2}{3}\xi^3\right), \tag{24}$$

where

$$\xi = (kL)^{1/3} \sin\theta. \tag{25}$$

The function $\Phi(\xi)$ has an optimum at $\xi=0.8$, meaning that the wave coupling efficiency and thus absorption is maximized at an angle scaling inversely with density scale length,

$$\sin\theta_{\mathrm{opt}} \approx 0.8(kL)^{-1/3}. \tag{26}$$

Here, L is defined by the ratio of the electron density n_e to the gradient of the electron density measured at the critical density n_c,

$$L = \left| \frac{n_e}{\nabla n_e} \right|_{n_e=n_c}. \tag{27}$$

If the condition (26) is even roughly satisfied, the resonant plasma wave can be driven to amplitudes many times larger than the nominal laser pump strength a_0,

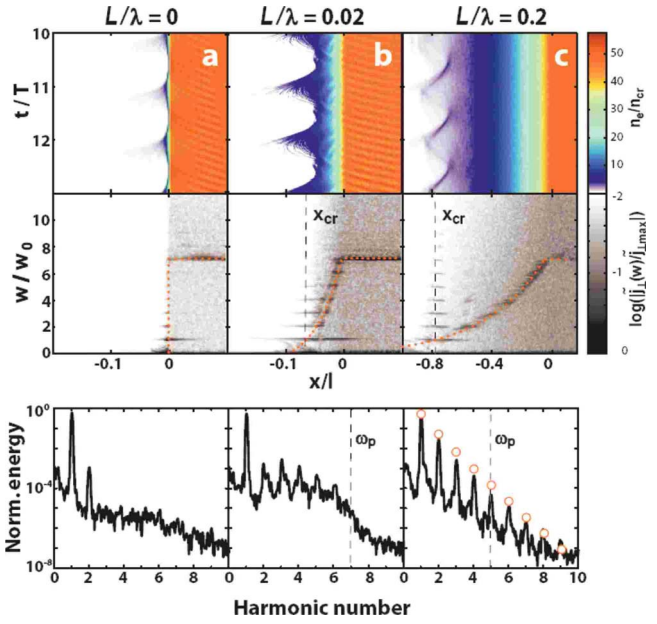

FIG. 9. (Color online) Transition from moving mirror regime ($L/\lambda=0$) to resonant regime ($L/\lambda=0.2$), showing density oscillations (top), location of harmonic current sources (middle), and spectra of reflected light (bottom). From Tarasevitch, Dietrich, and von der Linde, 2007.

and can thus itself become nonlinear. As pointed out by Erokhin *et al.* (1969), and verified by PIC simulations (Bulanov *et al.*, 1994), this implies that the plasma wave can act as a source of harmonics of the plasma frequency $N\omega_p$ at the critical density, which will in turn mix with the fundamental to produce current sources at $N\omega_0$. Because the strength of the plasma wave is angle dependent—varying according to Eq. (24)—harmonics generated in this fashion should also exhibit an angular dependence. Indeed, there is already some experimental evidence for this mechanism, albeit with ambiguous interpretations (see Sec. IV.F)

The transition between the stiff mirror $L/\lambda=0$ and resonance absorption regimes $L/\lambda > a_0/2\pi$ was investigated by Tarasevitch, Lobov, Wünsche, *et al.* (2007), who demonstrated that the location of the harmonic current sources is shifted toward the critical density surface with increasing density scale length (see Fig. 9).

E. Emission at the plasma frequency and its harmonics

Radiation at the local plasma frequency ω_p and its harmonics is a well-studied phenomenon in the astrophysical context—particularly in connection with certain types of solar flares (Ginzburg and Zhelezniakov, 1958; Melrose, 1980). Generally speaking, Langmuir waves can be excited by bunches of energetic electrons anywhere in a volume of plasma. If they are created close to the plasma surface, or in a strongly inhomogeneous region, nonlinear parametric processes can convert these electrostatic waves into electromagnetic radiation (Sturrock *et al.*, 1965; Chin-Fatt and Griem, 1970; Yoon, 1995, 1997; Willes *et al.*, 1996). In underdense plasmas (n_e

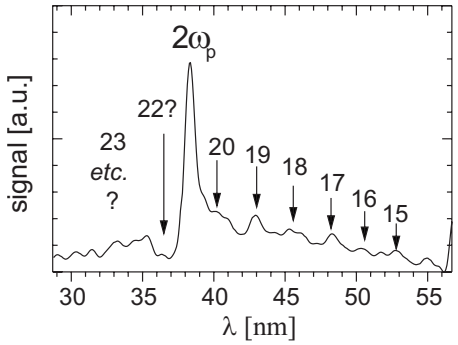

FIG. 10. Measured XUV spectrum showing the plasma frequency emission (i.e., emission at 2 ω_p). The other peaks may be identified with the harmonics of the laser fundamental. Adapted from Teubner *et al.*, 1999.

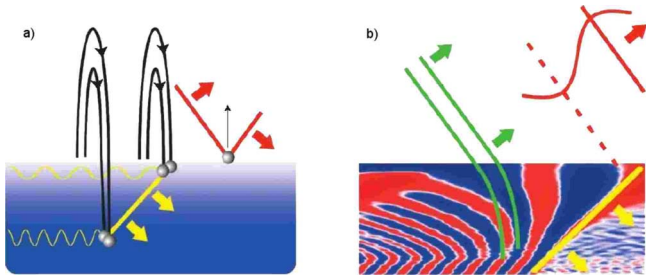

FIG. 11. (Color online) Coherent wake excitation: (a) Fast electron density bunch creates wake oscillations in density ramp with spatially varying wave vector. (b) Wake oscillations result in attosecond light emission where k becomes parallel to the target surface. From Thaury *et al.*, 2007.

$<10^{20}$ cm^{-3}), $2\omega_p$ emission can also be driven by laser wakefields, providing a novel source of terahertz radiation (Sheng *et al.*, 2005).

In the present laser-plasma context, where the laser pulse is incident on a finite-density profile, $2\omega_p$ emission can be triggered in inhomogeneous plasmas by inverse two-plasmon decay (Boyd, 1964; Meyer and Zhu, 1993) or inverse resonance absorption (Barr *et al.*, 1985). The connection of plasma harmonics with HHG has been demonstrated by many (Lichters *et al.*, 1996; Gibbon *et al.*, 1997, Boyd and Ondarza-Rovira, 2000; Ondarza-Rovira and Boyd, 2000) via PIC simulations that show plasma "line emission" at ω_p, $2\omega_p$, $3\omega_p$ on top of the usual optical spectrum. Significantly, this radiation is observed in both the reflected and transmitted spectra from thin foils and provides a direct means to determine the maximum electron density in such targets (Lichters, 1997; Lichters *et al.*, 1998). Plasma line emission at ω_p and $2\omega_p$ was also investigated experimentally: Fig. 10 shows a measured spectrum in which the $2\omega_p$ line may be clearly identified (Teubner *et al.*, 1997, 1999).

More recently, plasma emission has been proposed [Boyd and Ondarza-Rovira (2007)] as an explanation for periodic *modulations* found in the harmonic spectrum generated on density profiles with small but finite scale lengths (Teubner, Pretzler, Schlegel, *et al.*, 2003); see Sec. IV.F For example, these modulations can be seen in Fig. 7(c), even though the ω_p line itself (at $4.7\omega_0$) cannot be seen directly.

F. Coherent wake emission

The physical correlation between nonlinear surface motion and the production of energetic electrons in high-intensity laser plasma interactions has been known for some time (Brunel, 1987; Bulanov *et al.*, 1994; Gibbon, 2005). In general, the strong asymmetry of any longitudinal oscillations in a steep density profile almost inevitably leads to wave breaking, causing a certain fraction of electrons to be irreversibly accelerated into the target. This kinetic process results in absorption of laser energy, and would normally be regarded as detrimental to harmonic generation, compromising the coherence of the surface oscillations. On the other hand, fast electrons can themselves drive Langmuir waves, both in the overdense region leading to ω_p emission (Sec. III.E) and in the density ramps on the front (and possibly rear—Sec. IV.H) of the target.

The latter scenario has been identified as a potent source of HHG at moderate intensities (Quéré *et al.*, 2006). This mechanism, called coherent wave excitation (CWE) by the Saclay group, is triggered by the bunching of fast electrons in phase space as they reenter the target, an effect noted earlier (Bezzerides *et al.*, 1982; Brunel, 1987; Gibbon, 1996), but which had hitherto lacked quantitative analysis. The density bunching sets up a plasma wake oscillation with a wave vector $\mathbf{k}=(0,k_p(x)\sin\theta,0)$. Phase matching along this vector results in periodic bursts of radiation at the local plasma frequency $\omega_p(x)$, containing harmonics up to the maximum electron density n_e (see Fig. 11). CWE has been observed experimentally (Teubner *et al.*, 2004; Quéré *et al.*, 2006) and can be distinguished from relativistic OM harmonics via their spectral properties (see Sec. IV.F). By careful analysis of PIC simulations (Fig. 12), Quéré *et al.* were able to show that both mechanisms, namely, CWE and OMM, can be present at the same time but are active in different density regions. Finally, we note

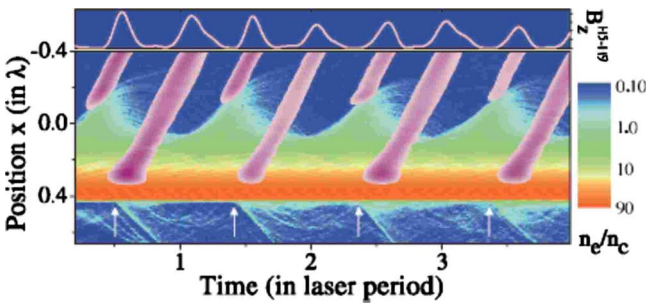

FIG. 12. (Color online) Electronic density on logarithmic scale and intensity of the harmonic pulses generated from a thin foil target. The upper diagram shows a temporal trace of the magnetic field, filtered between $H115$ and $H119$, showing that the harmonic pulses form a train of attosecond pulses. From Quéré *et al.*, 2006.

that the fast electrons driven by the Langmuir waves may lead to the generation of coherent transition radiation (see Sec. IV.I).

G. Multidimensional effects

The analyses and models of harmonic generation in the previous sections have implicitly assumed that the laser pulse is incident on a smooth, planar, overdense plasma target. In fact, this is slightly contradictory given the fact that the HHG process itself causes modulations in the density along its surface. This "surface rippling" has been examined by many (see, e.g., Veres *et al.*, 1999) who find that it may lead to significant enhancements in the low-order harmonics in a near-critical plasma (Singh *et al.*, 2003), or act as a diffraction grating for a probe pulse (Rzazewski *et al.*, 2000). In the latter scenario, the density modulations set up by the pump pulse scatter harmonic from the probe pulse into a rainbowlike fan of radiation, with reflection angles given by

$$\sin \alpha_n = \frac{1}{1+nN} \sin \theta + \frac{nN}{1+nN} \sin \phi, \tag{28}$$

where θ and ϕ are the incidence angles of the pump and probe, resectively, $N=\omega_N/\omega_0$ is the harmonic order, and n is the diffraction order. Rzazewski *et al.* proposed this technique as a means of testing the oscillating mirror model.

For pulses in the 100 fs–1 ps range, surface deformation is expected to result in multiple reflection surfaces and hence diffuse scattering of the harmonics. At sufficiently high intensities, surface deformity can be caused by Rayleigh-Taylor-like instabilities (Wilks *et al.*, 1992; Gamaly, 1993) driven by the imbalance of ponderomotive laser pressure to thermal plasma pressure. Evidence for this effect has been shown by Racz *et al.* (2005).

Extreme surface deformation can completely alter the nature of the reflected pulse—particularly in the so-called λ^3 regime. For tightly focused pulses on near-critical plasmas $[n_e \sim (1-2)n_c]$, the electron density is pushed so hard and rapidly that the reflection surface changes orientation during each optical cycle, leading to emission away from the specular direction (Naumova, Nees, Hou, *et al.*, 2004; Naumova, Nees, Sokolov, *et al.*, 2004) (see Fig. 13).

A recent study by Geissler *et al.* (2007) made use of postprocessed 3D PIC simulations to evaluate finite scale-length effects on the transverse spatial coherence of reflected harmonics in the far field. Despite limited resolution in these simulations, they showed that Rayleigh-Taylor-like instabilities in micron-length profiles essentially occur on the laser pulse time scale (in their case 5 fs), subsequently leading to a deterioration in the transverse coherence length by a factor of 8 compared to an initial step profile.

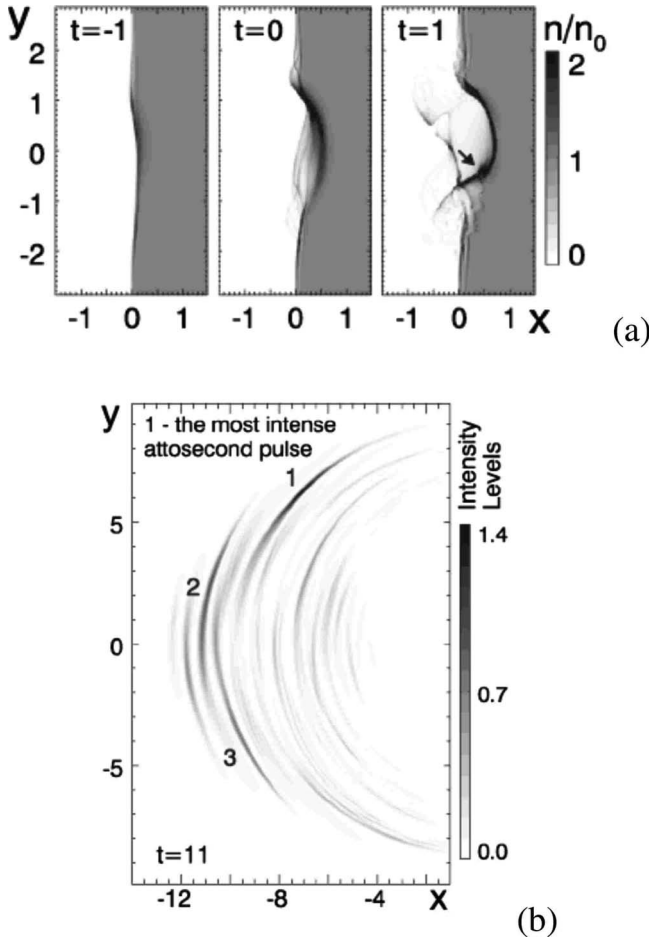

FIG. 13. Reflection of a 5 fs pulse with $a_0=3$ focused to 1 μm diameter from a plasma surface with $n_e=1.5n_c$: (a) electron density at three different optical cycles; (b) resulting reflected radiation pattern 11 cycles into the simulation. From Naumova, Nees, Sokolov, *et al.*, 2004.

H. Attosecond and subattosecond pulse generation

One of the most exciting aspects of HHG from solid targets is the prospect of harnessing the process to generate extremely intense electromagnetic pulses of attosecond duration. Low-intensity harmonics from gaseous media (Sec. II.D) have sparked a whole new field of attoscience (Hentschel *et al.*, 2001), so there is every reason to expect similar advances in the high-intensity regime. The suitability of solid targets for this purpose was first pointed out by Plaja *et al.* (1998), who showed that the reflected light spectra actually corresponds to a wave train $E(t)$ containing intensity spikes with durations 20× shorter than an optical period, or 100 as for a Ti:sapphire pump (see also von der Linde, 1999).

Since then, various schemes have been proposed to obtain *isolated* as pulses. These include the following:

(i) Selective filtering of the spectra, picking out a limited number of phase-locked (i.e., temporally coincident) harmonics (Gordienko *et al.*, 2004; Pirozhkov *et al.*, 2006; Tsakiris *et al.*, 2006; Geissler *et al.*, 2007).

(ii) Employing a deformable nanofoil target designed to enhance the reflected harmonic content within a

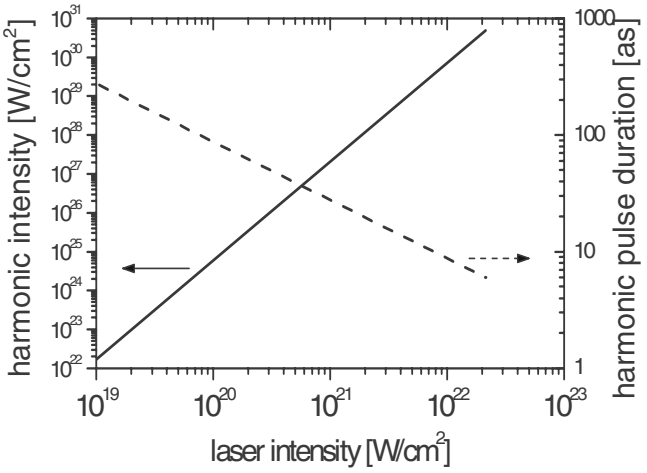

FIG. 14. Scaling for the focused harmonic intensity according to the coherent harmonic focusing scheme of Gordienko *et al.* (2005) (solid line), and scaling for the harmonic duration as a function of laser intensity (Nees *et al.*, 2005). From these curves, one may estimate that the intensity of the coherently focused harmonics scales approximately with $I_L^{2.5}$ and their pulse duration approximately with $I_L^{-0.5}$.

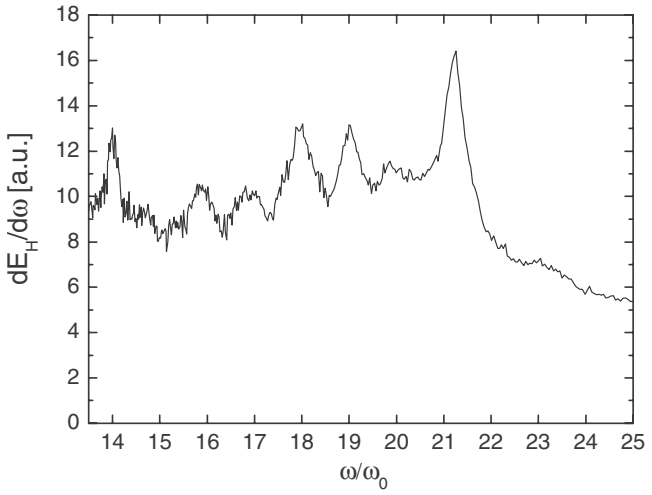

FIG. 15. Harmonic spectrum produced with an 800 nm, 35 fs laser pulse (fundamental) focused to an intensity of $I_0=5\times10^{17}$ W/cm^2 onto a massive glass target. The symbols ω and ω_0 are the angular frequency of the harmonics and laser fundamental, respectively. From Tarasevitch *et al.*, 2000.

single optical cycle (Mikhailova *et al.*, 2005).

(iii) Using a tightly focused, few-cycle pulse on a near-critical plasma to induce Doppler compression and deflection of the reflected light (Naumova, Nees, Hou, *et al.*, 2004; Naumova, Nees, Sokolov, *et al.*, 2004) (see also Fig. 13).

(iv) Exerting control over the surface dynamics via laser polarization (Baeva *et al.*, 2006b).

To date, none of these schemes has yet been tested in the laboratory, but it is almost certainly just a question of time before high-power attosecond pulses can be routinely produced.[1] Moreover, even shorter emission of harmonics may be expected in the future, as can be seen from Fig. 14. This may also give access to the zeptosecond range as discussed by Gordienko *et al.* (2004).

IV. EXPERIMENTAL INVESTIGATIONS OF HHG AT HIGH LASER INTENSITIES

Over the past decade, much higher-order harmonics have been observed in laser-plasma experiments compared to the investigations discussed in Sec. II: their properties have been analyzed in great detail, and the dependence of HHG efficiency on the experimental conditions has been determined. Various laser systems have been applied, namely, Nd:glass laser systems with picosecond pulses (Norreys *et al.*, 1996; Zhang *et al.*, 1996; Ishizawa *et al.*, 1999; Ishizawa *et al.*, 2000, 2001; Watts *et al.*, 2002), KrF* laser systems with subpicosecond pulses (Chambers *et al.*, 1998; Földes *et al.*, 1999; Veres *et al.*, 1999; Racz *et al.*, 2005), and Ti:sapphire laser systems with femtosecond pulses (Zepf *et al.*, 1998; von der Linde, 1999; Tarasevitch *et al.*, 2000, Teubner, Pretzler, Schlegel, *et al.*, 2003; Monot *et al.*, 2004; Teubner *et al.*, 2004). As a typical example from one of these experiments, Fig. 15 shows a harmonic spectrum produced with a fs laser pulse focused to an intensity of $I_0=5\times10^{17}$ W/cm^2.

A. Experiments with picosecond laser pulses at relativistic intensities

In a milestone experiment at Rutherford Appleton Laboratory (RAL), U.K., very high-order and shorter-wavelength harmonics were observed by Norreys *et al.* and Zhang *et al.* using $\lambda_0=1053$ nm laser pulses focused to an intensity up to 10^{19} W/cm^2 ($a_0=2.8$) (Norreys *et al.*, 1996; Zhang *et al.*, 1996). They reported on harmonics up to 68th order (with an indication for harmonics up to *H*75), which corresponds to a wavelength of 15.5 nm (14 nm for *H*75; see Fig. 16). However, in contrast to the experiments with high-intensity femtosecond laser pulses, there are some important differences. Those experiments were performed with substantially longer pulses (2.5 ps) and at much higher intensity (up to 10^{19} W/cm^2), which leads to a more complicated interaction and thus harmonic generation. On the one hand, the longer pulse duration leads to a more expanded density profile during the interaction of the ps laser pulse with the plasma; on the other hand, the plasma is strongly compressed by the ponderomotive force of the laser, which leads to profile steepening and hole boring (Wilks *et al.*, 1992; Zepf *et al.*, 1996). In significant contrast to the theoretical predictions (see Sec. III), the observed source parameters showed that the moving mirror model could not be simply applied under such conditions and the divergence angle $\Delta\theta_H$ of harmonics is

[1]Subfemtosecond pulse trains emitted from laser-irradiated solid-density plasmas have now been observed by Nomura *et al.* (2009).

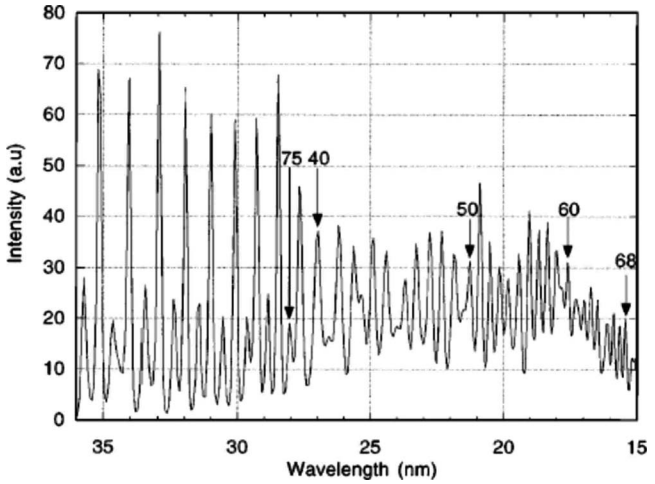

FIG. 16. Harmonic spectrum generated with a 2.5 ps laser pulse focused to $I_0=10^{19}$ W/cm^2 and measured in reflection geometry. The harmonic orders are indicated by the arrows. From Norreys *et al.*, 1996.

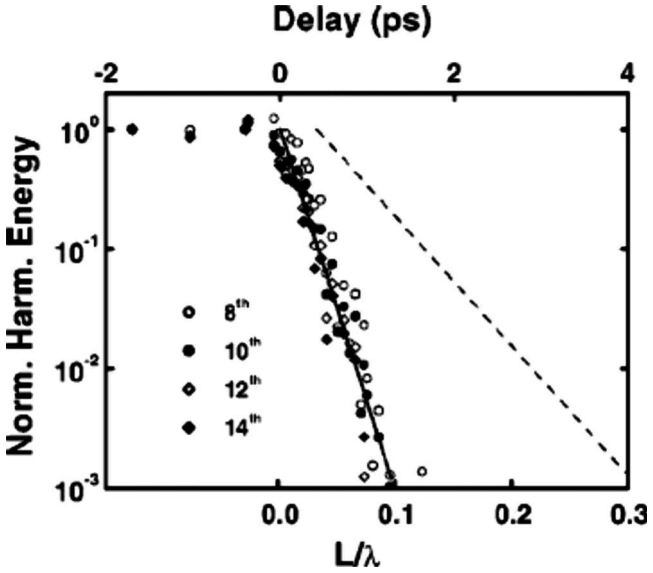

FIG. 17. Energy of different harmonics as a function of scale length L. L is modified by introducing a well-defined prepulse with specific delay before the main laser pulse. Similar results were obtained by Zepf *et al.* (1998). From Tarasevitch *et al.*, 2000.

not confined to a cone around the line of specular reflection (see also Sec. IV.D).

B. Influence of plasma density gradient on harmonics generated with femtosecond laser pulses

The influence of the plasma density scale length L was first investigated using femtosecond laser pulses by Zepf *et al.* (1998) and Tarasevitch *et al.* (2000). The experiments were performed with high-contrast ratio femtosecond laser pulses ($\lambda_0=790$ nm, τ_0 between 35 and 150 fs, 10 Hz repetition rate) focused to an intensity I_0 between 10^{17} and 10^{18} W/cm^2. Harmonics were observed up to high orders, namely, up to $H16_{800}$ (Zepf *et al.*, 1998) and $H21_{800}$ (Tarasevitch *et al.*, 2000); see Fig. 17. Some experiments were also carried out with a 395 nm fundamental leading to a maximum observable $H7_{395}$ (Zepf *et al.*, 1998).

To change L in a controlled manner, the accepted method is to apply a well-defined prepulse in advance of the high-contrast-ratio laser pulse (main pulse) (Kühlke *et al.*, 1987; Teubner *et al.*, 1992). Zepf *et al.* (1998) and Tarasevitch *et al.* (2000) applied this technique, and their experiments have shown that an increase of L up to a value $L/\lambda_0>0.2,\ldots,1$ leads to a strong decrease of the harmonics (see Fig. 17). Larger values of L lead to less efficient harmonic generation and to a weaker scaling with laser intensity (see Sec. IV.C). Furthermore, a prepulse not only leads to significantly less intense harmonics, but also decreases the order of the highest observable harmonic. These experimental observations were in qualitative agreement with PIC simulations where realistic electron density profiles and scale lengths were computed as a function of prepulse intensity and delay to the main pulse from hydrodynamic calculations (using the hydrodynamic code MULTI-FS) and measured pulse shapes of the laser driving pulse (Zepf *et al.*, 1998).

From these investigations, one can conclude that clean conditions and a preferably prepulse-free laser pulse are essential for the HHG process with femtosecond laser pulses. Consequently, in most recent experiments on HHG, considerable care is taken to obtain a high contrast ratio, either by frequency doubling of the laser pulse (Teubner, Pretzler, Schlegel, *et al.*, 2003; Teubner *et al.*, 2004; Tarasevitch, Dietrich, and von der Linde, 2007) or by applying an additional plasma mirror (Doumy, Dobosz, D'Oliveira, *et al.*, 2004; Doumy, Quere, Gobert, *et al.*, 2004; Monot *et al.*, 2004).

However, we remark that, although the scale length L should be short, an aptly chosen finite value may allow efficient HHG via the resonance absorption process (see, e.g., Földes *et al.*, 1999; Eidmann *et al.*, 2005). Measurements of Chambers *et al.* (1998), for example, show that there is an angle of incidence of the laser irradiation where HHG is strongest, an effect attributed to optimization of resonance absorption and thus of HHG. This also means that the ASE must be well below 10^7 W/cm^2 to allow control over L using deliberate prepulses (Földes *et al.*, 1999). For too strong ASE, the HHG process will be similar to that in underdense plasmas or gases (see Sec. II.D).

For picosecond laser pulses, the situation is different. For $I_L<10^{17}$ W/cm^2, Ishizawa *et al.* (2001) showed that an optimized prepulse can lead to an increase of HHG (they investigated $H3$ and $H5$). This was attributed to the optimization of resonance absorption (see Sec. III.D) leading to more strongly driven plasma wave oscillations and hence HHG. For much higher laser intensities, the situation can change again. Although the experimental results of Norreys *et al.* (1996) are nominally in good agreement with PIC simulations of Gibbon

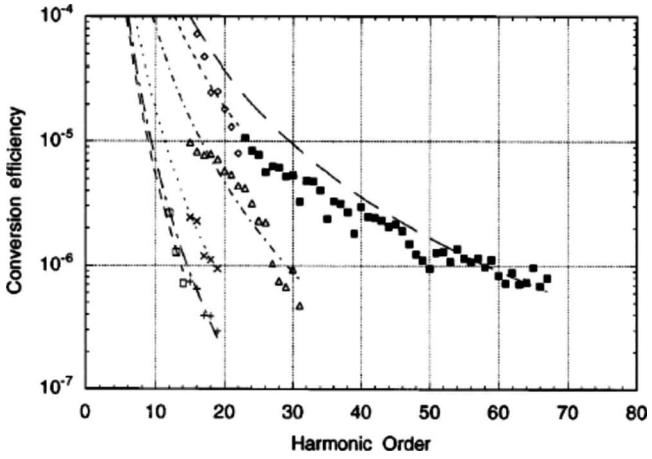

FIG. 18. Conversion efficiencies (assuming isotropic radiation) vs harmonic order for various irradiances for a 2.5 ps laser pulse focused to $I_0=10^{19}$ W/cm^2. Solid squares, $I_0\lambda^2=1.0\times10^{19}$ W μm^2 cm^{-2}; open diamonds, $I_0\lambda^2=6.3\times10^{18}$ W μm^2 cm^{-2}; open triangles, $I_0\lambda^2=5.5\times10^{18}$ W μm^2 cm^{-2}; diagonal crosses, $I_0\lambda^2=3.0\times10^{18}$ W μm^2 cm^{-2}; horizontal crosses, $I_0\lambda^2=2.2\times10^{18}$ W μm^2 cm^{-2}; and open squares, $I_0\lambda^2=4.7\times10^{17}$ W μm^2 cm^{-2}. Curve fits are best power-law fits, except for $I_0\lambda^2=1.0\times10^{19}$ W μm^2 cm^{-2} where the curve is fitted to the 50–68th harmonic to illustrate the onset of saturation for the lower harmonics From Norreys *et al.*, 1996.

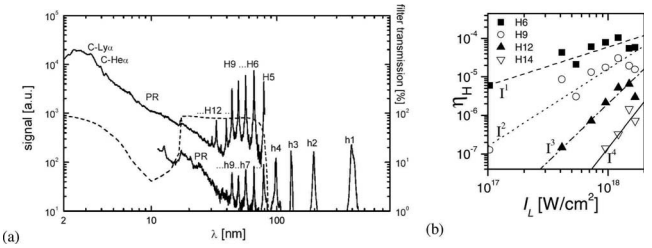

FIG. 19. Harmonic spectra, x-ray spectrum, and conversion efficiency. (a) Harmonic spectra and x-ray spectrum from glass and carbon targets, respectively. Some of the harmonics are indicated. Upper spectrum (Teubner, Pretzler, Schlegel, *et al.*, 2003): harmonics from a glass target observed in the direction of the specular reflected laser light (harmonics with short and long wavelengths are blocked by the 100-nm-thick Al light protection filter, dashed curve). At the short-wavelength side, the harmonic spectrum is followed by the plasma emission, here the *K*-shell X radiation of a carbon plasma (C-Ly-α, C-He-α), bremsstrahlung, and radiation due to transitions of lower ionization stages (all this is sitting on a background originating from the second diffraction order of the grating; "PR"). Lower spectrum (Teubner *et al.*, 2004): harmonics from a 62-nm-thick carbon foil target observed from the rear side of a thin foil target (see Sec. IV.H). (b) Conversion efficiency η_H as a function of laser intensity I_0 for a glass target for selected harmonics (squares *H*6, circles *H*9, up triangles *H*12, down triangles *H*14, and stars *H*11; note, here the laser fundamental is $\lambda_0=395$ nm). The lines in (b) indicate a scaling with I^1 to I^4 (Teubner, Pretzler, Schlegel, *et al.*, 2003).

(1996), due to the relatively long pulse duration, no steep electron density gradient is expected. Moreover, the experiments showed that the harmonic yield was independent of the prepulse level over a large range. Since efficient HHG requires a short scale length, it is likely that profile steepening via the ponderomotive force during the whole ps pulse duration ensured that the scale length remained small enough ($L/\lambda_0\leqslant0.2$) for effective HHG as discussed in Sec. III.B.

C. Conversion efficiency and scaling of harmonic yield with laser intensity and laser wavelength

The conversion efficiency η of laser energy into the energy of the harmonics has been estimated or measured in various experiments (Norreys *et al.*, 1996; Chambers *et al.*, 1998; Zepf *et al.*, 1998; Tarasevitch *et al.*, 2000; Teubner, Pretzler, Schlegel, *et al.*, 2003; Teubner *et al.*, 2004). Using picosecond laser pulses focused to an intensity $I_0=10^{19}$ W/cm^2, Norreys *et al.* reported a conversion efficiency of $\eta>10^{-4}$ for $H10_{1053}$ and a strong decrease with harmonic order to $\eta\sim10^{-6}$ for $H65_{1053}$ (Norreys *et al.*, 1996)—Fig. 18.

The conversion efficiency of femtosecond laser pulses into harmonics has to date mainly been measured at lower intensities only. For *p*-polarized femtosecond laser pulses, Tarasevitch *et al.* (2000) calibrated their spectrometer using a high-current hollow-cathode source as a radiant intensity standard in the wavelength range of the harmonics (Hollandt *et al.*, 1994). They reported that the conversion efficiency is comparable to that of gas harmonics, i.e., $\eta\approx10^{-6}$ (e.g., for $H10_{800}$) or harmonics generated in underdense plasmas. It is also of the same order of magnitude as the conversion efficiency of a $\lambda_0=1053$ nm picosecond laser pulse focused to the same intensity and converted into a harmonic of the same wavelength (i.e., $H13_{1053}$) (Norreys *et al.*, 1996).

Using *p*-polarized femtosecond laser pulses, Teubner, Pretzler, Schlegel, *et al.* (2003) estimated the conversion efficiency in two independent ways. Talking into account the spectrometer response, first they compared the harmonic signals to those of the Ly-α line from the *K*-shell spectrum of carbon measured with the same diagnostics (here conversion efficiency is known; the accuracy was within an order of magnitude). Second, they compared all harmonics to the rear-side-reemitted fundamental and second-order harmonic (see Sec. IV.H), additionally measured with calibrated detectors in the near-infrared and visible region, respectively (Teubner *et al.*, 2004; Eidmann *et al.*, 2005). For example, Fig. 19(a) shows such typical harmonic spectra together with the well-characterized plasma emission (*K*-shell x radiation) of a carbon target. They reported that depending on the harmonic order, approximately $\eta=10^{-5}$ to $>10^{-4}$ of the laser energy could be converted to an individual harmonic that is at least one or two orders of magnitude larger than the reported values for gas harmonics [see Fig. 19(b)].

The scaling of the conversion efficiency of the harmonics with laser intensity (*p*-polarized laser pulses) may be seen from Fig. 19(b) and has also been reported by Zepf *et al.* (1998). It is different for the different or-

ders. Low-order harmonics scale only weakly with I_0 (e.g., with $I_0^{0.8}$ for $H2_{800}$ to $I_0^{3.2}$ for $H10_{800}$ and approximately I_0^1 for $H6_{395}$) whereas higher orders show a strong scaling: $\eta \propto I_0^4$ for $H14_{395}$. However, it is important to note that a strong scaling is observed only for high-contrast laser pulses and a steep density gradient (Zepf *et al.*, 1998). Harmonics from poor-contrast laser pulses scale much more weakly with I_0—indeed, this may be because L also depends on I_0.

For the highest orders observed for fs HHG ($\geqslant$16th order), the scaling with I_0 is weaker [observed in the experiment by Teubner, Pretzler, Schelgel, *et al.* (2003); see Fig. 20, and PIC simulations (Schlegel, 2006)]. The reason for this is still under discussion. The physical reason is not yet clear, but may have to do with the different physical mechanisms for fs HHG as discussed by Quéré and co-workers (Quéré *et al.*, 2006; Thaury *et al.*, 2007); see Sec. III.F.

For (sub)picosecond 248 nm laser pulses and laser intensities below 10^{16} W/cm^2, Földes *et al.* obtained a scaling of $H2_{248}$ and $H3_{248}$ signals approximately proportional to I_0^2 (corresponding to $\eta \propto I_0^1$) with a threshold between 4×10^{14} and 1×10^{15} W/cm^2 (for $H2_{248}$) and 3×10^{15} W/cm^2 (for $H3_{248}$), respectively (Földes *et al.*, 1996). Similar results were reported by Chambers *et al.* for picosecond 248 nm laser pulses and laser intensities up to 10^{18} W/cm^2. The scaling on I_0 for $H3_{248}$ and $H4_{248}$ is similar with an $\eta \sim 7\times10^{-5}$ (for $H3_{248}$) and $\eta \sim 5\times10^{-6}$ (for $H4_{248}$) at 10^{18} W/cm^2. But again, in the latter experiments a preplasma was present, due to the picosecond pulse duration and the limited contrast ratio, and this prevents a stronger scaling with I_0. For picosecond 1053 nm laser pulses, Norreys *et al.* (1996) found a stronger scaling for higher harmonics (e.g., η approximately proportional to I_0^2 for $H20_{1053}$, i.e., the energy of the harmonic is approximately proportional to I_0^3), consistent with the empirical scaling predicted by Eq. (23).

The influence of the laser wavelength on the conversion efficiency may be estimated from Eq. (23). According to this scaling, for the same wavelength of the harmonic λ_H and the same laser intensity, a laser pulse with a wavelength λ_0' should yield a higher conversion efficiency η' than that of a laser pulse with a wavelength λ_0 (i.e., yielding to η): due to $N'/N=(\lambda_0'/\lambda_H)/(\lambda_0/\lambda_H)$, according to Eq. (23) at intensities below 10^{18} W/cm^2 (where we can take $\alpha \approx 5$), the conversion efficiency is increased by a factor $\eta'/\eta \propto (\lambda_0'/\lambda_0)^4 (N'/N)^{-5} = \lambda_0/\lambda_0'$.

This was also concluded by Chambers *et al.* (1998) and Zepf *et al.* (1998). Indeed, the measurements of Zepf *et al.* performed with two different laser wavelengths (i.e., $\lambda_0=790$ and 395 nm, repectively) lend experimental support to this conjecture. Also, comparison of the experiments by Tarasevitch *et al.* (2000), performed at $\lambda_L=800$ nm, and Teubner, Pretzler, Schlegel, *et al.* (2003), performed at $\lambda_L=395$ nm, seems to confirm this: the conversion efficiency into harmonic emission at 80 nm is approximately 6×10^{-5} for 395 nm laser pulses focused to 1.5×10^{18} W/cm^2 (Teubner, Pretzler, Schlegel, *et al.*, 2003) and thus approximately a factor of 50 larger when compared to harmonic generation with 800 nm laser pulses focused to 5×10^{17} W/cm^2 (Tarasevitch *et al.*, 2000). Within the experimental error, this result is expected from the scaling law given by Eq. (23). Neverthe-

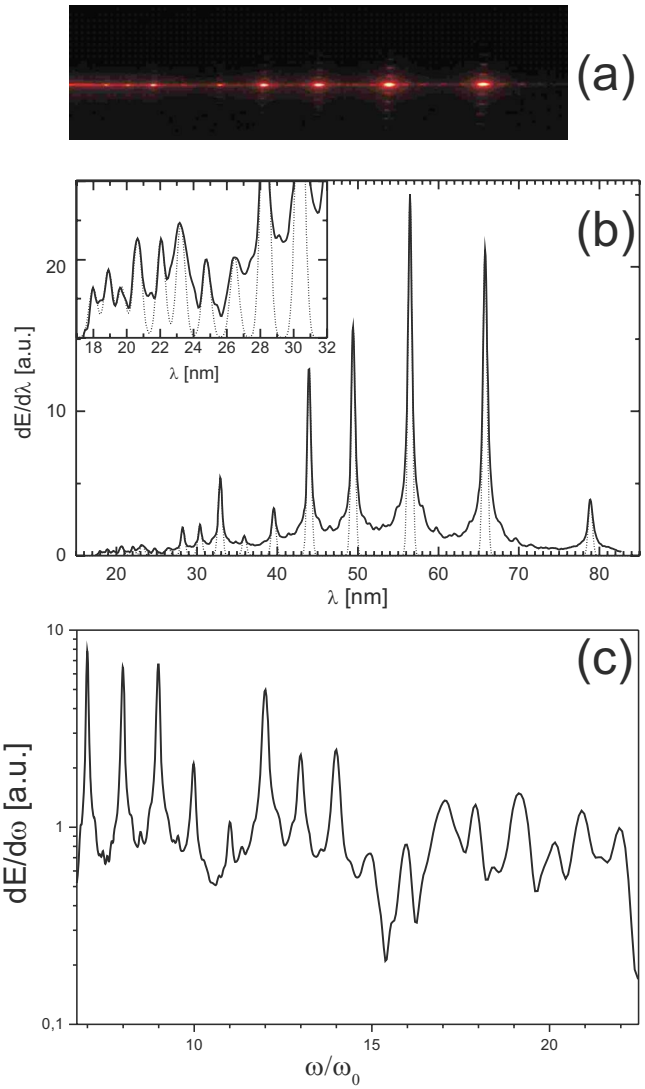

FIG. 20. (Color online) Harmonic spectrum from a glass target measured with *p*-polarized light at $I_0=1.5\times10^{18}$ W/cm^2 ($\tau_0=120$ fs, $\lambda_0=395$ nm; front side observation in specular direction) (Teubner, Pretzler, Schlegle, *et al.*, 2003). (a) Raw data on CCD. (b) Spectrum. The dotted line in (b) corresponds to the spectrometer function (spectral resolution full width at half maximum $\Delta\lambda_{res}=0.6$ nm; the profiles are plotted at the theoretical position of the harmonics). The inset shows the short-wavelength part of the spectrum until the cutoff of the Al filter at 17 nm. At wavelengths >60 nm, the Al filter also begins to become opaque so that the fifth harmonic at 80 nm is significantly reduced. (c) Harmonics as a function of harmonic order on a logarithmic scale. This spectrum shows the shortest wavelength, spectrally resolved fs harmonics from LPP observed to date. In particular, an irregular structure at the highest orders is clearly recognized (Teubner, Pretzler, Schlegel, *et al.*, 2003). Note that the spectra shown are as measured, i.e., they are neither corrected for filter transmission and detector efficiency [see Fig. 2(c)] nor for the different solid angle of emission.

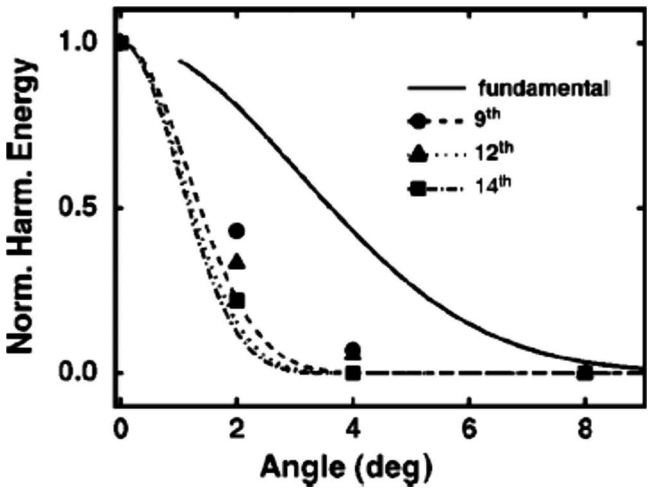

FIG. 21. Angular distribution of the 9th, 12th, 14th harmonic, and of the reflected 800-nm-laser fundamental. Dashed, dotted, and dash-dotted lines represent the calculated distribution for the 9th, 12th, and 14th harmonics, respectively. From Tarasevitch *et al.*, 2000.

less, it should be noted that, in general, it is not easy to compare different experiments, in particular when the conditions vary strongly.

Care should be taken in generalizing this result, however, since the spectral rolloff generally flattens with increasing intensity (see Fig. 8). In the extreme relativistic regime for which Eq. (21) is expected to apply, the scaling may be reversed.

D. Angular and spatial properties

Another important characteristic of the harmonics is their emission direction and their divergence. For femtosecond laser pulses and different harmonic orders, this has been measured by Zepf *et al.* (1998), Tarasevitch *et al.* (2000), and Monot *et al.* (2004). It has been found that under clean conditions, the harmonics are emitted entirely in the specular direction of the fundamental laser light. The divergence angle of emission of the Nth harmonic $\Delta\Theta_N$ was much smaller than that of the incident fundamental light $\Delta\Theta_0$. From nonlinear optics in the perturbative regime, one would naively expect a harmonic intensity scaling $I_N=I_L^N$, which for a Gaussian beam leads to a reduction in the emission spot size of each harmonic, scaling as $\phi_N=\phi_0/N^{1/2}$. Under these circumstances, the angular divergence $\Delta\Theta_N=2\pi\lambda_N/\phi_N=\Delta\Theta_0 N^{-1/2}$, a scaling apparently consistent with measurements by Tarasevitch *et al.* (2000) at intensities of 5×10^{17} W/cm^2 (see Fig. 21). These authors concluded that the emitted harmonics are nearly diffraction limited and spatially highly coherent. Monot *et al.* obtained similar results, though their $\Delta\Theta_N$ was somewhat broader than that measured by Tarasevitch *et al.*

On the other hand, from Sec. IV.C we have seen that both PIC simulations and experimental results suggest a much weaker scaling $\sim I_0^{1.5-2}$ for the nonlinear HHG regime (at intensities, say $>10^{18}$ W/cm^2) with a much weaker dependence on harmonic order. This implies that the emission size of each harmonic is roughly the same, so that one can expect an angular divergence

$$\Delta\Theta_N=\frac{\Delta\Theta_0}{N}. \tag{29}$$

This divergence scaling is indeed borne out by very recent experimental measurements at high contrast (Dromey *et al.*, 2009), demonstrating that relativistic HHG does produce diffraction-limited harmonics.

For picosecond laser pulses, the situation is different. For lower intensities, the emission is directed into the specular direction but becomes diffuse for high intensities, i.e., the harmonics are emitted into 2π steradian (Veres *et al.*, 1999; Ishizawa *et al.*, 2000). The transition from specular to diffuse occurs between $I_0=10^{16}$ (Veres *et al.*, 1999) and 10^{17} W/cm^2, for $\lambda_0=248$ nm (Chambers *et al.*, 1998), and diffuse emission strongly depends on the angle of incidence of the laser pulse. The divergence also increases when laser pulse duration is increased from a few ps to 100 ps (Ishizawa *et al.*, 2000).

Using ultraintense ($I_0=10^{19}$ W/cm^2, $a_0=2.8$) Nd:glass picosecond laser pulses, Norreys *et al.* (1996) and Zhang *et al.* (1996) found a nearly isotropic emission. This broad angular distribution was attributed to Rayleigh-Taylor-like surface rippling and to the strong ponderomotive pressure which pushes back the expanding plasma (see Sec. III.G). This has two important effects. First, the density profile near the critical density is steepened and allows efficient HHG. Second, at these high laser intensities the ponderomotive pressure may even impress the target surface and lead to a concave surface during the interaction, i.e., while harmonics are being generated. In this case, specular reflection gives way to diffuse reflection, as also observed in reflectivity measurements with $\tau_0=350$ fs, $\lambda_0=528$ nm laser pulses by Feurer *et al.* (1997), where for laser intensities exceeding several times 10^{18} W/cm^2 the reflectivity became completely diffuse.

The transverse and longitudinal coherence of 2.5 ps laser pulses has been measured by Zhang *et al.* (1996). For $H4_{1053}$ of the 1053 nm fundamental, they observed high temporal coherence with a coherence time in the range 0.02–0.4 ps (for I_0 between 5×10^{17} and 3×10^{18} W/cm^2). However, due to the nearly isotropic emission, they concluded that the source is spatially incoherent. This experimental observation may be explained at least partly by the theoretical work of Geissler *et al.* (2007), who showed that an extended density profile (i.e., a long-scale-length plasma) reduces the transverse (or spatial) coherence significantly.

At first glance, the imprint effect would appear to be detrimental with respect to enhancing the emitted harmonic power per solid angle at ultrahigh laser intensities. However, simulations suggest that, in contrast to the isotropic emission distribution, a controlled imprint could actually lead to a focusing of the harmonics (Naumova, Nees, Hou, *et al.*, 2004; Gordienko *et al.*, 2005; Nees *et al.*, 2005); see also Sec. III.G.

Finally, we remark that any transition from specular to diffuse emission has to be taken into account when determining the conversion efficiency. In this case, conversion of the laser energy into the total emitted harmonic radiation should be estimated from the harmonic signals measured within the acceptance angle of the spectrometer used. This was done in the experiment of Chambers *et al.* (1998), who for small laser intensities assumed specular reflection into a small solid angle (and thus collection of a large fraction of the total emitted harmonic radiation), but for large laser intensities supposed emission into 2π sr (and thus collection of only a small fraction of the total harmonic radiation).

E. Dependence on laser pulse polarization

The dependence of HHG on the polarization of the laser pulse has been investigated by several groups. For (sub)picosecond pulses, the experiments of Földes *et al.* (1999) showed that both the second- and third-order harmonics follow the (linear) polarization of the fundamental beam, but *p*-polarized laser light was found to be more efficient in the generation of $H2_{248}$, typically by a factor of 4; this is also an indication of the important role of resonance absorption (see Sec. III.D), and the efficiency was approximately the same for the generation of $H3_{248}$. Similar results were obtained by Ishizawa *et al.* (1999) and Eidmann *et al.* (2005). For ultraintense picosecond laser pulses ($I_0=10^{19}$ W/cm^2), Norreys *et al.* (1996) found no measurable difference for harmonics generated with *p*- and *s*-polarized laser pulses, respectively. Again, this was attributed to the surface rippling effect (see Sec. III.G).

Detailed measurements of the polarization dependence of HHG using femtosecond laser pulses have not yet been reported. However, the experimental results of Zepf *et al.* (1998) showed that the only measurable harmonic generated with an *s*-polarized pulse was $H3_{800}$, and even this harmonic was three orders of magnitude less intense than $H3_{800}$ generated with a *p*-polarized pulse. Similarly, in the experiment by Teubner, Pretzler, Schlegel, *et al.* (2003), a measurement was made using a $\lambda/2$ plate to change the degree of the (linear) polarization. As expected, it was found that the harmonic emission strongly decreases with that part of the electric field that is oriented parallel to the plane of incidence. This decrease of the electric field component is proportional to the cosine of the rotation angle of the half-wavelength plate, and thus the corresponding intensity scales with the square of the cosine. Then together with the scaling of the harmonics generated with *p*-polarized pulses on I_0 as discussed in Sec. IV.C, the scaling of the harmonics on polarization degree (i.e., rotation angle of the plate) could be well fitted: as observed in the experiment, $H7_{395}$ roughly scales with the fourth power of the cosine of the rotation angle. As a consequence, HHG has been achieved almost exclusively with *p*-polarized laser pulses up to now: only very recently have high-order harmonics with clean *s*-polarized femtosecond pulses been observed at relativistic intensities (Tarasevitch, Dietrich, and von der Linde, 2007).

F. High-contrast femtosecond experiments at relativistic intensities

Within the past five years, experiments with intense pulses but clean conditions with a steep-density-gradient plasma have been performed with high-contrast ratio femtosecond laser pulses at intensities exceeding 10^{18} W/cm^2. To achieve the high contrast, the original laser pulses of 790 nm wavelength are either frequency doubled to $\lambda_0=395$ nm or passed through a plasma mirror (PM) setup [see Gibbon (2007), and references therein].

In a series of experiments (Teubner, Pretzler, Schlegel, *et al.*, 2003; Teubner *et al.*, 2004; Eidmann *et al.*, 2005), frequency-doubled pulses with a duration between 120 and 150 fs were focused to an intensity between $I_0=10^{17}$ and several times 10^{18} W/cm^2. Different target materials were used (massive aluminum, copper, glass, glasslike carbon, and thin foils of aluminum, carbon, and plastic). The measurements were performed with *p*-polarized laser light. Figure 20 shows harmonics up to $N=22$nd order ($\lambda_{H22}=18$ nm). Note that, in contrast to Fig. 15 and most of the other experiments, in these experiments the laser fundamental was $\lambda_0=395$ nm and thus the harmonic orders are lower. Although it is expected that higher orders are generated as well, they could not be detected due to the aluminum filter applied in front of the spectrometer, which has a short-wavelength cutoff at 17 nm [see Fig. 2(c)]. Thus, to date these measurements represent the shortest wavelength resolved harmonics from the interaction of femtosecond laser pulses with plasmas.

From Fig. 20(c) one can also see that the intensity of the harmonics is strongest for the lowest order and decreases to shorter wavelengths. However, as Watts *et al.* (2002) and Teubner, Pretzler, Schlegel, *et al.* (2003) showed, in contrast to the expected well-known continuous "rolloff" of the high harmonic orders (see Secs. III.B and III.C and Fig. 8), the rolloff is overlaid by a modulation, and, in particular, well reproducible minima are present that are significantly less intense than the neighboring harmonics. This can seen more clearly in Fig. 22, where, for better visibility, all individual harmonics have been integrated over their line profile. In particular, the spectrum becomes very complex at the highest observed harmonic orders. Watts *et al.* (2002) observed similar modulations, but it has to be noted that due to the long pulse duration used in that experiment there are similar difficulties to those discussed in Sec. IV.B.

In addition, Teubner, Pretzler, Schlegel, *et al.* (2003) found significant differences for different target materials, i.e., the intensity of the harmonics and the position of the minima depend on the experimental conditions, in particular, on target material. Clear minima at different positions were observed with carbon and glass targets, but not with aluminum and copper targets, which show the normal rolloff behavior. By applying the oscillating

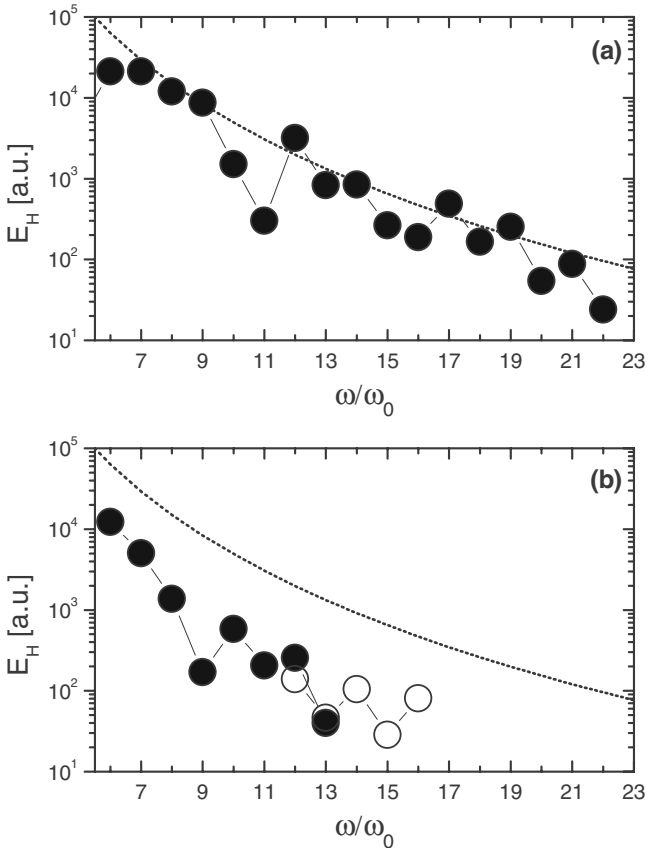

FIG. 22. Energy E_H of the individual harmonics from the spectrum shown in Fig. 20. The dashed line corresponds to the scaling of Eq. (23). (a) Glass target and (b) carbon target but otherwise the same experimental conditions. The open circles correspond to a measurement with five times better resolution. From Teubner, Pretzler, Schlegel, *et al.*, 2003.

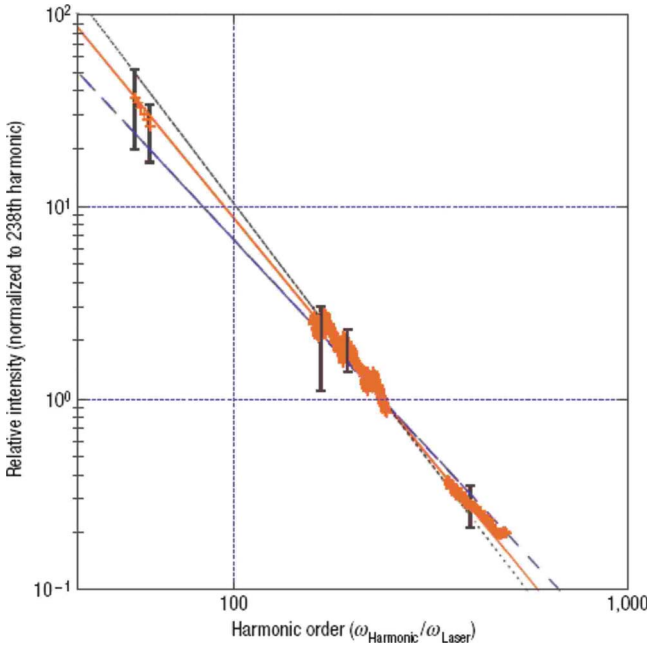

FIG. 23. (Color online) Relative intensity of harmonics normalized to the 238th harmonic (at the carbon K_p edge). The lines are fits to the data with the exponent p as a fitting parameter such that $I(N)/I(238)=N/238$ The best fit (solid line) corresponds to a value of $p=2.5$, in agreement with the OMM Eq. (19) or Eq. (20). From Dromey *et al.*, 2006.

mirror model and performing PIC simulations, the physical origin of these modulations can be explained by an intricate interplay of resonance absorption (Teubner *et al.*, 1993) and ponderomotive force. This leads to a complicated oscillation of the critical surface (Watts *et al.*, 2002; Teubner, Pretzler, Schlegel, *et al.*, 2003; Teubner, Wagner, Andiel, *et al.*, 2003) and thus to a time-dependent time retardation at the position of the spectrometer. The simple sinusoidal form of the OMM introduced in Sec. III.A can thus be generalized,

$$\xi(t) = \xi_1 \sin(\omega t + \varphi_1) + \xi_2 \sin(2\omega t + \varphi_2). \tag{30}$$

Depending on the actual plasma conditions, the relative contributions of the two dominant oscillation amplitudes ξ_1 and ξ_2 change, affecting the intensity of the harmonics and the positions of the minima as observed in the experiment.

Further support for those explanations was obtained from the simulated and observed spectral profiles of the harmonic lines, which were in good agreement (Teubner, Pretzler, Schlegel, *et al.*, 2003). The profiles of the "normal lines" correspond to that of the fundamental, although with a width that was somewhat larger than expected from simple nonlinear optics (see Sec. IV.G). By contrast, the "minimum lines" had a more complicated spectral and temporal structure and showed wings that were likely due to interference effects originating from the complex motion of the critical surface.

Although the complicated structure of the spectra can be explained qualitatively within the oscillating mirror model, a microscopic understanding is still lacking. We also note that Boyd and Ondarza-Rovira (2007) have recently proposed an alternative explanation for these modulations based on correlations with plasma frequency emission (see Sec. III.E).

Within the past two years, three high-contrast experiments at relativistic intensities have been reported (Dromey *et al.*, 2006; Tarasevitch, Dietrich, and von der Linde, 2007; Thaury *et al.*, 2007). In an experiment with the Vulcan petawatt laser (70 J, 1 μm, 600 fs, focal spot 8 μm), Dromey *et al.* deployed a double plasma mirror setup to improve its contrast by more than a factor of 10^4, permitting harmonic measurements down to a few nanometers. In the event, they claimed to have observed harmonics down to 4 nm, albeit in the form of a quasi-continuum where individual harmonics can no longer be properly resolved. Nevertheless, the spectral intensities appear to scale in good agreement with the relativistic limit predicted by Eq. (21) (see Fig. 23), with estimated efficiencies ranging from $\eta=3\times10^{-5\pm1}$ at 17 nm to $\eta=10^{-6\pm1}$ at 4 nm.

Thaury *et al.* (2007) also used a double PM in combination with a 10 TW, 60 fs Ti-sapphire laser to achieve probably the cleanest interaction conditions at relativistic intensities so far. The high quality of the harmonic

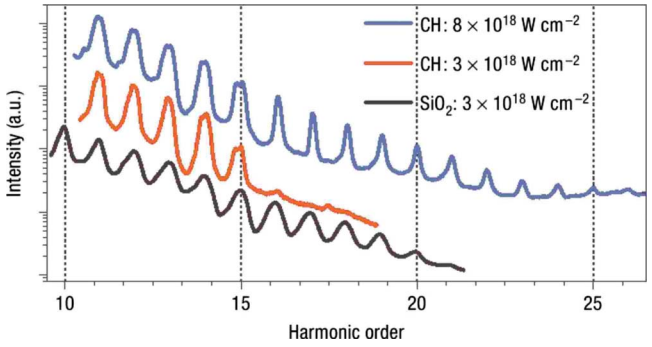

FIG. 24. (Color online) Harmonic spectra obtained by focusing high-intensity high-contrast 60 fs pulses on plastic and silica targets, for two laser intensities, showing transition from the CWE regime to relativistic OMM. In the *y*-direction, the relative positions of the curves are arbitrary. From Thaury *et al.*, 2007.

spectra (see Fig. 24) permitted the transition between the CWE (Sec. III.B) and OMM (Sec. III.F) regimes to be identified unambiguously for the first time.

To conclude, we note that while increase in laser intensities evidently improves the prospects for efficient surface harmonic generation, other mechanisms of short-wavelength incoherent radiation emission via relativistically accelerated electrons become more effective too, such as nonlinear Thomson scattering (Chen *et al.*, 1998) or bremsstrahlung from electrons interacting with ions inside the solid target (Schwoerer *et al.*, 2001). These effects may influence or even mask parts of the harmonic spectrum detected experimentally.

G. Spectral and temporal properties

Spectral profiles of individual harmonics from picosecond laser pulses were measured by Norreys *et al.* (1996) and Zhang *et al.* (1996). They reported a relatively large fractional bandwidth of the harmonics $\Delta\lambda_4/\lambda_4 \sim 2 \times 10^{-3}$, which is in contrast to theoretical predictions that describe bandwidth transform limited harmonics emitted in specular direction. Following the argumentation of these groups, the large bandwidth may be due to spectral broadening by self-phase-modulation in the preformed plasma. In particular, Zhang *et al.* showed that the experimental results are consistent with that explanation by Bulanov *et al.* (1996).

Ishizawa *et al.* (2002) find a blueshift for ps pulses up to 10^{17} W/cm^2, which increases with both I_L and harmonic order. From this they estimated a maximum expansion velocity of $v_p \sim 2 \times 10^7$ cm/s. As discussed by Lichters (1997), a larger linewidth may be due to a redshift of the harmonic emission during profile steepening (transient decrease of L) followed by a consecutive blueshift later on. Due to plasma expansion (or compression), there may be an additional absolute shift of the harmonic wavelengths. However, from the absolute accuracy of the wavelength of the lines measured by Teubner, Pretzler, Schlegel, *et al.* (2003), one can estimate an

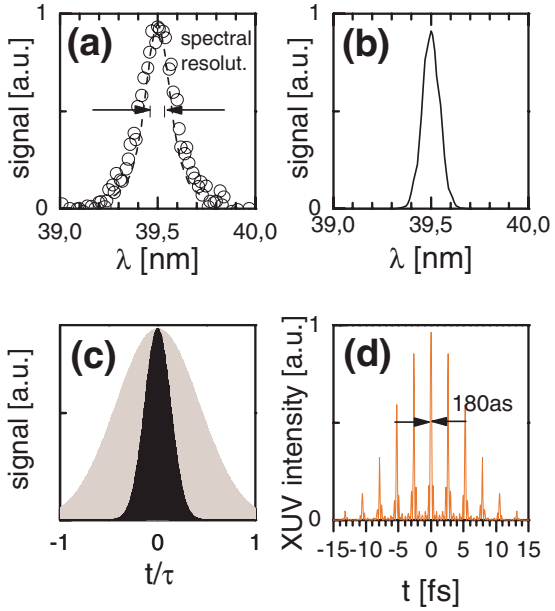

FIG. 25. (Color online) Spectral and temporal profiles of a typical harmonic. (a) Measured line profile of $H10_{395}$ from the spectrum shown in Fig. 20. (b) Corresponding simulated result from OMM of the spectral line shape. (c) Corresponding temporal structure obtained by Fourier transformation (black line; the fundamental is shown in gray). (d) Temporal structure of the intrinsically mode-locked harmonics $H20$ to $H24$ filtered by means of a 200 nm Ti filter. In (c) and (d) it is assumed that $I_0 = 10^{18}$ W/cm^2, $\lambda_0 = 790$ nm, and $\tau = 60$ fs (OMM simulation according to Teubner, Pretzler, Schlegel, *et al.* (2003) and Teubner, Wagner, Andiel, *et al.* (2003).

upper limit for the shift of the Nth harmonic of $|\Delta\omega_H|/\omega_H = 4\%$ and for the corresponding velocity of $|v_p| < 10^8$ cm/s.

Even though the high contrast in femtosecond experiments prevents preplasma-associated phenomena from occurring, large spectral widths have also been found here (Teubner, Pretzler, Schlegel, *et al.*, 2003). For instance, after deconvolution of the instrumental resolution, the spectral width of $H10_{395}$ is $\Delta\lambda_{10} = 0.17$ nm [full width at half-maximum (FWHM)], and as expected from nonlinear optics, within the experimental error the measured spectral width of $H9_{395}$ to $H16_{395}$ agrees with the scaling $\Delta\lambda_N \propto N^{-3/2}$.

These broad linewidths of the individual harmonics [see Fig. 25(a)] were expected to be consistent with a very short duration τ_N of the harmonics. Indeed, Teubner *et al.* concluded that in agreement with a scaling from the nonlinearity,

$$\tau_N = \tau_0 N^{-1/2}. \tag{31}$$

For example, $H10_{395}$ may be a factor of 3 shorter than the 130 fs fundamental (Teubner, Wagner, Andiel, *et al.*, 2003) [Fig. 25(c)].

Furthermore, several (von der Linde, 1999; Teubner, Wagner, Andiel, *et al.*, 2003; Tsakiris *et al.*, 2006) have argued that the duration of the harmonic emission may even be much shorter. In contrast to the gas harmonics,

in the case of harmonics from dense plasmas, the phases of the harmonics are expected to be inherently mode locked, in an analogous fashion to mode locking in laser physics. Thus, even for a laser pulse with a duration of 40–100 fs, a train of attosecond pulses could be expected if several or all phase-locked harmonics are collected together. As an example, Fig. 25(d) shows such a train that consists of peaks of 180 as width that are separated by one laser period. Such trains of attosecond pulses have also been observed in PIC simulations (Plaja *et al.*, 1998; Roso *et al.*, 2000; Tsakiris *et al.*, 2006). Finally, it should be noted that, as for gas harmonics (Hentschel *et al.*, 2001), even *single* attosecond pulses from dense plasmas should be possible—see Sec. III.H.

Measurements of the temporal characteristics of the harmonics (pulse duration, chirp) have not been reported up to now. However, in principle, for the harmonics from dense plasmas, the same established methods (Reider, 2004) such as laser-assisted XUV photoionization together with photoelectron spectroscopy (see, e.g., Drescher *et al.*, 2001; Aseyev *et al.*, 2003; Lopez-Martens *et al.*, 2004) or XUV spectral phase interferometry (Mairesse *et al.*, 2005) could be applied for the temporal characterization as in the case of the gas harmonics. A more direct measurement, in particular, an autocorrelation using two-photon ionization of helium (Ishizawa and Midorikawa, 2002; Papadogiannis *et al.*, 2003) with photons of two harmonics between $H7_{800}$ and $H13_{800}$ (Tzallas *et al.*, 2003), should be straightforward. Finally, we mention that ultrafast gating using a plasma shutter (Teubner *et al.*, 2001) would be an appropriate method to measure the pulse duration, as well as the chirp of the harmonics.

H. Investigations with thin foil targets

In addition to the HHG experiments with massive targets involving observation from the front side that were reviewed up to now, measurements using foil targets have been reported as well. The first experiments with fs laser pulses in which high-order harmonic emission from foil targets was observed from the rear side were by Teubner *et al.* (2004). Free-standing aluminum and carbon foils of 50 and 400 nm thickness, respectively, were irradiated under the same conditions as discussed in Sec. IV.F. Observation of the harmonics was made both in the specular reflection direction (observation from the laser-irradiated front side) and from the rear side. They reported that the spectra observed from the front side of the foil targets are weaker than those from massive targets (see Fig. 26) but otherwise do not differ too much.

The spectra observed from the rear side are even weaker (Fig. 26) but also more interesting, and yield much insight into the harmonic generation process itself. They show harmonics from second to tenth order and even light at the laser fundamental is *reemitted* from the rear side (Fig. 27). This was in total contrast to earlier model predictions (Lichters *et al.*, 1996; Gibbon, Altenbernd, Teubner, *et al.*, 1997) where it was assumed that low-order harmonics generated at the front side do not propagate through the foil plasma. In that case, it was expected that only harmonics with a frequency $\omega_N > \omega_p$ should be detectable, i.e., there should be a low-frequency cutoff. For a plasma that stays overdense during the harmonic generation process, this means that low-order harmonics generated at the front side could not propagate through the target. As shown by hydrocode simulations, transmission would only be possible after the plasma has expanded for several picoseconds, i.e., at a time when harmonic generation has stopped (Teubner *et al.*, 2004; Eidmann *et al.*, 2005). Thus, the cold target was overdense for the front-side generated harmonics with $N<5$ and even $N<9$ for the heated target. The high density was also deduced from x-ray spectra (Andiel *et al.*, 2001; Wagner *et al.*, 2002); furthermore, the spectral profiles of the simulated reemitted harmonics agree with those measured for solid-density targets only.

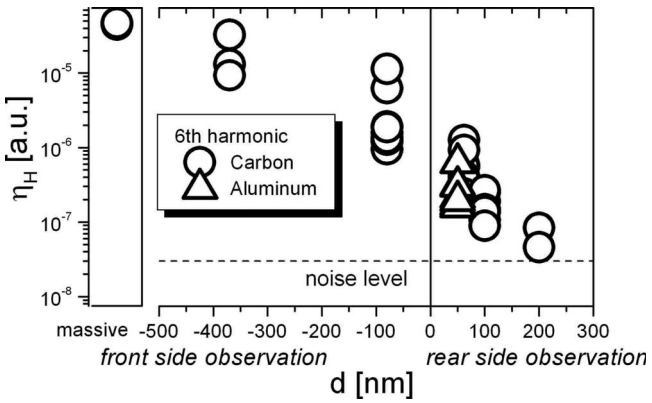

FIG. 26. Efficiency of the harmonic lines $H6_{395}$ and $h6_{395}$ as a function of foil thickness for rear side observation ($d>0$) and front side observation in specular direction (here the thickness is multiplied by −1, i.e., $d<0$) measured at an intensity of 1.5×10^{18} W/cm^2 (the symbols correspond to single-shot measurements, the symbol size corresponds to the accuracy); data from Teubner *et al.* (2004). For comparison, the intensity obtained from a massive target (Teubner, Pretzler, Schlegel, *et al.*, 2003) is displayed as well.

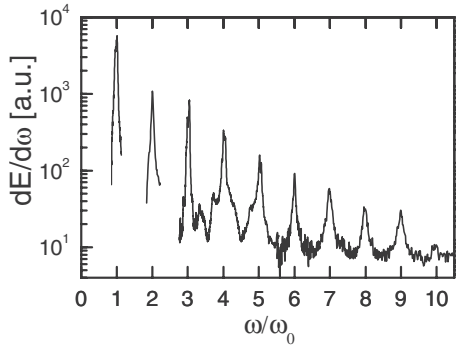

FIG. 27. Typical harmonic spectrum measured at the rear side of a 60-nm carbon foil. It was measured with *p*-polarized light at $I_0=2\times10^{18}$ W/cm^2 (pulse duration 130 fs, laser fundamental $\lambda_0=395$ nm).

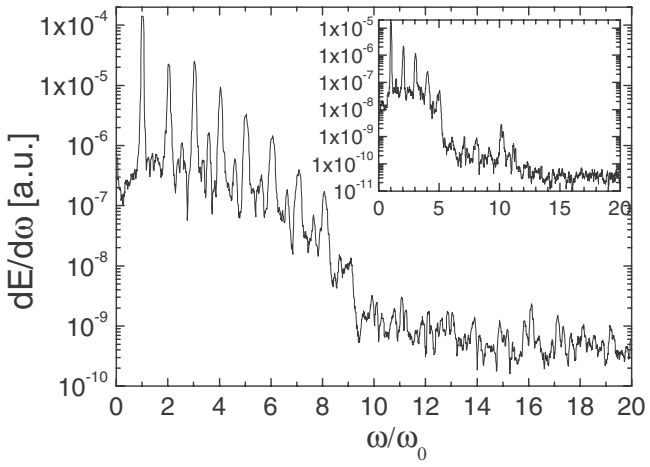

FIG. 28. PIC simulation with input parameters chosen to be close to the experimental conditions (see Fig. 27; from Teubner *et al.*, 2004). The high-frequency cutoff at $N_{\mathrm{cut}} \approx 10$ of the spectrum in Fig. 27 is well reproduced and indicates a density $n_e/n_c \approx 80$ (corresponds to five to six times ionized carbon). This was supported by additional diagnostics from measurements from carbon *K*-shell x-ray spectra. The inset shows a harmonic spectrum generated at ten times lower density, which resulted in $N_{\mathrm{cut}} \approx 5$.

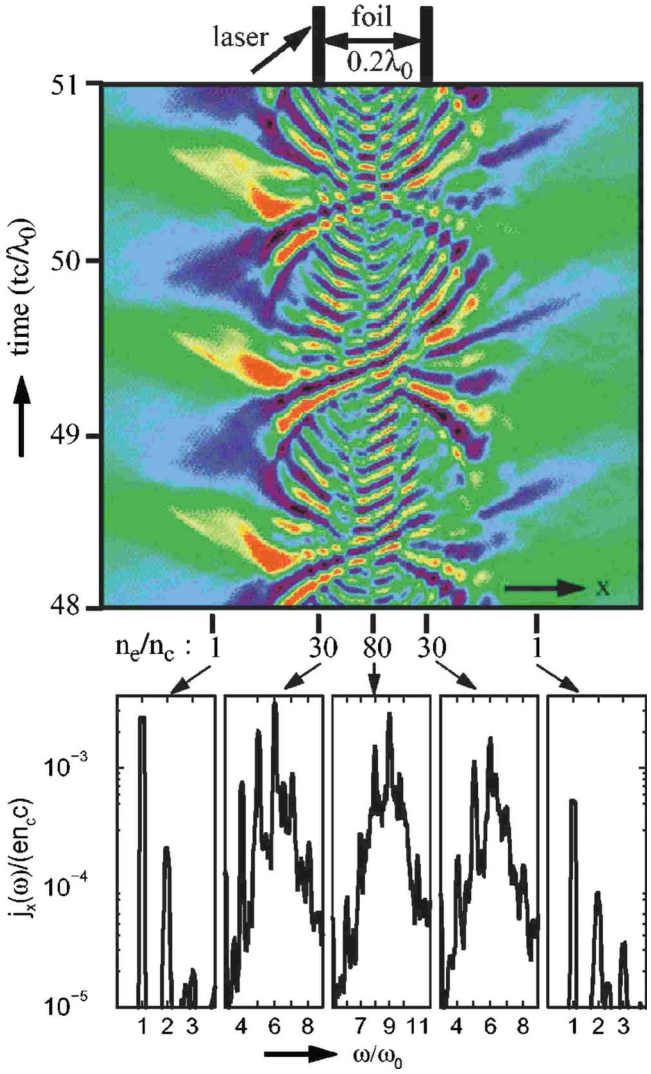

FIG. 29. (Color online) Current density j_x along the target normal for the experimental conditions of Fig. 27. At the top, the space-time mapping of j_x (in the laboratory frame) is shown. The thick bars indicate the unperturbed foil. At a few positions, the density at the time of the laser pulse maximum is given. The diagram at the bottom shows the Fourier spectrum of j_x at these indicated positions, with peaks at $\omega/\omega_0 = (n_e/n_c)^{1/2}$. From Teubner *et al.*, 2004.

However, the experiment of Teubner *et al.* showed a high-frequency cutoff at $N_{\mathrm{cut}} = \omega_p/\omega_0 = (n_{e,\mathrm{max}}/n_c)^{1/2}$, where $n_{e,\mathrm{max}}$ is the maximum density in the plasma, i.e., at a harmonic order between nine and ten in that experiment (Fig. 27). Additional PIC simulations were performed with input parameters carefully chosen close to the experimental conditions. The experimental observations were well reproduced, and further analysis showed that the high-frequency cutoff could be used as a density diagnostic (Fig. 28).

The physical process of harmonic generation was explained by energetic electron currents propagating from the interaction zone into the foil. In regions where the harmonic frequency equals multiples of ω_0 and is close to the local plasma frequency, excitation becomes resonant and leads to efficient generation of harmonic radiation (Teubner *et al.*, 2004). In the simulations, this can be seen by Fourier transformation of the current density (see Fig. 29). Following this, the lower harmonics are generated in regions where the density is lower, i.e., at both the front side and the rear side of the foil target (there is no transmission of harmonics from the front to the rear side). Somewhat higher-order harmonic orders originate from more dense regions. The highest-order harmonic frequency generated is close to the plasma frequency and comes from the vicinity of the center of the dense foil. Above this frequency a cutoff occurs, which is observed in the experiment (higher-order harmonics, if present, were below the noise level) and the simulation and is of interest for diagnostics to determine the maximum density in the foil during the interaction.

A further detailed investigation of the reemission process was performed by Eidmann and co-workers (Eidmann *et al.*, 2005). They found that the reemitted fundamental and second harmonic are already observed at low intensities ($a_0 = 0.1$ or 10^{17} W/cm^2 at $\lambda_0 = 395$ nm). The conversion efficiency increases with laser intensity and decreases with foil thickness but was still observable for a foil thickness up to one laser wavelength (i.e., 400 nm). As for harmonics observed from the front side, harmonics observed from the rear side were generated only if the incident laser pulse was *p* polarized (the reemitted fundamental was also *p* polarized). This, and the fact that the PIC simulations showed that efficient reemission of harmonics occurs only during a period when the electron density profile is optimal, indicates that high-energy electrons relevant for HHG are generated via resonance absorption (Eidmann *et al.*, 2005). Moreover, this optimal profile is present only for a short time,

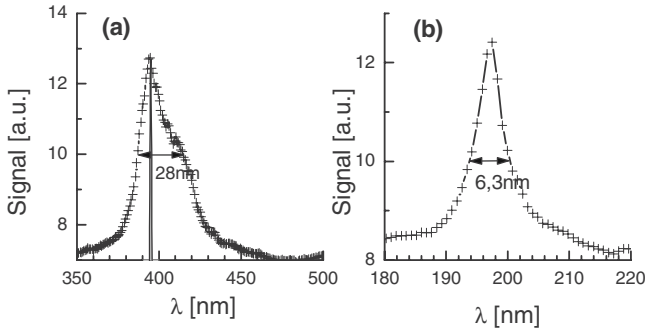

FIG. 30. Measured spectral line shapes of $h1$ and $h2$ from the spectrum displayed in Fig. 27. The spectral width is 28 nm (FWHM) for $h1_{395}$ and 6.3 nm (FWHM) for $h2_{395}$. In (a), for comparison, the profile of the incident fundamental is displayed as well (1.7 nm FWHM). [Plots made from the experimental data taken from Teubner *et al.* (2004).]

which leads to a short pulse duration of the harmonics and thus to a broad spectral width of them (Fig. 30). Dispersion of the electron bunches, phase-modulation effects, and complicated plasma dynamics (compression in the early phase and expansion later on) also lead to complicated temporal structure with spiking.

These results are also consistent with the findings of Quére *et al.* (2006), who attribute their low-intensity harmonics to the CWE mechanism. Thin foils could in principle support both resonance absorption and CWE for harmonic generation, which in turn exhibit a cutoff at ω_p, and relativistic OMM, which does not. Such a cutoff has been observed in lower-intensity experiments (at around $H15_{395}$ and $h10_{395}$) (Teubner *et al.*, 2004; Eidmann *et al.*, 2005; Quére *et al.* 2006). Further evidence for the former mechanisms can be derived from different scaling of the harmonics with I_0 below and above the cutoff (as discussed by Quére *et al.*, 2006 and in Sec. IV.C).

I. Coherent transition radiation

Another phenomenon that can lead to specific electron-generated line-emission-like radiation is optical transition radiation that occurs when energetic electrons traverse a boundary between regions of different dielectric function (Landau and Lifshitz, 1985). Thus, for instance, when electrons pass from the rear side of a foil target into vacuum, the coherent transition radiation component should be observable. In fact, using intense sub-ps laser pulses ($\lambda_0=1.06$ μm) focused to high intensity ($I_0=10^{18}$–10^{19} W/cm^2) onto foil targets with a thickness up to several tens or hundreds of microns, several have investigated this feature (Santos *et al.*, 2002; Baton *et al.*, 2003; Zheng *et al.*, 2003, 2004; Beg *et al.*, 2004; Popescu *et al.*, 2005). In particular, intense line emission was observed from the rear side of the foil at the laser fundamental frequency ω_0 (with a spectral width of $\Delta\omega/\omega\sim0.019$ FWHM) (Zheng *et al.*, 2004), at $2\omega_0$ ($\Delta\omega/\omega\sim0.038$) (Baton *et al.*, 2003), and at multiples of $2\omega_0$–$5\omega_0$ (Popescu *et al.*, 2005). In all these experiments, the radiation could be attributed to coherent transition radiation (CTR), although Santos *et al.* (2002) and Baton *et al.* (2003) argued that part of the emission may be due to synchrotron radiation originating from outgoing electrons, but not sufficiently to modify these principal conclusions on CTR.

Following the discussion of the cited works, CTR relies on high-energy electrons that are accelerated via resonance absorption (Zheng *et al.*, 2004), some kind of Brunel effect ("vacuum heating") or the $\mathbf{v}\times\mathbf{B}$ mechanism (Baton *et al.*, 2003), or a mixture of those processes (Popescu *et al.*, 2005). In this way, a series of microbunches of electrons are generated with a time separation given by $2\pi c/\omega_0$, or by $\pi c/\omega_0$ in the case of the $\mathbf{v}\times\mathbf{B}$ mechanism. Due to the very short and narrow electron bunches, the transition radiation fields of all electrons are added coherently when they traverse the foil vacuum interface (if the wavelength is larger than the bunch length). This coherent superposition then leads to a much higher radiation power proportional to N_{el}^2, where N_{el} is the number of relevant electrons when compared to an incoherent superposition (power proportional to N_{el}).

In a theoretical investigation, Baton *et al.* suggested a formula for the CTR spectrum where the frequency distribution is proportional to the electron flux and to

$$\frac{\sin^2\theta\left(\frac{1}{2}M\omega\delta T\right)}{\sin^2\theta\left(\frac{1}{2}\omega\delta T\right)},$$

where δT is the temporal separation between bunches and M is the number of bunches (Baton *et al.*, 2003). This result corresponds to the coherent superposition of the fields of each of the bunches and thus leads to electromagnetic emission peaked at multiplies of ω_0 (including ω_0 itself; without coherence, the spectrum would be broadband and nearly flat) (Zheng *et al.*, 2003). The typical energy of involved electrons is of the order of MeV (Baton *et al.*, 2003; Zheng *et al.*, 2004; Popescu *et al.*, 2005). Typically the electron jets consist of a few tens of bunches and carry of the order of 10^{-4} of the incident laser pulse energy (Popescu *et al.*, 2005). It should be noted that if, as in the investigations of Popescu *et al.*, both ω_0 and $2\omega_0$ microbunches are present, then the relative electron numbers within the bunches and the relative phase between both components become important and may either enhance or cancel specific frequencies.

In this context, it is relevant to ask how, in particular, harmonics observed from the rear side of very thin (a few tens of nanometers) foil targets (Teubner *et al.*, 2004) are connected to CTR. For this case, Popescu *et al.* (2005) argued that the radiation could be explained in terms of CTR. However, we note that although a contribution of CTR to rear side emitted harmonics is still an open question, there are arguments that might exclude this process either totally for the rear side emitted harmonic generation mechanism or might make it a partial

contribution only. First, due to the relatively short wavelength of the laser fundamental in the experiment of Teubner *et al.* (i.e., $\lambda_0=395$ nm), those high-energy electrons had a much lower hot-electron temperature than the MeV from typical CTR experiments (e.g., Popescu *et al.*, 2005, and the other works mentioned above). In other words, the necessary ultrarelativistic electrons—those with an energy higher than the electron temperature—are not really present. Second, for the reemitted light observed in the experiments of Teubner *et al.* (2004) and Eidmann *et al.* (2005), one may exclude CTR for the reemitted harmonics because CTR is expected in the direction of the high-energy electrons, which is mainly along the target normal and not in the direction of the incident laser pulse (which was the observation direction in these experiments).

Consequently, we note that the contribution of CTR to the harmonic generation process for the rear side reemitted harmonics is not clear to date. If CTR plays a role, then we would expect that it may be of relevance for the harmonics observed from the front side too. In any case, the CTR process is inherently included in PIC simulations of harmonic generation, even though it may not be distinguishable from other kinetic processes, e.g., in Teubner *et al.* (2004) and Eidmann *et al.* (2005), and could be suppressed to some extent in 1D codes using the boost technique (Sec. III.C).

V. APPLICATIONS, CONCLUSION, AND OUTLOOK

Any serious application of short-wavelength, coherent light poses constraints and demands on the radiation source, which will often determine the choice between two competing alternatives. Before we consider potential applications of HHG as an XUV source, it is helpful to compare harmonics against other sources such as free electron and x-ray lasers.

A. Brilliance of harmonics of picosecond and femtosecond laser pulses and comparison to other XUV sources

Based on the previous analysis, it is interesting to compare the conversion efficiency and harmonic yield for picosecond (Norreys *et al.*, 1996; Chambers *et al.*, 1997) and femtosecond laser pulses (Tarasevitch *et al.*, 2000; Teubner, Pretzler, Schlegel, *et al.*, 2003). As an example, we compare $H38_{1053}$ from the experiment of Norreys *et al.* (1996) ($I_0=10^{19}$ W/cm^2, $\tau_0=2.5$ ps, $\lambda_0=1053$ nm) with a harmonic at the same wavelength (i.e., 28 nm, corresponding to 44 eV photon energy), but generated with a femtosecond laser pulse ($H14_{395}$; $I_0=2\times10^{18}$ W/cm^2, $\tau_0=120$ ps, $\lambda_0=395$ nm) (Teubner, Pretzler, Schlegel, *et al.*, 2003).

For the picosecond laser pulse $\eta\sim4\times10^{-6}$ (assuming isotropic emission into $\Delta\Omega_H=4\pi$ sr), which means that approximately 10^{13} photons in total are emitted into the accessible half-space in front of the target, yielding a total power of 10–100 MW or 1–10 MW/sr (Norreys *et al.*, 1996). For the femtosecond laser pulse η is of the same order, but the supplied laser energy is a factor of 60 mJ/20 $J\sim1/300$ weaker and thus the number of emitted photons is of the order of 10^{10}. However, the pulses are much shorter and the emission is strongly directed. One may estimate a power of

$$P_{H14}\sim\frac{\eta_{H14}E_0}{\tau_{H14}}\sim\frac{2\times10^{-6}\times60\text{ mJ}}{(120\text{ fs})/\sqrt{14}}\sim4\text{ MW}. \quad (32)$$

This power is emitted into $\sim10^4$ mrad^2 or 9×10^{-3} sr. Thus, femtosecond HHG leads to a power per solid angle of approximately 400 MW/sr, which is at least an order of magnitude larger when compared to picosecond HHG.

Table II summarizes some properties of harmonics obtained for different experimental conditions from LPP. It may be seen that with intense laser pulses, a very high number of XUV photons may be obtained in the photon energy region between 20 and 70 eV. Harmonics with shorter wavelengths or higher photon energies are also expected to be present, but have not been definitively demonstrated for fs HHG up to now (see Sec. IV.F). But even with a moderate laser intensity (e.g., 10^{17} W/cm^2), the harmonic yield is considerable. Assuming that the harmonics can be well focused, the achievable intensity is quite substantial: in fact, harmonics generated with fs laser pulses may be one of the most intense sources in the wavelength range of a few tens of nanometers, i.e., they have a high peak brilliance

$$B_{\text{peak}}=\frac{N_{\text{pho}}}{\Delta\Omega\Delta A\tau},$$

where N_{pho} is the number of photons, $\Delta\Omega\Delta A$ is the etendue, and τ is the emission duration (the spectral peak brilliance B is B_{peak} within a narrow spectral band, which is usually 0.1% relative bandwidth). This may be seen by comparing their characteristics with other sources, such as x-ray lasers (XRLs), also listed in Table II and III. Here, as an example, the emission parameters of DESY's XUV free electron laser (XFEL) FLASH and gas harmonics are also given, all with respect to the same wavelength range of 20–50 nm.

Although a detailed discussion on all these sources is beyond the scope of this review, it may be seen from Table II that many of them have their advantages with respect to specific requirements such as high XUV energy or photon number per pulse (in particular for an XRL or XFEL), small divergence, very short pulse duration (fs harmonics, XFEL, but this excludes XRL), or high spectral peak brilliance, which allows for high intensity when focused onto a sample.

A further source property relevant for application is coherence, which is already much better for a harmonic than for an XRL. Another important feature is if the XUV wavelength may be adapted to a specific application, as in the case of harmonics or for the tunable XFEL, or if, conversely, the application must be adapted to the XUV source, as in the case of an XRL.

From the discussion in Sec. II.D, it may be seen that in contrast to HHG in gases, for plasma-based HHG,

TABLE II. Examples of harmonic properties from present experimental data given for picosecond and femtosecond pulse HHG. For comparison corresponding parameter are provided for other XUV sources emitting in the same wavelength range. Order-of-magnitude estimates are made only. Vulcan is laser facility at Rutherford Laboratory, Didcot, UK. ATLAS is a laser system at the Max-Planck-Institute för Quantenoptik, Garching, Germany. Vulcan-XRL is the Ne-like Ge, saturated XRL at Vulcan. GRIP XRL is the grazing incidence pumped XRL at Max-Born-Institute, Berlin, Germany, using two laser pulses (ps and fs). The capillary discharge XRL does not make use of a laser driver. Its η is estimated from the condenser pump energy. SXRL is seeded XRL (generated with a 1 J, 30 fs laser), e.g., amplified *H*25 generated in gas (generated with a 20 mJ, 30 fs laser). η of the SXRL is the energy of the amplified *H*25 divided by the total laser energy (see pulse generation and XRL pump laser). For the SXRL, the pulse duration is limited by the spectral width of the XRL amplifier. $\Delta\omega/\omega$ for *H*38 of LPP from Vulcan was no measured, but a rough estimate could be obtained from the scaling according to Secs. IV.D and IV.G [$\Delta\omega_N/\omega_N \approx (\Delta\omega_0/\omega_0)N^{-1/2}$]. The spectral resolution was not sufficient to obtain a reliable value for $\Delta\omega/\omega$ of *H*20 of LPP from ATLAS; however, it was estimated from extrapolation of the data from Teubner, Pretzler, Schlegel, *et al.* (2003) (see also Sec. IV.G). For the optimized gas, harmonic *H*27 optimistic band width limit was assumed. From wavelength, photon energy, XUV energy, divergence, duration, peak power, source size, and $\Delta\omega/\omega$, the peak brilliance was estimated (in the usual units used at synchrotrons). Note that the value given for the optimized gas harmonic *H*27 is the highest pulse energy and brilliance of a gas harmonic at this wavelength, but note that usually for higher pulse energy of the gas harmonics, their coherence is lower. The divergence $\Delta\theta$ is the full angle for actual experiment shown.

Harmonic (or XRL or XFEL) properties	*H*48 of LPP from Vulcan	*H*38 of LPP from Vulcan	*H*14 of LPP from ATLAS	*H*10 of LPP from laser of Univ. of Essen	*H*6 of LPP from ATLAS	*H*20 Source of LPP from ATLAS	Vulcan XRL	GRIP XRL	Capillary discharge XRL	XFEL FLASH (present status)	SXRL	Optimized gas harmonic *H*27
λ (nm)	22	28	28	80	66	20	19.6	10–60	47	32	33	30
Photon energy (eV)	56	44	44	15	19	63	64	20–125	26	39	38	41
Conversion eff. η	10^{-8}	10^{-6}	10^{-6}	10^{-6}	10^{-4}	10^{-7}	10^{-5}	10^{-5}	10^{-5}		10^{-6}	10^{-6}–10^{-5}
E ($=E_0\eta$)(μJ)	0.4	80	10^{-1}	7×10^{-3}	6	10^{-2}	900	1–15	880	100	0.7	10^{-3}–10^{-1}
Number of photons	10^{10}	10^{13}	10^{10}	10^{10}	10^{12}	10^{9}	10^{14}	10^{11}	10^{14}	10^{13}	10^{11}	10^{8}–10^{11} (but typ. 10^{7}–10^{8})
Divergence $\Delta\theta$ (mrad)	2000	2000	100	40	160	85	7 ($\perp$) 30 ($\parallel$)	1–10	2	0.1	1	1–4
Solid angle of emission $\Delta\Omega$ (sr)	2π	$2\pi(4\pi)$	10^{-2}	10^{-3}	10^{-2}	10^{-2}	10^{-4}	10^{-6}–10^{-4}	10^{-6}	10^{-8}	10^{-6}	10^{-6}
Pulse duration τ	0.5 ps	0.5 ps	32 fs	38 fs	49 fs	27 fs	40 ps	2–30 ps	$\leq$1 ns	30 fs	500 ps	7 fs
Peak power P (W)	10^{6}	10^{8}	10^{6}	10^{6}	10^{8}	10^{5}	10^{7}	10^{5}	10^{6}	10^{9}	10^{6}	10^{4}–10^{7}
Source size (μm)	3	10	1	4	2	1	150	20–100	300	150	150	60
$\Delta\omega/\omega$	10^{-2}	10^{-3}	10^{-3}		10^{-2}	10^{-3}	10^{-4}	10^{-3}–10^{-4}	10^{-4}	10^{-2}	10^{-4}	10^{-2}
B [photons/(s mm^2 mrad^2) in 0.1% relative bandwidth]	10^{21}	10^{23}	10^{25}	10^{25}	10^{26}	10^{24}	10^{24}	10^{24}	10^{25}	10^{29}	10^{26}	10^{22}–10^{26}
Diffraction limit	100 times	300 times	2 times	1 time	2 times	2 times	20–100 times	6–8 times	1–2 times	1 time	1–2 times	1–2 times
Laser properties									No driver laser	No driver laser		
Laser: λ_0 (nm)	1053	1053	395	800	395	395	1053	1053, 800	no laser	no laser	815	~800
Laser: τ_0 (fs)	1000	2500	120	120	120	120	10^{5}	10^{3} & 10^{5}	no laser	no laser	30	30–60
Laser: E_0 (J)	20	20	6×10^{-2}	70	6×10^{-2}	5×10^{-2}	150	10^{-1}	no laser	no laser	1 & 0.02	$10^{-3}$$10^{-2}$
Laser: I_0 (W/cm^2)	4×10^{18}	10^{19}	2×10^{18}	5×10^{17}	2×10^{18}	2×10^{18}		10^{11} & 10^{14}	no laser	no laser	2×10^{17} & 10^{15}	10^{14}–10^{15}
Respetition rate	single short	single shot	10 Hz	10 Hz	10 Hz	10 Hz	single shot	single shot or 10 Hz	1–10 Hz	10 Hz 3000 bunches per pulse	10 Hz	10–20 Hz
Estimated from Refs.	Chambers *et al.*, 1997	Norreys *et al.*, 1996; Zhang *et al.*, 1996	Teubner, Pretzler, Schlegel, *et al.*, 2003	Tarasevitch *et al.*, 2000	Teubner, Pretzler, Schlegel, *et al.*, 2003	Teubner, Pretzler, Schlegel, *et al.*, 2003	Zhang *et al.*, 1996	Janulewicz *et al.*, 2004; Janulewicz, 2007	Rocca *et al.* 1994; Janulewicz *et al.*, 2004	Materlik and Tschentscher, 2001; Tschentscher, 2004, 2007;Ackermann *et al.*, 2007	Zeitoun *et al.*, 2004	Hergottct *et al.*, 2002; Takahashi *et al.*, 2002; Janulewicz *et al.*, 2004

TABLE III. Brilliance and expected intensity for present and future XFEL and synchrotrons at approximately 40 eV (i.e., 31 nm). For the intensity it is assumed that the full beam is focused with a perfect $f/1$ optic. For comparison, the estimate for $H14$ is from the data given in Table II. Note that due to imperfections and lower f-numbers, all achievable intensities in experiments are expected to be lower than the listed values.

Source	Order of magnitude of peak brilliance [photons/(s mm^2 mrad^2) in 0.1% relative bandwidth]	Order of magnitude of expected intensity (W/cm^2) at ~30 nm
FLASH (seeded; planned; from Fig. 2.3.1 in Materlik and Tschentscher, 2001)	10^{31}	10^{22}
FLASH	10^{29}	10^{20}
DESY TTF-FEL (spontaneous)	10^{23}	10^{14}
BESSY II U-125	10^{21}	10^{12}
$H14$ from plasma surface (present)	10^{25}	10^{15}
$H14$ from plasma surface (expected for laser intensity of 10^{19} W/cm^2)	10^{28}	10^{19}
TUIXS[a]	10^{26}	10^{18}

[a]Development within the European network Table-top Ultra Intense X-ray Source (TUIXS) for a 100 μJ pulse energy SXRL (Zeitoun, 2006) (estimated values from boosting SXRL in Table II to 100 μJ pulse energy).

there are much better prospects for reaching higher harmonic intensity. For HHG in gases this would require the separate amplification of a single harmonic—the SXRL scheme (see, e.g., Zeitoun *et al.*, 2004; Fajardo *et al.*, 2006; Zeitoun, 2006). Again, we point out that the advantage of HHG from LPP when compared to that in gases is not only the higher conversion efficiency but also the higher laser intensity that could be applied (thus even for a constant value of η, I_H would still increase with I_L). Moreover, in particular, further development of the XFEL will lead to an unrivaled source of ultrahigh brilliance in the XUV. But, in general, one should be aware that the necessary effort for the different sources is quite different. In particular, it is (very) large in the case of HHG from ps LPP, most XRL, SXRL, and XFEL.

Figure 31 visually summarizes spectral peak brilliance values for important sources in the photon energy range between 10 and 100 eV. We restrict the figure to this range because this is the spectral range presently accessible with HHG from fs plasmas (values that are achieved in experiment or that could be credibly derived from measurements; closed circles). The figure also includes values that are expected for the near future: first a conservative and then a somewhat more progressive extrapolation, both based on brilliance values deduced from measurements at $I_L=2\times10^{18}$ W/cm^2. For this extrapolation, we used the scaling of the harmonics intensity on laser intensity for the different harmonic numbers (or photon energies); see Figs. 32 and 19(b). Then, using the values of B shown as closed circles and scaling them for a five times higher laser intensity (this is a quite reasonable estimate), the obtained expected spectral peak brilliance values are shown as open circles. The

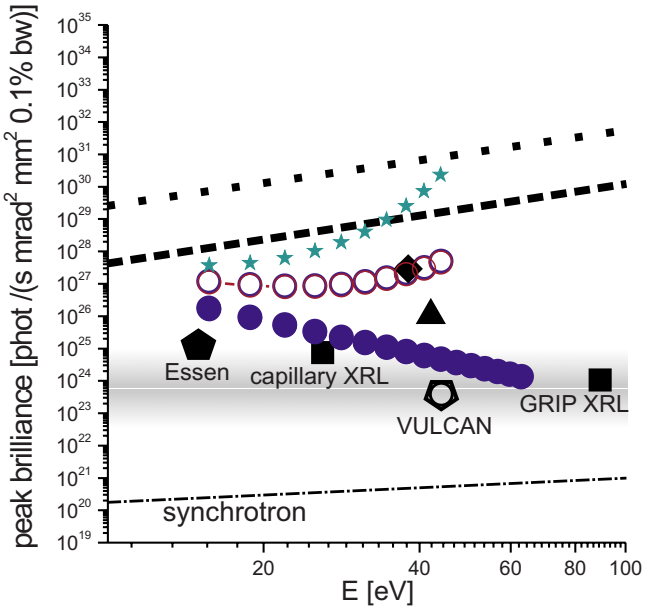

FIG. 31. (Color online) XUV spectral peak brilliance from present sources and future expectations. The symbols correspond to estimates for the harmonics from Teubner, Pretzler, Schlegel, *et al.* (2003a) (closed circles). These are expected to be shifted to the positions of the open circles or stars for more optimized conditions (see text). The other symbols are labeled according to the first row in Table II (the triangle corresponds to the most brilliant gas harmonic to date; see the last column in Table II). The diamond indicates the SXRL. The broken and dotted lines indicate the brilliance of the XFEL at present and in the future, respectively [data from Materlik and Tschentscher (2001) and Ackermann *et al.* (2007)]. For comparison, the brilliance of a typical synchrotron is displayed as the line near the bottom of the diagram. The gray background indicates the typical brilliance for gas harmonics.

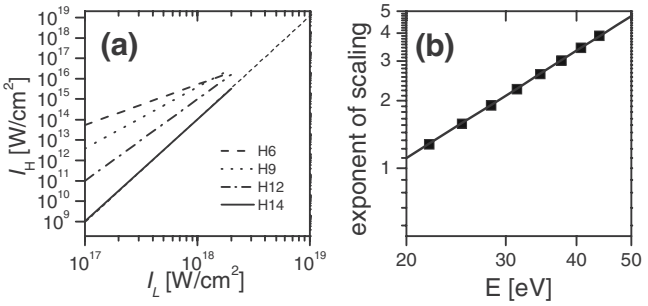

FIG. 32. Scaling of harmonics on laser intensity and harmonic photon energy. (a) Estimated achievable intensity of the high-order harmonics produced with pulses of the order of $\tau_0 \approx 100$ fs and $\lambda_0 \approx 400$ nm [estimated from the data in Teubner, Wagner, Andiel, *et al.* (2003)]. The thin dashed line is an extrapolation of the intensity of the 14th harmonic that may be achieved for laser intensities up to 10^{19} W/cm^2. For higher intensities ($\sim 10^{19}$ W/cm^2 for $\lambda_0 = 400$ nm), two-or three-dimensional effects may become important and lead to less focusable harmonics (see Sec. III.G). However, for ultrahigh intensities, a scaling may be obtained from Fig. 14. The accuracy of η_H and I_H is within one order of magnitude. (b) Dependence of the coefficient Γ with which the harmonics scale on I_L (i.e., $I_H \propto \eta_H I_L = I_L^{\Gamma}$) on photon energy of the harmonics [obtained from data from Fig. 19(b)].

somewhat more progressive extrapolation for 10 times higher laser intensity yields the values shown as stars, but of course due to the scaling based on weakly relativistic laser intensity, we would expect an even stronger enhancement of B in the strongly relativistic regime.

We note that the above scalings are realistic for $N \leqslant 15$ (i.e., below approximately 50 eV photon energy), but at present due to the lack of further measurements and well enough understood interaction physics, an extrapolation to higher laser intensities would not be reliable for higher photon energies (see discussion in Sec. IV.C). Moreover, this is the case for the photon energy range beyond 100 eV, where no HHG with fs laser plasma interaction has been demonstrated experimentally.

High spectral peak brilliance values for shorter wavelengths have been reported using the Vulcan petawatt ps laser. Dromey *et al.* (2006) reported $B \sim 10^{24}$ photons/mm^2 mrad^2 s in 0.1% relative bandwidth at 17 nm (i.e., ~70 eV), $B \sim 10^{22}$ photons/mm^2 mrad^2 s in 0.1% relative bandwidth at 4 nm (i.e., ~300 eV), and $B \sim 10^{20}$ photons/mm^2 mrad^2 s in 0.1% relative bandwidth at 1 nm (i.e., ~1.2 keV). But these values are obtained with ps laser pulses and thus it is expected that properties such as harmonic pulse duration, divergence, etc., are dominated by the processes prevalent in ps laser plasma interaction discussed in Sec. IV (see also Table II). Nevertheless, these brilliance values indicate the potential progress for fs HHG.

To provide reliable estimates of the spectral peak brilliance based on theoretical grounds without any experimental support would be premature given the present understanding of the HHG physics. Of course, for a laser intensity of several times 10^{20} W/cm^2 within a 3 fs laser pulse as assumed in the theoretical feasibility study of Tsakiris *et al.* (2006), one may estimate a spectral peak brilliance of $B > 10^{30}$ photons/mm^2 mrad^2 s in 0.1% relative bandwidth at 32 nm (i.e., ~50 eV) or $B > 10^{28}$ photons/mm^2 mrad^2 s in 0.1% relative bandwidth at 1 nm (i.e., ~1 keV). Thus this study is very encouraging. But as those authors state, "the question is to what extent this potential can be exploited in a realistic experiment" and in this respect such estimates are very speculative. Practical limitations are of a technological nature and related to the development of suitable high-power laser systems, as dicussed in this work or that of Nees *et al.* (2005).

B. Focusing and spectral control

The intensity I_H that could be achieved by focusing high-order harmonics onto a sample can be estimated either from the brilliance data given in Table II [for a perfect beam and a perfect optics one gets $I_H \sim B\Delta\Omega\Delta A E_{\text{pho}}/(2\lambda_H f/D)^2$ or $I_H \sim B E_{\text{pho}}/(f/D)^2$, where $\Delta\Omega\Delta A$ is the etendue, E_{pho} is the photon energy, λ_H is the harmonic wavelength, and f/D is the f-number of the applied focusing optics] or just by taking into account the conversion efficiency, the divergence of the harmonics $\Delta\theta_N$ (for a given source area that is determined by the experiment), and their pulse duration τ_N. As discussed by Tarasevitch *et al.* (2000), the emitted fs harmonics are expected to be nearly diffraction limited so that it should be possible to focus them to a small spot with a diameter

$$\phi_N = \frac{\phi_L \lambda_H}{\lambda_L} = \frac{\phi_L}{N}. \tag{33}$$

The solid angle of emission scales according to Eq. (29), which leads to the high focusability of the harmonics.

Although the pulse duration of harmonics has not yet been measured (Sec. IV.G), a short duration of the harmonic pulses is expected [see Eq. (31)]. The values of τ_N for the single Nth harmonic pulse from fs LPP and gases given in Table II are the result of such an estimate, as is the power P. In addition, it may be recalled that due to inherent mode locking of several harmonics together, a train of spikes with a duration of a few hundred attoseconds each (see Secs. III.H and IV.G) is generated that leads to an even higher peak power.

Taking into account the conversion efficiency, the ultrashort pulse duration, and the spot size of a harmonic that is several times diffraction limited, for instance, focusing the ninth harmonic at 44 nm ($\lambda_0 = 395$ nm; see Fig. 32) should yield a harmonic intensity exceeding 10^{15} W/cm^2, even for the less than optimal conditions in that experiment.

To summarize, the achievable intensity for the measured harmonics may be estimated as

$$I_N \approx I_L \eta_N \left(\frac{\tau_0}{\tau_N}\right)\left(\frac{\phi_0}{\phi_N}\right)^2 = I_L \eta_N N^{5/2}, \quad (34)$$

which is plotted in Fig. 32. The extrapolation of our estimate shows that even a single harmonic may reach an intensity similar to that of the driving laser pulse. Further potential may be realized by applying laser pulses of shorter pulse duration and higher intensity: due to the scaling of Eq. (23) with λ_0 and N, short wavelength lasers are preferable.

Extraordinarily high intensities could be achieved, in particular, when harmonics in a larger spectral range are contained within an attosecond pulse in the focus. For such a case, Tsakiris *et al.* (2006) showed, for example, that the intensity may even exceed that of an XFEL by many orders of magnitude. But again, to demonstrate such high intensities in a real experiment remains a tremendous challenge for the future.

On a more speculative note, recent simulations show that even higher intensities may be achieved by coherent focusing of all high harmonics, the so-called coherent harmonic focusing scheme (Gordienko *et al.*, 2005), potentially giving intensities of the order of 10^{22}–10^{30} W/cm^2 for laser intensities of the order of 10^{19}–10^{23} W/cm^2 (see Fig. 14). Alternative schemes have also been proposed by Naumova, Nees, Hou, *et al.* (2004) which exploit the relativistic pulse compression produced by a near-critical plasma surface to reduce the duration of the reflected (harmonic-rich) pulse into the attosecond range, while also permitting tight focusing arrangements (Nees *et al.*, 2005); see Sec. III.H (Fig. 14; this is the so-called λ^3 regime).

Today, however, such large intensities (see Fig. 32 and Table III) may be difficult to achieve experimentally because first one must demonstrate this high-brilliance source, and second, one must apply an appropriate optics with large collection angle, high optical quality, and large f number. Here we emphasize that an ultrabright harmonic pulse requires a high conversion efficiency yielding a high photon number and simultaneously high spatial and temporal coherence that allows for high focusability and the shortest possible pulse duration (requirement for a diffraction-limited beam and a bandwidth-limited pulse). This is particularly the case when a group of phase-locked harmonics are to be superimposed to create an even shorter pulse. Thus all necessary source parameters must be determined experimentally, and it would be advantageous to demonstrate that they could be obtained simultaneously even when an ultrahigh-power laser pulse is used as the driver.

Then to achieve ultrahigh intensity, e.g., for an application, in a second step either an additional nearly perfect optics must collect as much of the emitted harmonics as possible and, focus them possibly to a diffraction limited spot, or such perfect focusing must be performed during the laser-plasma interaction itself as discussed in theory. But this must also be proven in an experiment, and this is difficult because today the optics for the XUV range is not yet as developed as that for the near-infrared to UV region. Nevertheless, the harmonic intensity may still be remarkable and further advances in XUV optics will bring us closer to the theoretical value. For example, a recent development of SMT has shown that a high reflectivity mirror for 13 nm radiation yields a focal spot size of ~30 nm (Zeiss, 2006).

C. Applications of fs-high-order harmonics from LPP (i.e., coherent VUV and XUV radiation)

As a consequence of the estimates in Sec. V.B, it can be concluded that the fs LPP harmonic source can be extremely intense. Thus it may be promising for applications that require a powerful, coherent source in the vacuum ultraviolet (VUV) or XUV region. In particular, this includes investigations of ultrafast ionization of atoms, molecules, and clusters in strong fields of short wavelengths (see, e.g., Wabnitz *et al.*, 2002), ultrafast spatial interferometry in XUV (see, e.g., Salières *et al.*, 1999), and investigations of electron packets and photoelectron spectroscopy on ultrafast time scales (see, e.g., Drescher *et al.*, 2002; Asevey *et al.*, 2003; Niikura *et al.*, 2005; Yudin *et al.*, 2006) and the whole field of novel attosecond physics (for an overview, see, e.g., Ivanov and Walmsley, 2005; Knight and Marangos, 2006). One may also envisage many other novel applications such as nonlinear optics in XUV (Schnürer *et al.*, 1999; Sekikawa *et al.*, 2004; Tzallas *et al.*, 2004; Benis *et al.*, 2006; Misoguti *et al.*, 2006) for which the intense fs harmonics from LPP show particularly good potential.

Due to their short wavelength, fs harmonics from LPP provide an excellent tool for laser-plasma diagnostics, especially to diagnose warm and hot dense matter. This should provide additional insight into the interaction physics, including the process of harmonic generation itself. For this purpose, the harmonics have been used as a diagnostic tool to probe plasma properties (Theobald *et al.*, 1996, 1999; Merdji *et al.*, 2000; Teubner *et al.*, 2004; Dobosz *et al.*, 2005) and to examine high-energy electron jets from the interaction process. One highlight in this respect is the measurement of gigagauss magnetic fields generated during ultrahigh-intensity short pulse laser-solid target interaction experiments (Tatarakis, Gopal, Watts, *et al.*, 2002; Tatarakis, Watts, Beg, *et al.*, 2002; Wagner *et al.*, 2004).

Attosecond pulses created by surface harmonics should contain significantly more photons than are currently available from gas harmonics, and so enhance the potential of this new type of light source for real-time molecular imaging.

In general, there will be a virtually unlimited number of applications for intense ultrashort XUV pulses in the future. Although the XFEL may be the source of choice for applications that require the most intense pulses, there will still be an enormous potential for the still very intense fs harmonics from LPP (see Fig. 31); see Materlik and Tschentscher (2001) for a recent overview of such applications.

D. Conclusion and outlook

Since the first experiments and theoretical investigations on HHG from fs and ps laser-pulse-generated plasmas, much progress has been made. Today, very intense harmonics can already be generated. In the near future, the harmonics from femtosecond laser-produced plasmas will represent a coherent source much brighter than most other XUV sources apart from the XFEL with its extraordinary brilliance. Moreover, there is no fundamental limitation in using the highest possible laser intensities available, so that even when the conversion efficiency saturates, a further increase of harmonic intensity should be possible by scaling the laser energy.

Theory shows that the duration of the harmonics could be ultrashort, namely, in the femtosecond or attosecond range, and in the future the zeptosecond regime may even be reached. Several groups are presently attempting to confirm these predictions by high-precision measurements. It is expected that experimental verification of femtosecond and attosecond pulse durations will follow soon.

Within the past decade, the harmonics from fs LPPs have been quantitatively characterized. Parameters such as the energy, pulse duration, divergence, polarization, conversion efficiency, etc. of the harmonics are now well known from theory and experiment. The dependence of these parameters on the experimental conditions such as laser intensity, angle of incidence, and laser polarization has been studied in sufficient detail that it is now possible to optimize the generation process to obtain intense and ultrashort pulses in the XUV.

Both experimental and theoretical investigations have also given much insight into the interaction of high-intensity laser light with solid targets and plasmas and into the HHG process itself. Several mechanisms are now thought to be responsible for the generation of the harmonics, such as resonance absorption, relativistic surface oscillations, and plasma waves induced by bunches of energetic electrons, which play a particularly important role in experiments using thin foil targets. Related phenomena such as plasma line emission and coherent transition radiation have also been identified within the context of HHG.

Currently there are still a lot of open questions, making HHG not only a lively field of investigation in its own right, but also giving hope for potential applications. Future research is likely to concentrate on (i) making use of fs harmonics as a diagnostic tool for the laser-plasma interaction process itself; (ii) control of fs harmonic properties, which still have the potential to achieve much higher conversion efficiency and thus harmonic power and brilliance (the main goals here are to increase the harmonic order, i.e., to reduce the harmonic wavelength, and to reduce the harmonic pulse duration); and finally (iii) practical exploitation of fs harmonics in applications that require *intense* XUV light and give access to new fields of physics such as nonlinear optics in the XUV region.

ACKNOWLEDGMENTS

U.T. thanks K. A. Janulewicz, Th. Tschentscher, and Ph. Zeitoun for information on the actual state of the art of the XRL, XFEL, and SXRL, respectively. We are also indebted to F. Quéré for clarifying discussions concerning the OMM and CWE mechanisms of surface harmonic generation, and to M. Zepf for pointing out an error in the angular divergence for harmonics quoted in an earlier version of the manuscript.

REFERENCES

Ackermann, W., *et al.*, 2007, "Operation of a free-electron laser from the extreme ultraviolet to the water window," Nat. Phys. **1**, 336–342.

Akhiezer, A. I., and R. V. Polovin, 1956, "Theory of wave motion of an electron plasma," Sov. Phys. JETP **3**, 696–705.

Akiyama, Y., K. Midorikawa, Y. Matsunawa, Y. Nagata, M. Obara, H. Tashiro, and K. Toyoda, 1992, "Generation of high-order harmonics using laser-produced rare-gas-like ions," Phys. Rev. Lett. **69**, 2176–2179.

Altenbernd, D., U. Teubner, P. Gibbon, E. Förster, P. Audebert, J. P. Geindre, J. C. Gauthier, G. Grillon, and A. Antonetti, 1997, "Soft x-ray brilliance of femtosecond and picosecond laser-plasmas," J. Phys. B **30**, 3969–3982.

Andiel, U., K. Eidmann, and K. Witte, 2001, "Time-resolved x-ray *K*-shell spectra from high density plasmas generated by ultrashort laser pulses," Phys. Rev. E **63**, 026407.

Aseyev, S. A., Y. Ni, L. J. Frasinski, H. G. Muller, and M. J. J. Vrakking, 2003, "Attosecond angle-resolved photoelectron spectroscopy," Phys. Rev. Lett. **91**, 223902.

Baeva, T., S. Gordienko, and A. Pukhov, 2006a, "Relativistic control for single attosecond x-ray burst generation," Phys. Rev. E **74**, 065401.

Baeva, T., S. Gordienko, and A. Pukhov, 2006b, "Theory of high-order harmonic generation in relativistic laser interaction with overdense plasma," Phys. Rev. E **74**, 046404.

Balcou, Ph., R. Haroutunian, S. Sebban, G. Grillon, A. Rousse, G. Mullot, J.-P. Chambaret, G. Rey, A. Antonetti, D. Hulin, L. Roos, D. Descamps, M. B. Gaarde, A. L'Huillier, E. Constant, E. Mevel, D. von der Linde, A. Orisch, A. Tarasevitch, U. Teubner, D. Klöpfel, and W. Theobald, 2002, "High-order-harmonic generation: Towards laser-induced phase-matching control and relativistic effects," Appl. Phys. B: Lasers Opt. **74**, 509–515.

Barr, H. C., T. J. M. Boyd, G. A. Gardner, and R. Rankin, 1985, "Inverse resonance-absorption in an inhomogeneous magnetized plasma," Phys. Fluids **28**, 16–18.

Baton, S. D., J. J. Santos, F. Amiranoff, H. Popescu, L. Gremillet, M. Koenig, E. Martinolli, O. Guilbaud, C. Rousseaux, M. Rabec Le Gloahec, T. Hall, D. Batani, E. Perelli, F. Scianitti, and T. E. Cowan, 2003, "Evidence of ultrashort electron bunches in laser-plasma interactions at relativistic intensities," Phys. Rev. Lett. **91**, 105001.

Beg, F. N., M. S. Wei, E. L. Clark, A. E. Dangor, R. G. Evans, P. Gibbon, A. Gopal, K. L. Lancaster, K. W. D. Ledingham, P. McKenna, P. A. Norreys, M. Tatarakis, M. Zepf, and K. Krushelnick, 2004, "Return current and proton emission from short pulse laser interactions with wire targets," Phys. Plasmas **11**, 2806–2813.

Benis, E. P., D. Charalambidis, T. N. Kitsopoulos, G. D. Tsakiris, and P. Tzallas, 2006, "Two-photon double ionization of

rare gases by a superposition of harmonics," Phys. Rev. A **74**, 051402(R).
Benitez, E. L., D. E. Husk, S. E. Schnatterly, and C. Tarrio, 1991, "A surface recombination model applied to large features in inorganic phosphor efficiency measurements in the soft x-ray region," J. Appl. Phys. **70**, 3256–3260.
Bezzerides, B., R. D. Jones, and D. W. Forslund, 1982, "Plasma mechanism for ultraviolet harmonic radiation due to intense CO_2 light," Phys. Rev. Lett. **49**, 202–205.
Bobin, J. L., 1985, "High intensity laser plasma interaction," Phys. Rep. **122**, 173–274.
Bourdier, A., 1983, "Oblique incidence of a strong electromagnetic wave on a cold inhomogeneous electron plasma: Relativistic effects," Phys. Fluids **26**, 1804–1807.
Boyd, T. J. M., 1964, "Emission of radio noise by plasmas," Phys. Fluids **7**, 59–63.
Boyd, T. J. M., and R. Ondarza-Rovira, 2000, "Plasma line emission from short pulse laser interactions with dense plasmas," Phys. Rev. Lett. **85**, 1440–1443.
Boyd, T. J. M., and R. Ondarza-Rovira, 2007, "Plasma modulation of harmonic emission spectra from laser-plasma interactions," Phys. Rev. Lett. **98**, 105001.
Brunel, F., 1987, "Not-so-resonant, resonant absorption," Phys. Rev. Lett. **59**, 52–55.
Brunel, F., 1990, "Harmonic generation due to plasma effects in a gas undergoing multiphoton ionization in the high-intensity limit," J. Opt. Soc. Am. B **7**, 521–526.
Bulanov, S. V., N. M. Naumova, T. Z. Esirkepov, and F. Pegoraro, 1996, "Evolution of the frequency spectrum of a relativistically strong laser pulse in a plasma," Phys. Scr., T **T63**, 258–261.
Bulanov, S. V., N. M. Naumova, and F. Pegoraro, 1994, "Interaction of an ultrashort, relativistically strong laser pulse with an overdense plasma," Phys. Plasmas **1**, 745–757.
Burnett, N. H., H. A. Baldis, M. C. Richardson, and G. D. Enright, 1977, "Harmonic generation in CO_2-laser target interaction," Appl. Phys. Lett. **31**, 172–174.
Carman, R. L., D. W. Forslund, and J. M. Kindel, 1981a, "Visible harmonic emission as a way of measuring profile steepening," Phys. Rev. Lett. **46**, 29–32.
Carman R. L., D. W. Forslund, and J. M. Kindel, 1981b, "Observation of harmonics in the visible and ultraviolet created in CO_2-laser produced plasmas," Phys. Rev. A **24**, 2649–2663.
Chambers, D. M., P. A. Norreys, A. E. Dangor, R. S. Majoribanks, S. Moustaizis, D. Neely, S. G. Preston, J. S. Wark, I. Watts, and M. Zepf, 1998, "Feasibility study of high harmonic generation from short wavelength lasers interacting with solid targets," Opt. Commun. **148**, 289–294.
Chambers, D. M., S. G. Preston, M. Zepf, M. Castro-Colin, M. H. Key, J. S. Wark, A. E. Dangor, A. Dyson, D. Neely, and P. A. Norreys, 1997, "Imaging of high harmonic radiation emitted during the interaction of a 20 TW laser with a solid target," J. Appl. Phys. **81**, 2055–2058.
Chen S.-Y., A. Maksimchuk, E. Esarey, and D. Umstadter, 2000, "Observation of phase-matched harmonic generation," Phys. Rev. Lett. **84**, 5528–5531.
Chen, S.-Y., A. Maksimchuk, and D. Umstadter, 1998, "Experimental observation of relativistic nonlinear Thomson scattering," Nature **396**, 653–655.
Chin-Fatt, C., and H. R. Griem, 1970, "Enhanced radiation from a theta-pinch plasma," Phys. Rev. Lett. **25**, 1644–1646.
Denisov, N. G., 1957, "On a singularity of the field of an electromagnetic wave propagated in an inhomogeneous plasma," Sov. Phys. JETP **4**, 544–553.
Dobosz, S., G. Doumy, H. Stabile, P. D'Oliveira, P. Monot, F. Reau, S. Hüller, and Ph. Martin, 2005, "Probing hot and dense laser-induced plasmas with ultrafast XUV pulses," Phys. Rev. Lett. **95**, 025001
Donnelly, T. D., T. Ditmire, K. Neuman, M. D. Perry, and R. W. Falcone, 1996, "High-order harmonic generation in atom clusters," Phys. Rev. Lett. **76**, 2472–2475.
Doumy, G., S. Dobosz, P. D'Oliveira, P. Monot, M. Perdrix, F. Quere, F. Reau, Ph. Martin, P. Audebert, J. C. Gauthier, and J. P. Geindre, 2004, "High order harmonic generation by nonlinear reflection of a pedestal-free intense laser pulse on a plasma," Appl. Phys. B: Lasers Opt. **78**, 901–904.
Doumy, G., F. Quere, O. Gobert, M. Perdrix, Ph. Martin, P. Audebert, J. C. Gauthier, J.-P. Geindre, and T. Wittmann, 2004, "Complete characterization of a plasma mirror for the production of high-contrast ultraintense laser pulses," Phys. Rev. E **69**, 026402.
Drake, J. F., P. K. Kaw, Y. C. Lee, G. Schmidt, C. S. Liu, and M. N. Rosenbluth, 1974, "Parametric instabilities of electromagnetic waves in plasmas," Phys. Fluids **17**, 778–785.
Drescher, M., M. Hentschel, R. Kienberger, G. Tempea, C. Spielmann, G. A. Reider, P. B. Corkum, and F. Krausz, 2001, "X-ray pulses approaching the attosecond frontier," Science **291**, 1923–1927.
Drescher, M., M. Hentschel, R. Kienberger, M. Uiberacker, V. Yakovlev, A. Scrinzi, Th. Westerwalbesloh, U. Kleineberg, U. Heinzmann, and F. Krausz, 2002, "Time-resolved atomic inner-shell spectroscopy," Nature **419**, 803–807
Dromey, B., D. Adams, R. Hoerlein, Y. Nomura, S. G. Rykovanov, D. C. Carroll, P. S. Foster, S. Kar, K. Markey, P. McKenna, D. Neely, M. Geissler, G. D. Tsakiris, and M. Zepf, 2009, "Diffraction-limited performance and focusing of high harmonics from relativistic plasmas," Nat. Phys. **5**, 146–152.
Dromey, B., M. Zepf, A. Gopal, K. Lancaster, M. S. Wei, K. Krushelnick, M. Tatarakis, N. Vakakis, S. Moustaizis, R. Kodama, M. Tampo, C. Stoeckl, R. Clarke, H. Habara, D. Neely, S. Karsch, and P. Norreys, 2006, "High harmonic generation in the relativistic limit," Nat. Phys. **2**, 456–459.
Eidmann, K., T. Kawachi, A. Marcinkevicius, R. Bartlome, G. D. Tsakiris, K. Witte, and U. Teubner, 2005, "Fundamental and harmonic emission from the rear side of a thin overdense foil irradiated by an intense ultrashort laser pulse," Phys. Rev. E **72**, 036413.
Erokhin, N., V. E. Zakharov, and S. S. Moiseev, 1969, "Second harmonic generation by an electromagnetic wave incident on inhomogeneous plasma," Sov. Phys. JETP **29**, 101.
Fajardo, M., Ph. Zeitoun, G. Faivre, S. Sebban, T. Mocek, S. Hallou, D. Aubert, Ph. Balcou, F. Burgy, D. Douillet, P. Mercère, A. S. Morlens, J. P. Rousseau, C. Valentin, S. Kazamias, G. de Lachèze-Murel, T. Lefroud, H. Merdji, S. le Pape, M. F. Ravet, F. Delmotte, and J. Gautier, 2006, "Second generation x-ray lasers," J. Quant. Spectrosc. Radiat. Transf. **99**, 142–152.
Feurer, T., W. Theobald, R. Sauerbrey, I. Uschmann, D. Altenbernd, U. Teubner, P. Gibbon, E. Förster, G. Malka, and J. L. Miquel, 1997, "Onset of diffuse reflectivity and fast electron flux inhibition in 528-nm-laser-solid interactions at ultrahigh intensity," Phys. Rev. E **56**, 4608–4614.
Flettner, A., T. Pfeifer, D. Walter, C. Winterfeldt, C. Spielmann, and G. Gerber, 2003, "High-harmonic generation and plasma radiation from water microdroplets," Appl. Phys. B: Lasers Opt. **77**, 747–751.

Földes, I. B., J. S. Bakos, Z. Bakonyi, T. Nagy, and S. Szatmari, 1999, "Harmonic generation in plasmas of different density gradients," Phys. Lett. A **258**, 312–316.

Földes, I. B., J. S. Bakos, G. Veres, Z. Bakonyi, T. Nagy, and S. Szatmari, 1996, "Harmonic generation in a UV laser plasma," IEEE J. Sel. Top. Quantum Electron. **2**, 776–781.

Gamaly, E. G., 1993, "Instability of the overdense plasma boundary induced by the action of a powerful photon beam," Phys. Rev. E **48**, 2924–2928.

Ganeev, R. A., M. Suzuki, M. Baba, and H. Kuroda, 2005, "Harmonic generation from chromium plasma," Appl. Phys. Lett. **86**, 131116.

Ganeev, R. A., M. Suzuki, M. Baba, H. Kuroda, and T. Ozaki, 2005, "High-order harmonic generation from boron plasma in the extreme-ultraviolet range," Opt. Lett. **30**, 768–770.

Gavrila, M., 1992, *Atoms in Intense Laser Fields* (Academic, Boston).

Geissler, M., S. Rykovanov, J. Schreiber, J. Meyer-ter-Vehn, and G. D. Tsakiris, 2007, "3D simulations of surface harmonic generation with few-cycle pulses," New J. Phys. **9**, 218.

Gibbon, P., 1994, "Efficient production of fast electrons from femtosecond laser interaction with solid targets," Phys. Rev. Lett. **73**, 664–667.

Gibbon, P., 1996, "Harmonic generation by femtosecond laser-solid interaction: A coherent 'water-window' light source?," Phys. Rev. Lett. **76**, 50–53.

Gibbon, P., 1997, "High-order harmonic generation in plasmas," IEEE J. Quantum Electron. **33**, 1915–1924.

Gibbon, P., 2005, *Short Pulse Interactions with Matter: An Introduction* (Imperial College, London).

Gibbon, P., 2007, "Cleaner petawatts with plasma optics," Nat. Phys. **3**, 369–370.

Gibbon, P., D. Altenbernd, U. Teubner, E. Förster, P. Audebert, J. P. Geindre, J. C. Gauthier, and A. Mysyrowicz, 1997, "Plasma density determination by transmission of laser-generated surface harmonics," Phys. Rev. E **55**, R6352–R6355.

Gibbon, P., A. A. Andreev, E. Lefebvre, G. Bonnaud, H. Ruhl, J. Delettrez, and A. Bell, 1999, "Calibration of 1D boosted kinetic codes for modeling high-intensity laser-solid interactions," Phys. Plasmas **6**, 947–953.

Gibbon, P., and A. R. Bell, 1992, "Collisionless absorption in sharp-edged plasmas," Phys. Rev. Lett. **68**, 1535–1538.

Ginzburg, V. L., 1964, *The Propagation of Electromagnetic Waves in Plasmas* (Pergamon, New York).

Ginzburg, V. L., and V. V. Zhelezniakov, 1958, "On the possible mechanisms of sporadic solar radio emission (radiation in an isotropic plasma)," Sov. J. Astron. **2**, 653–668.

Gordienko, S., A. Pukhov, O. Shorokhov, and T. Baeva, 2004, "Relativistic Doppler effect: Universal spectra and zeptosecond pulses," Phys. Rev. Lett. **93**, 115002.

Gordienko, S., A. Pukhov, O. Shorokhov, and T. Baeva, 2005, "Coherent focusing of high harmonics: A new way towards the extreme intensities," Phys. Rev. Lett. **94**, 103903.

Grebogi, C., V. K. Tripathi, and H.-H. Chen, 1983, "Harmonic generation of radiation in a steep density profile," Phys. Fluids **26**, 1904–1908.

Gruner, S. M., M. W. Tate, and E. F. Eikenberry, 2002, "Charge-coupled device area x-ray detectors," Rev. Sci. Instrum. **73**, 2815–2842.

Henke, B. L., E. M. Gullikson, and J. C. Davis, 1993, "X-ray interactions: Photoabsorption, scattering, transmission, and reflection at $E=50-30000$ eV, $Z=1-92$," At. Data Nucl. Data Tables **54**, 181–342.

Hentschel, M., R. Kienberger, Ch. Spielmann, G. A. Reider, N. Milosevic, T. Brabec, P. Corkum, U. Heinzmann, M. Drescher, and F. Krausz, 2001, "Attosecond metrology," Nature **414**, 509–513.

Hergott, J.-F., M. Kovacev, H. Merdji, C. Hubert, Y. Mairesse, E. Jean, P. Breger, P. Agostini, B. Carre, and P. Salieres, 2002, "Extreme-ultraviolet high-order harmonic pulses in the microjoule range," Phys. Rev. A **66**, 021801.

Hollandt, J., M. Kühne, and B. Wende, 1994, "High-current hollow-cathode source as a radiant intensity standard in the 40–125 nm wavelength range," Appl. Opt. **33**, 68–74.

Hu, S. X., and Z. Z. Xu, 1997, "Enhanced harmonic emission from ionized clusters in intense laser pulses," Appl. Phys. Lett. **71**, 2605–2607.

Hüller, S., and J. Meyer-ter-Vehn, 1993, "High-order harmonic radiation from solid layers irradiated with subpicosecond laser pulses," Phys. Rev. A **48**, 3906–3909.

Ishizawa, A., R. A. Ganeev, T. Kanai, H. Kuroda, and T. Ozaki, 2002, "Measurements of blue shifts due to collisionless absorption in harmonic generation from subpicosecond laser-produced plasma," Phys. Rev. E **66**, 026414.

Ishizawa, A., K. Inaba, T. Kanai, T. Ozaki, and H. Kuroda, 1999, "High-order harmonic generation from a solid surface plasma by using a picosecond laser," IEEE J. Quantum Electron. **35**, 60–65.

Ishizawa, A., T. Kanai, T. Ozaki, and H. Kuroda, 2000, "The spatial distribution of high-order harmonics from solid surface plasmas," IEEE J. Quantum Electron. **36**, 665–668.

Ishizawa, A., T. Kanai, T. Ozaki, and H. Kuroda, 2001, "Enhancement of high-order harmonic generation efficiency from solid-surface plasma by controlling the electron density gradient of picosecond laser-produced plasmas," IEEE J. Quantum Electron. **37**, 384–389.

Ishikawa, K., and K. Midorikawa, 2002, "Two-photon ionization of He^+ as a nonlinear optical effect in the soft-x-ray region," Phys. Rev. A **65**, 043405.

Ivanov, M. Yu., and I. A. Walmsley, 2005, Eds., "Special issue: Attosecond science," J. Mod. Opt. 52, Nos. 2–3.

Jackson, J. D., 1975, *Classical Electrodynamics*, 2nd ed. (Wiley, New York), Chap. 14.

Janulewicz, K. A., 2007, private communication.

Janulewicz, K. A., A. Lucianetti, G. Priebe, and P. V. Nickles, 2004, "Review of state-of-the-art and output characteristics of table-top soft x-ray lasers," X-Ray Spectrom. **33**, 262–266.

Jasny, J., U. Teubner, W. Theobald, C. Wülker, J. Bergmann, and F. P. Schäfer, 1994, "A single-shot spectrograph for the soft x-ray region," Rev. Sci. Instrum. **65**, 1631–1635.

Kato, S., B. Bhattacharyya, A. Nishiguchi, and K. Mima, 1993, "Wave breaking and absorption efficiency for short pulse *p*-polarized laser light in a very steep density radient," Phys. Fluids B **5**, 564–570.

Kingham, R. J., P. Gibbon, W. Theobald, L. Veisz, and R. Sauerbrey, 2001, "Phase modulation ultra-short pulses reflected from high density plasmas," Phys. Rev. Lett. **86**, 810–813.

Knight, P. L., and J. P. Marangos, 2006, Eds., "Special issue: High field attosecond physics," J. Mod. Opt. 53, Nos. 1–2.

Kohlweyer, S., G. D. Tsakiris, C.-G. Wahlström, C. Tillman, and I. Mercer, 1995, "Harmonic generation from solid-vacuum interface irradiated at high laser intensities," Opt. Commun. **117**, 431–438.

Kruer, W. L., 1988, *The Physics of Laser Plasma Interactions* (Addison-Wesley, New York).

Kühlke, D., U. Herpes, and D. von der Linde, 1987, "Soft x-ray emission from sub-picosecond laser-produced plasmas," Appl. Phys. Lett. **50**, 1785–1787.

Landau, L. D., and L. M. Lifshitz, 1985, *Elektrodynamik der Kontinua* (Akademie-Verlag, Berlin), pp. 506–510.

L'Huillier, A., and P. Balcou, 1993, "High-order harmonic generation in rare gases with a 1-ps 1053-nm laser," Phys. Rev. Lett. **70**, 774–777.

Lichters, R., 1997, Ph.D. thesis, Technical University München.

Lichters, R., J. Meyer-ter-Vehn, and A. Pukhov, 1996, "Short-pulse laser harmonics from oscillating plasma surfaces dreven at relativistic intensity intensity," Phys. Plasmas **3**, 3425–3437.

Lichters, R., J. Meyer-ter-Vehn, and A. Pukhov, 1998, *Radiation at* $2\omega_p$ *from Inverse Two-plasmon Decay in Overdense Plasma Driven by Ultra-short Laser Pulses*, AIP Conf. Proc. No. 426 (AIP, Woodbury, NY), pp. 41–48.

Lopez-Martens, R., J. Mauritsson, P. Johnsson, K. Varju, A. L'Huillier, W. Kornelis, J. Biegert, U. Keller, M. Gaarde, and K. Schafer, 2004, "Characterization of high-order harmonic radiation on femtosecond and attosecond time scales," Appl. Phys. B: Lasers Opt. **78**, 835–840.

Luther-Davies, B., E. G. Gamalii, Y. Wang, A. V. Rode, and V. T. Tikhonchuk, 1992, "Matter in ultrastrong laser fields," Sov. J. Quantum Electron. **22**, 289–325.

Maiman, T. H., 1960, "Stimulated optical radiation in ruby," Nature **187**, 493–494.

Mairesse, Y., O. Gobert, P. Breger, H. Merdji, P. Meynadier, P. Monchicourt, M. Perdrix, P. Salières, and B. Carre, 2005, "High harmonic XUV spectral phase interferometry for direct electric-field reconstruction," Phys. Rev. Lett. **94**, 173903.

Materlik, G., and Th. Tschentscher, 2001, Eds., "TESLA Technical Design Report Part V—The X-ray Free Electron Laser," DESY 2001-011, pp. V-1 to V-533 DESY, Hamburg.

McPherson, A., G. Gibson, H. Jara, U. Johann, T. S. Luk, I. A. McIntyre, K. Boyer, and C. K. Rhodes, 1987, "Studies of multiphoton production of vacuum ultraviolet-radiation in the rare gases," J. Opt. Soc. Am. B **4**, 595–601.

Melrose, D. B., 1980, "The emission mechanisms for solar radio bursts," Space Sci. Rev. **26**, 3–38.

Merdji, H., P. Salières, L. Ledéroff, J.-F. Hergott, B. Carré, D. Joyeux, D. Descamps, J. Norin, C. Lyngå, A. L'Huillier, C.-G. Wahlström, M. Bellini, and S. Hüller, 2000, "Coherence properties of high-order harmonics: Application to high-density laser-plasma diagnostic," Laser Part. Beams **18**, 495–502.

Meyer, J., and Y. Zhu, 1993, "Measurement of two plasmon decay instability development in k space of a laser produced plasma and its relation to 3/2-harmonic genetration," Phys. Rev. Lett. **71**, 2915–2918.

Mikhailova, Yu. M., V. T. Platonenko, and S. G. Rykovanov, 2005, "Generation of an attosecond x-ray pulse in a thin film irradiated by an ultrashort ultrarelativistic laser pulse," JETP Lett. **81**, 571–574.

Misoguti, L., I. P. Christov, S. Backus, M. M. Murnane, and H. C. Kapteyn, 2006, "Nonlinear wave-mixing processes in the extreme ultraviolet," Phys. Rev. A **72**, 063803.

Monot, P., G. Doumy, S. Dobosz, M. Perdrix, P. D'Oliveira, F. Quéré, R. Réau, P. Martin, P. Audebert, J.-C. Gauthier, and J.-P. Geindre, 2004, "High-order harmonic generation by nonlinear reflection of an intense high-contrast laser pulse on a plasma," Opt. Lett. **29**, 893–895.

Montgomery, D., and P. Tidman, 1964, "Secular and nonsecular behavior for the cold plasma equations," Phys. Fluids **7**, 242–249.

Mori, W. B., C. D. Decker, and W. P. Leemans, 1993, "Relativistic harmonic content of nonlinear electromagnetic waves in underdense plasmas," IEEE Trans. Plasma Sci. **21**, 110–119.

Mourou, G., 1997, "The ultrahigh-peak-power laser: present and future," Appl. Phys. B: Lasers Opt. **65**, 205–211.

Mourou, G. A., T. Tajima, and S. V. Bulanov, 2006, "Optics in the relativistic regime," Rev. Mod. Phys. **78**, 309–371.

Mulser, P., 1979, in *Laser-Plasma Interactions*, edited by R. A. Cairns and J. J. Sanderson (SUSSP, Edinburgh), Vol. 1, pp. 91–144.

Murnane, M. M., H. C. Kapteyn, S. P. Gordon, and R. W. Falcone, 1994, "Ultrashort x-ray pulses," Appl. Phys. B: Lasers Opt. **58**, 261–266.

Naumova, N. M., J. A. Nees, B. Hou, G. A. Mourou, and I. V. Sokolov, 2004, "Isolated attosecond pulses generated by relativistic effects in a wavelength-cubed focal volume," Opt. Lett. **29**, 778–780.

Naumova, N. M., J. A. Nees, I. V. Sokolov, B. Hou, and G. A. Mourou, 2004, "Relativistic generation of isolated attosecond pulses in a λ^3 focal volume," Phys. Rev. Lett. **92**, 063902.

Nees, J., N. Naumova, E. Power, V. Yanovsky, I. Sokolov, A. Maksimchuk, S.-W. Bahk, V. Chvykov, G. Kalintchenko, B. Hou, and G. Mourou, 2005, "Relativistic generation of isolated attosecond pulses: A different route to extreme intensity," J. Mod. Opt. **52**, 305–319.

Niikura, H., F. Le Gare, D. M. Villeneuve, and P. B. Corkum, 2005, "Attosecond dynamics using sub-laser-cycle electron pulses," J. Mod. Opt. **52**, 453–464.

Nomura, Y., R. Hoerlein, P. Tzallas, B. Dromey, S. Rykovanov, Zs. Major, J. Osterhoff, S. Karsch, L. Veisz, M. Zepf, D. Charalambidis, F. Krausz, and G. D. Tsakiris, 2009, "Attosecond phase locking of harmonics emitted from laser-produced plasmas," Nat. Phys. **5**, 124-128.

Norreys, P. A., K. M. Krushelnick, and M. Zepf, 2004, "PW lasers: Matter in extreme laser fields," Plasma Phys. Controlled Fusion **46**, B13–B21.

Norreys, P. A., M. Zepf, S. Moustaizis, A. P. Fews, J. Zhang, P. Lee, M. Bakarezos, C. N. Danson, A. Dyson, P. Gibbon, P. Loukakos, D. Neely, F. N. Walsh, J. S. Wark, and A. E. Dangor, 1996, "Efficient XUV harmonics generated from picosecond laser pulse interactions with solid targets," Phys. Rev. Lett. **76**, 1832–1835.

Ondarza-Rovira, R., and T. J. M. Boyd, 2000, "Plasma harmonic emission spectra from laser interactions with dense plasma," Phys. Plasmas **7**, 1520–1530.

Papadogiannis, N. A., L. A. A. Nikolopoulos, D. Charalambidis, G. D. Tsakiris, P. Tzallas, and K. Witte, 2003, "Two-photon ionization of He through a superposition of higher harmonics," Phys. Rev. Lett. **90**, 133902.

Peatross, J., J. L. Chaloupka, and D. D. Meyerhofer, 1994, "High-order harmonic generation with an annular laser beam," Opt. Lett. **19**, 942–944.

Perry, M. D., and G. Mourou, 1994, "Terawatt to petawatt subpicosecond lasers," Science **264**, 917–924.

Pirozhkov, A. S., S. V. Bulanov, T. Zh. Esirkepov, M. Mori, A. Sagisaka, and H. Daido, 2006, "Attosecond pulse generation in the relativistic regime of the laser-foil interaction: The sliding mirror model," Phys. Plasmas **13**, 013107.

Platonenko, V. T., and V. V. Strelkov, 1998, "Generation of high-order harmonics in a high-intensity laser radiation field,"

Quantum Electron. **28**, 564–583.
Plaja, L., L. Roso, K. Rzazewski, and M. Lewenstein, 1998, "Generation of attosecond pulse trains during the reflection of a very intense laser on a solid surface," J. Opt. Soc. Am. B **15**, 1904–1911.
Popescu, H., S. D. Baton, F. Amiranoff, C. Rousseaux, M. Rabec Le Gloahec, J. J. Santos, L. Gremillet, M. Koenig, E. Martinolli, T. Hall, J. C. Adam, A. Heron, and D. Batani, 2005, "Subfemtosecond, coherent, relativistic, and ballistic electron bunches generated at ω_0 and $2\omega_0$ in high intensity laser-matter interaction," Phys. Plasmas **12**, 063106.
Quéré, F., C. Thaury, P. Monot, S. Dobosz, Ph. Martin, J.-P. Geindre, and P. Audebert, "Coherent wake emission of high-order harmonics from overdense plasmas," 2006, Phys. Rev. Lett. **96**, 125004.
Racz, E., I. B. Földes, G. Kocsis, G. Veres, K. Eidmann, and S. Szatmari, 2005, "On the effect of surface rippling on the generation of harmonics in laser plasmas," Appl. Phys. B: Lasers Opt. **82**, 13–18.
Reider, G. A., 2004, "XUV attosecond pulses: Generation and measurement," J. Phys. D **37**, R37–R48.
Rocca, J. J., V. N. Shlyaptsev, F. G. Tomasel, O. D. Cortazar, D. Hartshorn, and J. L. A. Chilla, 1994, "Demonstration of a discharge pumped table-top soft x-ray laser," Phys. Rev. Lett. **73**, 2192–2195.
Roso, L., L. Plaja, K. Rzazewski, and D. von der Linde, 2000, "Beyond the moving mirror model: Attosecond pulses from a relativistically moving plasma," Laser Part. Beams **18**, 467–475.
Rzazewski, K., L. Plaja, L. Roso, and D von der Linde, 2000, "Probe-field reflection on a plasma surface driven by a strong electromagnetic field," J. Phys. B **33**, 2549–2558.
Salieres, P., L. Le Deroff, T. Auguste, P. Monot, P. D'Oliveira, D. Campo, J. F. Hergott, H. Merdji, and B. Carre, 1999, "Frequency-domain interferometry in the XUV with high-order harmonics," Phys. Rev. Lett. **83**, 5483–5486.
Santos, J. J., F. Amiranoff, S. D. Baton, L. Gremillet, M. Koenig, E. Martinolli, M. Rabec Le Gloahec, C. Rousseaux, D. Batani, A. Bernardinello, G. Greison, and T. Hall, 2002, "Fast electron transport in ultraintense laser pulse interaction with solid targets by rear-side self-radiation diagnostics," Phys. Rev. Lett. **89**, 025001.
Sarachik, E. S., and G. T. Schappert, 1970, "Classical theory of the scattering of intense laser radiation by free electrons," Phys. Rev. D **1**, 2738–2753.
Schlegel, T., 2006, private communication.
Schnürer, M., Z. Cheng, M. Hentschel, G. Tempea, P. Kálmán, T. Brabec, and F. Krausz, 1999, "Absorption-limited generation of coherent ultrashort soft-x-ray pulses," Phys. Rev. Lett. **83**, 722–725.
Schwoerer, H., P. Gibbon, S. Düsterer, R. Behrens, C. Ziener, C. Reich, and R. Sauerbrey, 2001, "MeV x-rays and photoneutrons from femtosecond laser-produced plasmas," Phys. Rev. Lett. **86**, 2317–2320.
Sekikawa, T., A. Kosuge, T. Kanai, and S. Wanatabe, 2004, "Nonlinear optics in the extreme ultraviolet," Nature **432**, 605–608.
Sheng, Z. M., K. Mima, J. Zhang, and H. Sanuki, 2005, "Emission of electromagnetic pulses from laser wakefields through linear mode conversion," Phys. Rev. Lett. **94**, 095003.
Siegman, A. E., 1986, *Lasers* (University Science Books, Mill Valley, CA).
Singh, K. P., V. L. Gupta, and V. K. Tripathi, 2003, "Relativistic laser harmonic generation from plasmas with density ripple," Opt. Commun. **226**, 377–386.
Spielmann, Ch., N. H. Burnett, S. Sartania, R. Koppitsch, M. Schnürer, C. Kan, M. Lenzner, P. Wobrauschek, and F. Krausz, 1997, "Generation of coherent x-rays in the water window using 5-femtosecond laser pulses," Science **278**, 661–664.
Stamper, J. A., R. H. Lehmberg, A. Schmitt, M. J. Herbst, F. C. Young, J. H. Gardner, and S. P. Obenshain, 1985, "Evidence in the second-harmonic emission for self-focusing of a laser pulse in a plasma," Phys. Fluids **28**, 2563–2569.
Strickland, D., and G. Mourou, 1985, "Compression of amplified chirped optical pulses," Opt. Commun. **56**, 219–211.
Sturrock, P. A., R. H. Ball, and D. E. Baldwin, 1965, "Radiation at the plasma frequency and its harmonic from a turbulent plasma," Phys. Fluids **8**, 1509–1516.
Takahashi E., Y. Nabekawa, and K. Midorikawa, 2002, "Generation of 10-mJ coherent extreme-ultraviolet light by use of high-order harmonics," Opt. Lett. **27**, 1920–1922.
Tarasevitch, A., C. Dietrich, and D. von der Linde, 2007, "High order harmonics from plasma surfaces," in *Lectures in Strong Field Physics*, edited by T. Brabec (Springer-Verlag, Berlin, in press).
Tarasevitch, A., K. Lobov, C. Wünsche, and D. von der Linde, 2007, "Transition to the relativistic regime in high order harmonic generation," Phys. Rev. Lett. **98**, 103902.
Tarasevitch, A., A. Orisch, D. von der Linde, Ph. Balcou, G. Rey, J.-P. Chambaret, U. Teubner, D. Klöpfel, and W. Theobald, 2000, "Generation of high-order spatially coherent harmonics from solid targets by femtosecond laser pulses," Phys. Rev. A **62**, 023816.
Tatarakis, M., A. Gopal, I. Watts, F. N. Beg, A. E. Dangor, K. Krushelnick, U. Wagner, P. A. Norreys, E. L. Clark, M. Zepf, and R. G. Evans, 2002, "Measurements of ultrastrong magnetic fields during relativistic laser-plasma interactions," Phys. Plasmas **9**, 2244–2250.
Tatarakis, M., I. Watts, F. N. Beg, E. L. Clark, A. E. Dangor, A. Gopal, M. G. Haines, P. A. Norreys, U. Wagner, M.-S. Wei, M. Zepf, and K. Krushelnick, 2002, "Measuring huge magnetic fields," Nature **415**, 280.
Teubner, U., D. Altenbernd, P. Gibbon, E. Förster, A. Mysyrowicz, P. Audebert, J.-P. Geindre, J. C. Gauthier, R. Lichters, and J. Meyer-ter-Vehn, 1997, "Observation of VUV radiation at wavelengths in the ω_p- and $2\omega_p$-wavelength range emitted from femtosecond laser-plasmas," Opt. Commun. **144**, 217–221.
Teubner, U., J. Bergmann, B. van Wonterghem, F. P. Schäfer, and R. Sauerbrey, 1993, "Angle-dependent x-ray emission and resonance absorption in a laser-produced plasma generated by a high intensity ultrashort pulse," Phys. Rev. Lett. **70**, 794–797.
Teubner, U., K. Eidmann, U. Wagner, U. Andiel, F. Pisani, G. D. Tsakiris, K. Witte, J. Meyer-ter-Vehn, T. Schlegel, and E. Förster, 2004, "Harmonic emission from the rear side of thin overdense foils irradiated with intense ultrashort laser pulses," Phys. Rev. Lett. **92**, 185001.
Teubner, U., P. Gibbon, D. Altenbernd, D. Oberschmidt, E. Förster, A. Mysyrowicz, P. Audebert, J.-P. Geindre, and J. C. Gauthier, 1999, "Plasma frequency and harmonic emission from fs-laser plasmas," Laser Part. Beams **17**, 613–619.
Teubner, U., P. Gibbon, E. Förster, F. Falliès, P. Audebert, J. P. Geindre, and J. C. Gauthier, 1996, "Subpicosecond KrF*-laser plasma interaction at intensities between

10^{14} W/cm^2 and 10^{17} W/cm^2," Phys. Plasmas **3**, 2679–2685.
Teubner, U., G. Kühnle, and F. P. Schäfer, "Detailed study of the effect of a short prepulse on soft x-ray spectra generated by a high-intensity KrF* laser pulse," 1992, Appl. Phys. B: Photophys. Laser Chem. **54**, 493–499.
Teubner, U., G. Pretzler, Th. Schlegel, K. Eidmann, E. Förster, and K. Witte, 2003, "Anomalies in high-order harmonic generation at relativistic intensities," Phys. Rev. A **67**, 013816.
Teubner, U., W. Theobald, C. Wülker, and E. Förster, 1995, "X-ray spectra from high-intensity subpicosecond laser produced plasmas," Phys. Plasmas **2**, 972–981.
Teubner, U., U. Wagner, U. Andiel, F. Pisani, K. Eidmann, G. D. Tsakiris, T. Schlegel, E. Förster, and K. Witte, 2003, "Intense high-order harmonics generated with femtosecond laser pulses at relativistic intensities interacting with high density plasmas," Proc. SPIE **5196**, 146–155.
Teubner, U., U. Wagner, and E. Förster, 2001, "Sub-ten-femtosecond gating of optical pulses," J. Phys. B **34**, 2993–3002.
Thaury, C. F. Quéré, J.-P. Geindre, A. Levy, T. Ceccotti, P. Monot, M. Bougeard, F. Reau, P. D'Oliveira, P. Audebert, R. Marjoribanks, and Ph. Martin, 2007, "Plasma mirrors for ultrahigh-intensity optics," Nat. Phys. **3**, 424–429.
Theobald, W., R. Häßner, R. Kingham, R. Sauerbrey, R. Fehr, D. O. Gericke, M. Schlanges, W.-D. Kraeft, and K. Ishikawa, 1999, "Electron densities, temperatures, and the dielectric function of femtosecond-laser-produced plasmas," Phys. Rev. E **59**, 3544–3553.
Theobald, W., R. Häßner, C. Wülker, and R. Sauerbrey, 1996, "Temporally resolved measurement of electron densities ($>10^{23}$ cm^{-3}) with high harmonics," Phys. Rev. Lett. **77**, 298–301.
Theobald, W., C. Wülker, S. Szatmari, F. P. Schäfer, and J. S. Bakos, 1995, "Investigation of the interaction of subpicosecond KrF* laser pulses with a preformed carbon plasma," Appl. Phys. B: Lasers Opt. **61**, 593–600.
Tsakiris, G. D., K. Eidmann, J. Meyer-ter-Vehn, and F. Krausz, 2006, "Route to intense single attosecond pulses," New J. Phys. **8**, 1–19.
Tschentscher, Th., 2004, "Investigation of ultrafast processes using x-ray free-electron laser radiation," Chem. Phys. **299**, 271–276.
Tschentscher, Th., 2007, private communication.
Tzallas, P., D. Charalambidis, N. A. Papadogiannis, K. Witte, and G. D. Tsakiris, 2003, "Direct observation of attosecond light bunching," Nature **426**, 267–271.
Tzallas, P., K. Witte, G. D. Tsakiris, N. A. Papadogiannis, and D. Charalambidis, 2004, "Extending optical fs metrology to XUV attosecond pulses," Appl. Phys. A: Mater. Sci. Process. **79**, 1673–1677.
Veisz, L., W. Theobald, T. Feurer, H. Schwoerer, I. Uschmann, O. Renner, and R. Sauerbrey, 2004, "Three-halves harmonic emission from femtosecond laser-produced plasmas with steep density gradients," Phys. Plasmas **11**, 3311–3323.
Veres, G., J. S. Bakos, I. B. Földes, K. Gal, Z. Juhasz, G. Kocsis, and S. Szatmari, 1999, "Polarization of harmonics generated by ultrashort KrF*-laser pulses on solid surfaces," Europhys. Lett. **48**, 390–396.
von der Linde, D., 1999, "Generation of high order optical harmonics from solid surfaces," Appl. Phys. B: Lasers Opt. **68**, 315–319.
von der Linde, D., T. Engers, G. Jenke, P. Agostini, G. Grillon, E. Nibbering, A. Mysyrowicz, and A. Antonetti, 1995, "Generation of high-order harmonics from solid surfaces by intense femtosecond laser pulases," Phys. Rev. A **52**, R25–R27.
von der Linde, D., and K. Rzàzewski, 1996, "High order optical harmonic generation from solid surfaces," Appl. Phys. B: Lasers Opt. **63**, 499–506.
von der Linde, D., H. Schulz, T. Engers, and H. Schüler, 1992, "Second harmonic generation in plasmas produced by intense femtosecond laser pulses," IEEE J. Quantum Electron. **QE-28**, 2388–2397.
Wabnitz, H., *et al.*, 2002, "Multiple ionization of atom clusters by intense soft x-rays from a free-electron laser," Nature **420**, 482–485.
Wagner, U., U. Andiel, U. Teubner, and K. Eidmann, 2002, unpublished.
Wagner, U., M. Tatarakis, A. Gopal, E. L. Clark, A. E. Dangor, R. G. Evans, M. G. Haines, S. P. D. Mangles, P. A. Norreys, M.-S. Wei, M. Zepf, and K. Krushelnick, 2004, "Laboratory measurements of 0.7 GG magnetic fields generated during high-intensity laser interactions with dense plasmas," Phys. Rev. E **70**, 026401.
Watts, I., M. Zepf, E. L. Clark, M. Tatarakis, K. Krushelnick, A. E. Dangor, R. M. Allott, R. J. Clarke, D. Neely, and P. A. Norreys, 2002, "Dynamics of the critical surface in high-intensity laser-solid interactions: Modulation of the XUV harmonic spectra," Phys. Rev. Lett. **88**, 155001.
Wilks, S. C., J. M. Dawson, W. B. Mori, T. Katsouleas, and M. E. Jones, 1989, "Photon accelerator," Phys. Rev. Lett. **62**, 2600–2603.
Wilks, S. C., W. L. Kruer, and W. Mori, 1993, "Odd harmonic generation of ultra-intense laser pulses reflected from an overdense plasma," IEEE Trans. Plasma Sci. **21**, 120–124.
Wilks, S. C., W. L. Kruer, M. Tabak, and A. B. Langdon, 1992, "Absorption of ultra-intense laser pulses," Phys. Rev. Lett. **69**, 1383–1386.
Willes, A. J., P. A. Robinson, and D. B. Melrose, 1996, "Second harmonic electromagnetic emission via Langmuir wave coalescence," Phys. Plasmas **3**, 149–159.
Yoon, P. H., 1995, "Plasma emission by a nonlinear beam instability," Phys. Plasmas **2**, 537–548.
Yoon, P. H., 1997, "Plasma emission by a nonlinear beam instability in a weakly magnetized plasma," Phys. Plasmas **4**, 3863–3881.
Yu, W., M. Y. Yu, Z. M. Sheng, and J. Zhang, 1998, "Model for fast electrons in ultrashort-pulse laser interaction with solid targets," Phys. Rev. E **58**, 2456–2460.
Yudin, G. L., A. D. Bandrauk, and P. B. Corkum, 2006, "Chirped attosecond photoelectron spectroscopy," Phys. Rev. Lett. **96**, 063002.
Zeiss, 2006, "Spiegelsysteme für EUV-Lithographie," Phys. J. **Nr. 1**, 74.
Zeitoun, P., 2006, private communication. See also http://www.tuixs.org/
Zeitoun, Ph., G. Faivre, S. Sebban, T. Mocek, A. Hallou, M. Fajardo, D. Aubert, Ph. Balcou, F. Burgy, D. Douillet, S. Kazamias, G. de Lacheze-Murel, T. Lefrou, S. le Pape, P. Mercere, H. Merdji, A. S. Morlens, J. P. Rousseau, and C. Valentin, 2004, "A high-intensity highly coherent soft x-ray femtosecond laser seeded by a high harmonic beam," Nature **431**, 426–429.
Zepf, M., 2008, private communication.
Zepf, M., G. D. Tsakiris, G. Pretzler, I. Watts, D. M. Chambers, P. A. Norreys, U. Andiel, A. E. Dangor, K. Eidmann, C. Gahn, A. Machacek, J. S. Wark, and K. Witte, 1998, "Role of

the plasma scale length in the harmonic generation from solid targets," Phys. Rev. E **58**, R5253–R5256.

Zepf, M., *et al.*, 1996, "Measurements of hole boring velocities and inferred energy absorption fractions for laser interaction with solid targets at 10^{19} W cm^{-2} μm^2," Phys. Plasmas **3**, 3242–3244.

Zhang, J., M. Zepf, P. A. Norreys, A. E. Dangor, M. Bakarezos, C. N. Danson, A. Dyson, A. P. Fews, P. Gibbon, M. H. Key, P. Lee, P. Loukakos, S. Moustaizis, D. Neely, F. N. Walsh, and J. S. Wark, 1996, "Coherence and bandwidth measurements of harmonics generated from solid surfaces irradiated by intense picosecond laser pulses," Phys. Rev. A **54**, 1597–1603.

Zheng, J., K. A. Tanaka, T. Miyakoshi, Y. Kitagawa, R. Kodama, T. Kurahashi, and T. Yamanaka, 2003, "Theoretical study of transition radiation from hot electrons generated in the laser-solid interaction," Phys. Plasmas **10**, 2994–3003.

Zheng, J., K. A. Tanaka, T. Sato, T. Yabuuchi, T. Kurahashi, Y. Kitagawa, R. Kodama, T. Norimatsu, and T. Yamanaka, 2004, "Study of hot electrons by measurement of optical emission from the rear surface of a metallic foil irradiated with ultraintense laser pulses," Phys. Rev. Lett. **92**, 165001.